DISCLAIMER

This report was prepared as an account of work sponsored by an agency of the United States Government. Neither the United States Government nor any agency thereof, nor any of their employees, makes any warranty, express or implied, or assumes any legal liability or responsibility for the accuracy, completeness, or usefulness of any information, apparatus, product, or process disclosed, or represents that its use would not infringe privately owned rights. Reference herein to any specific commercial product, process, or service by trade name, trademark, manufacturer, or otherwise does not necessarily constitute or imply its endorsement, recommendation, or favoring by the United States Government or any agency thereof. The views and opinions of authors expressed herein do not necessarily state or reflect those of the United States Government or any agency thereof. Reference herein to any social initiative (including but not limited to Diversity, Equity, and Inclusion (DEI); Community Benefits Plans (CBP); Justice 40; etc.) is made by the Author independent of any current requirement by the United States Government and does not constitute or imply endorsement, recommendation, or support by the United States Government or any agency thereof.

Savannah River National Laboratory®

A U.S. DEPARTMENT OF ENERGY NATIONAL LAB • SAVANNAH RIVER SITE • AIKEN, SC • USA

Slow Strain Rate Testing of A537 Tank Wall Material

Chris Rasmussen

Bruce Wiersma

Max Neveau

October 2025

SRNL-STI-2025-00337, Revision 0

DISCLAIMER

This work was prepared under an agreement with and funded by the U.S. Government. Neither the U.S. Government or its employees, nor any of its contractors, subcontractors or their employees, makes any express or implied:

- warranty or assumes any legal liability for the accuracy, completeness, or for the use or results of such use of any information, product, or process disclosed; or
- representation that such use or results of such use would not infringe privately owned rights; or
- endorsement or recommendation of any specifically identified commercial product, process, or service.

Any views and opinions of authors expressed in this work do not necessarily state or reflect those of the United States Government, or its contractors, or subcontractors.

Printed in the United States of America

Prepared for
U.S. Department of Energy

SRNL-STI-2025-00337
Revision 0

Keywords: Stress Corrosion Cracking, Corrosion Control, Waste Tanks

Retention: Permanent

Tracking Number: 10562

Slow Strain Rate Testing of A537 Tank Wall Material

Chris Rasmussen

Bruce Wiersma

Max Neveau

October 2025

Savannah River National Laboratory is operated by Battelle Savannah River Alliance for the U.S. Department of Energy under Contract No. 89303321CEM000080

Reviews and Approvals

AUTHORS:

Chris Rasmussen, Materials Science and Disposition, Senior Engineer Date

Bruce Wiersma, Materials Science and Disposition, Advisory Engineer Date

Max Neveau, Materials Science and Disposition, Engineer Date

TECHNICAL REVIEWERS:

Roderick Fuentes, Materials Science and Disposition, Senior Engineer Date

APPROVAL:

Morgan Whiteside, Materials Science and Disposition, Manager Date

Keisha Martin, SRMC, Safety Programs and Regulatory, Technical Reviewer Date

Logan Ballard, SRMC, Safety Programs and Regulatory, Manager Date

Acknowledgements

The authors gratefully acknowledge the assistance of Maxwell Alderman in conducting the tests. The authors also appreciated feedback and recommendations from Dr. Roderick Fuentes on the set-up of the potentiostat and electrochemical cell for the load frame.

Executive Summary

At Savannah River Site (SRS), High-Level Waste is stored in below-grade carbon steel tanks. This waste in part consists of sludge, salt cake, and/or supernate. Preparation of this waste for future processing involves dissolution of the salt cake layer. The salt dissolution process can create conditions that leave the carbon steel tanks susceptible to localized corrosion. The salt to be dissolved contains high concentrations of nitrate, that once released, create an environment that may be conducive to pitting corrosion and/or stress corrosion cracking (SCC) of carbon steel.

The salt dissolution process also liberates interstitial liquid trapped between the salt crystals. This liquid is initially high in nitrite and hydroxide concentration. High pH and greater ratios of nitrite to nitrate act as inhibitors to minimize corrosion of carbon steel in high nitrate environments. However, as dissolution proceeds, the concentration of nitrate will increase, while the hydroxide and nitrite concentration of the interstitial liquid will deplete and become insufficient to prevent the onset of corrosion attack. Tank blending and the addition of inhibitors are used to ensure adequate concentrations of hydroxide and nitrite. However, this is not desirable during salt dissolution as it can reduce process efficiency and increase the amount of waste that needs processing.

This testing program was designed to examine the risk of SCC associated with utilizing the pitting factor (PF) and nitrite/nitrate (NO_2^-/NO_3^-) ratio limits for handling dissolved salt solutions at an elevated temperature in the carbon steel waste tanks. The previously identified limits are a PF of 1.2 and an NO_2^-/NO_3^- ratio of 0.15. The results indicate that as long as the NO_2^-/NO_3^- ratio exceeds 0.1 and the PF is above approximately 0.8, there is a discernible safety margin between the open circuit potential (OCP) and the critical cracking potential (CCP) observed during applied potential testing. However, this margin, defined by the difference between the OCP and CCP, is relatively narrow, ranging from 0.1 to 0.25 volts. This small margin raises concerns about potential shifts in OCP during waste retrieval operations, which could inadvertently increase the risk of SCC if the OCP approaches or exceeds the CCP. These results confirm that dissolved salt solutions provide a potent chemistry that, under certain conditions, makes carbon steel susceptible to SCC.

The next question to consider is the influence these results have on decisions for storage and retrieval of waste from the tanks. For Type III/IIIA waste tanks, the risk of SCC remains very low. First, and most importantly, the post-weld stress relief of the tanks has reduced the residual stress near the welds. Thus, without the stress component, SCC risk is minimized. The material of construction (A537 Carbon steel) for the Type III/IIIA tanks is superior to the steel in its resistance to SCC than the steel that was utilized for the Type I, II, and IV tanks (A285 carbon steel). From a chemistry control standpoint for a Type III/IIIA tank directly involved with handling dissolved salt solutions, the PF and NO_2^-/NO_3^- ratio limits may be utilized wherein chemistry control provides an extra layer of defense against SCC. Chemistry control for a Type III/IIIA tank minimizes the risk for a tank that may receive the dissolved salt solution, particularly if that tank is a Type I, II, or IV waste tank.

On the other hand, if the dissolved salt solution is handled by a Type I, II, or IV waste tank the risk of SCC is real. The potent chemistry, absence of stress relief, and inferior material result in a condition that is conducive to cracking. Efforts should be made to either avoid transferring

waste that may not meet the PF and NO_2^-/NO_3^- ratio criteria to one of these tanks or if it is unavoidable, take measures to minimize the consequences of a leak. As shown by these tests, even if the PF and NO_2^-/NO_3^- ratio criteria are met, there is a risk that the tank potential may be disturbed in the positive direction and the risk of SCC increase.

The following recommendations are made if the tank farm operator desires to investigate the risk of SCC to the tanks further.

1. Perform additional SSRT to further define the CCP for the PF and NO_2^-/NO_3^- ratio. These tests confirmed that dissolved salt solutions are potent SCC contributors. A larger matrix of simulant chemistry and applied potentials would further define the critical potential.
2. Rather than applying a potential, during the test add oxidizing species to the simulant and perform the same tests. This approach would determine which species could influence the tank potential and how much of that species is necessary to increase the tank potential above the CCP. If a species is discovered limits on this species could be developed.
3. Perform long-term OCP measurements to determine if the potential has stabilized after 24 hours at a value below the CCP. An envelope of dissolved salt solution chemistry would be investigated.
4. Perform electrochemical polarization studies in the tank simulants to define the range of the passive region or if there is an active-passive transition that may indicate susceptibility to SCC. An envelope of dissolved salt solution chemistry would be investigated.

Finally, if the tank farm facility desires more information on the SCC susceptibility of an actual tank, consideration should be given to the installation of a reference electrode to measure the actual tank potential. This tank potential may be compared with the CCP. Tank potential monitoring is currently performed for the Hanford tanks and has been done periodically in the SRS waste tanks. However, risk for SCC at the anticipated storage and retrieval conditions, the materials of construction, tank fabrication procedures, and expected service life should be considered prior to installation of a reference electrode.

Table of Contents

List of Tables

List of Figures

List of Abbreviations

A537	A537 Low-carbon steel
ASTM	American Society for Testing and Materials
CCP	Critical Cracking Potential
CMTR	Certified Mill Test Report
CPP	Cyclic potentiodynamic polarization
LW	Liquid Waste
M	Molar
OCP	Open circuit potential
Pa	Pascal
PF	Pitting factor
SCC	Stress corrosion cracking
SCE	Saturated calomel electrode
SEM	Scanning Electron Microscope
SRMC	Savannah River Mission Completion
SRNL	Savannah River National Laboratory
SRS	Savannah River Site
SSRT	Slow strain rate testing
TTQAP	Task Technical and Quality Assurance Plan
TTR	Task Technical Request
UTS	Ultimate Tensile Strength
V	Volt

1.0 Introduction

At Savannah River Site (SRS), High-Level Waste is stored in below-grade tanks constructed of carbon steel. This waste is composed of sludge, salt cake, and/or supernate. Waste retrieval of the salt cake crystals, which are composed of soluble sodium salts with a highly alkaline interstitial liquid involves water additions to dissolve the crystals [1]. The salt dissolution process may create waste solutions that are corrosive towards the carbon steel. The salt cake contains high concentrations of nitrate, that once released, create an environment that may be conducive to pitting corrosion and/or stress corrosion cracking (SCC) of carbon steel. Recently, SRS has adopted the Pitting Factor approach for mitigation of pitting during salt dissolution [2]. A program was undertaken to assess if this approach will be effective if the dissolved salt solutions are at higher temperatures (e.g., 75 °C) [3].

A review was performed to provide background on the SCC mechanism, the occurrence of SCC in the SRS waste tanks, and the testing that was performed to provide the inhibitor limits for the waste tank to mitigate this mechanism. The next sections of this report contain the review to help develop the basis for the tests performed in this program.

1.1 Background on SCC Mechanism

Stress corrosion cracking occurs in many metals and alloys due to the synergistic action of corrosion and stress. Neither significant corrosion nor stress alone would cause structural failure, but together they can. Figure 1-1 schematically shows the processes involved. Carbon steels are susceptible to SCC in nitrate solutions as well as in caustic solutions and several other environments [4]. The precise mechanism of this form of failure is not universally agreed upon, but it is related to the observation that in a crack, the chemistry of the solution can be very different from that in the bulk solution. The most generally accepted mechanism is the stress maintains a crevice in which the solution at the crack tip is aggressive towards the metal [5]. A characteristic of nitrate SCC is that it is intergranular, that is, the grain boundaries of the metal are preferentially attacked (Figure 1-2).

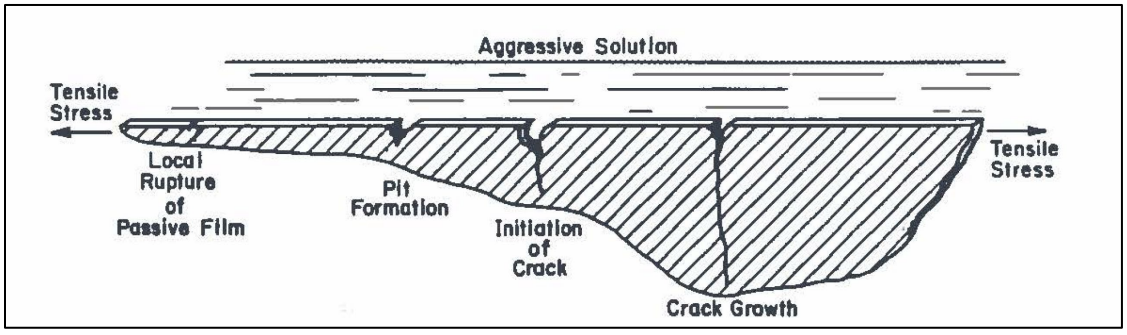

Figure 1-1 Illustration of the conditions necessary for a crack to initiate and propagate through a metal [5]

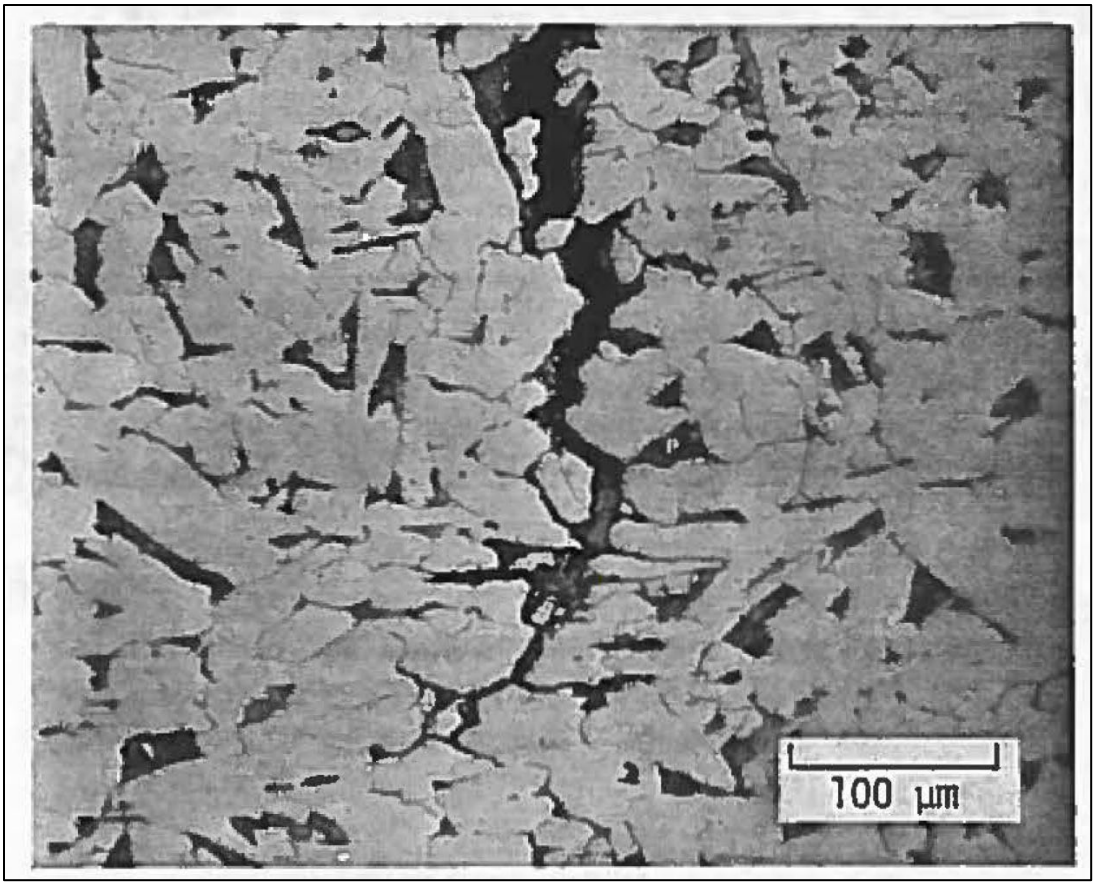

Figure 1-2 Intergranular stress corrosion cracking in carbon steel [6].

Corrosion of a metal requires transfer of electrons between the anodic (oxidation) and cathodic (reduction) sites. The OCP is the equilibrium potential at no current and indicates its initial tendency for corrosion. However, applying potential and determining the resulting current density of a specimen in solution provides information about the system's tendency to corrode or passivate. Polarization curves, current density versus potential, for actual waste versus simulants, demonstrate this information (Figure 1-3)[5]. The low current density in the region between 0 and 0.3 V vs. saturated calomel electrode (SCE) indicates a passive system with low corrosion rates. On the other hand,between -0.2 and 0 V vs. SCE, the current goes through a maximum, a behavior that is consistent with active corrosion (i.e., a high corrosion rate). An active-passive transition, as demonstrated here, is characteristic of a system that is susceptible to SCC.

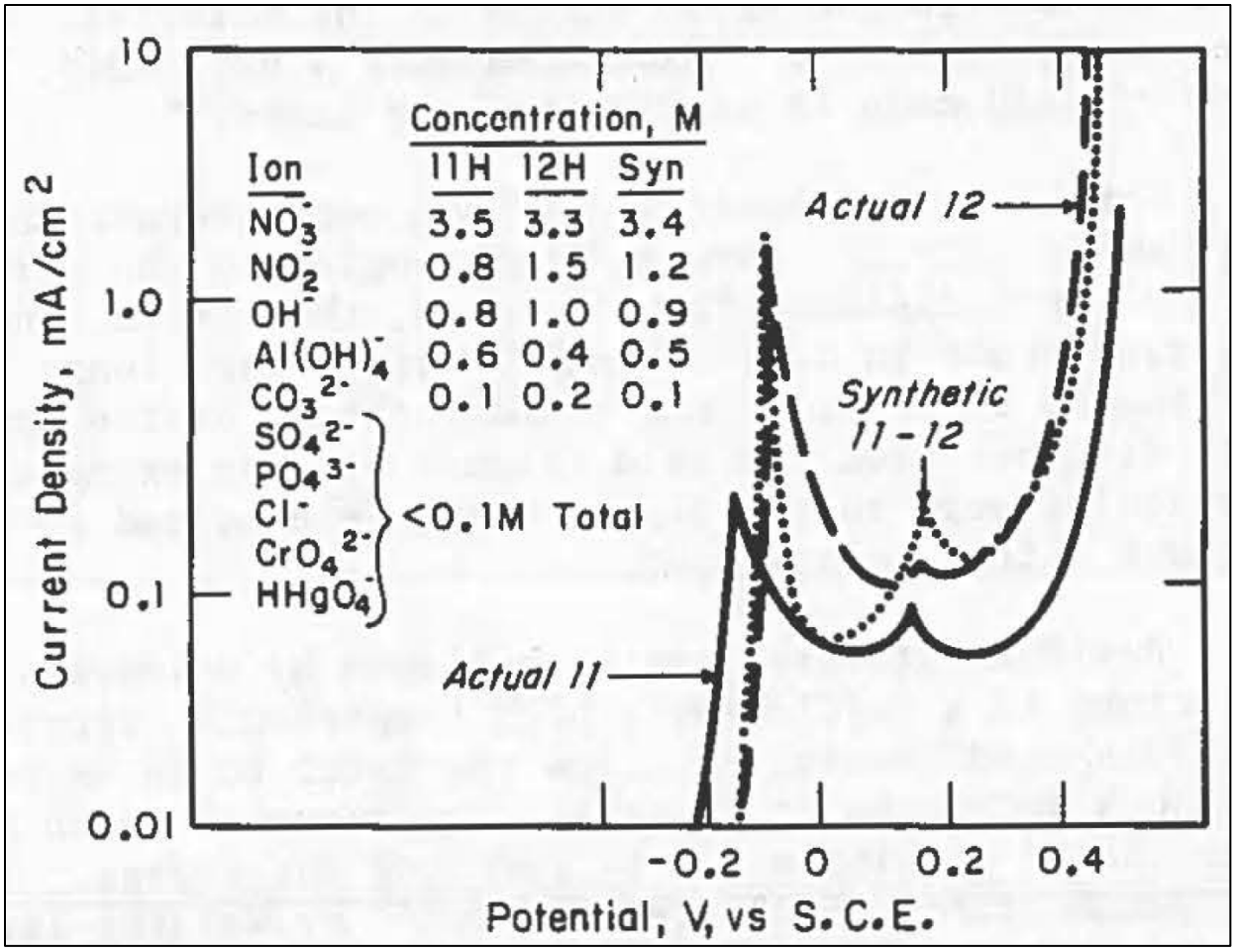

Figure 1-3 Polarization curve for carbon steel in a nitrate containing waste [5].

Besides an aggressive environment, the other necessary condition is the presence of tensile stresses in the metal. In the waste tanks, the highest stresses are near welds, which are referred to as residual stress. These stresses can exceed the yield stress of the material; however, they are typically short-range (~ 3 inches on either side of the weld). Residual stress can be relieved by uniformly heating the structure to a sufficiently high temperature (approximately 1100 °F in mild steels). Such heat treatment should also reduce the risk of SCC [7]. The Type III/IIIA tanks received heat treatment, while the Type I, II, and IV tanks did not[8].

Stress-corrosion cracking has been the principal degradation mechanism for the primary liner in waste storage tanks that have not been post-weld stress-relieved. These tanks were constructed in the 1950s and are referred to as non-compliant. Eight Type I waste tanks and all four Type II waste tanks have developed through-wall leak sites. Leaks developed in tanks 9H, 10H, 14H and 16H within less than two years after being placed in service [9].

Much of what is known with regard to flaws in waste tanks at SRS was learned in conjunction with the leakage incident in Tank 16H, a Type II tank, that occurred in the early 1960s [10]. Data on flaw characteristics was gathered through visual inspections of the tank, destructive examination of a tank sample and laboratory testing on welded plates. Type I tanks also contain

similar flaws, which is not unexpected given that they were constructed of the same materials, were not post-weld heat treated, and were exposed to similar waste chemistry.

Two disks, each 5-5/8 inches in diameter, were extracted from the wall of Tank 16 in 1965 [11]. The disks were extracted from the horizontal weld between the upper knuckle and the upper primary shell plate and both contained leak sites. The steel at this site had been exposed to radioactive waste for approximately 7 months. Metallographic examination revealed three cracks on one of the samples, with two of the cracks being through-wall. The cracks were intergranular and essentially perpendicular to the horizontal weld (Figure 1-4).

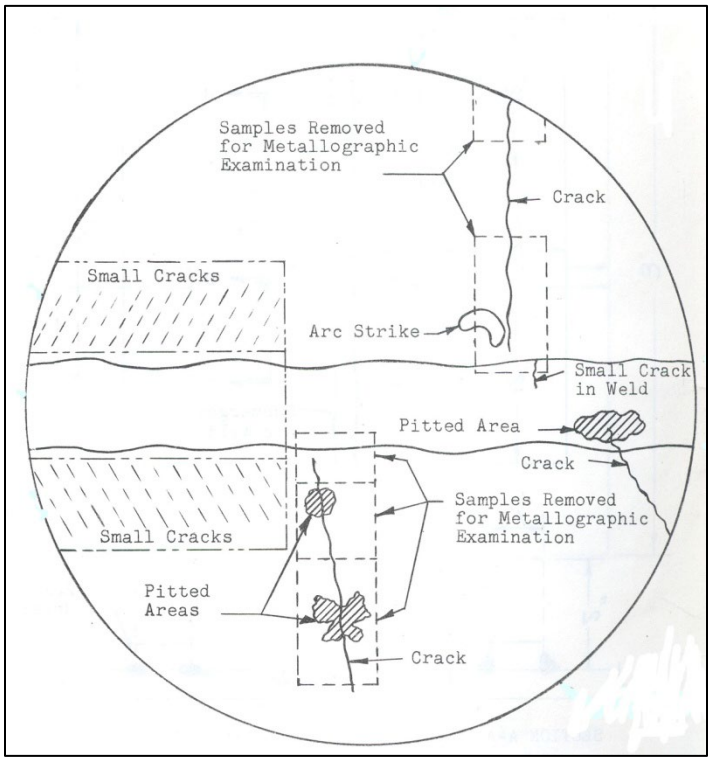

Figure 1-4 Drawing of interior surface of sample removed from Tank 16H [11]

The microstructure of the sample was consistent with the theory that the presence of grain boundary carbides in low carbon steel increases the tendency towards intergranular cracking (Figure 1-5). These carbides would be re-dissolved due to the welding process, and hence not present in the weld or immediately adjacent to the weld. This observation would explain why the two major cracks did not propagate into the weld and the numerous surface cracks did not extend into the narrow zone immediately adjacent to the weld.

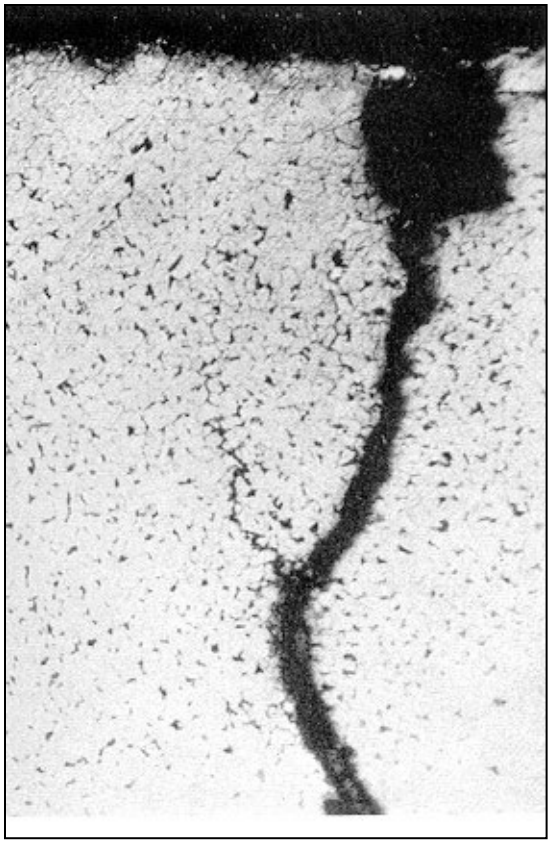

Figure 1-5 Shallow cracks on interior surface of Tank 16 sample [11]

The flaw lengths were also determined. In June 1962, the vertical weld in the upper primary shell beneath an inspection port was sandblasted and then inspected with dye penetrant[12]. Ten large cracks were visible without magnification. The cracks were essentially perpendicular to the weld bead (Figure 1-6). Four of the cracks were estimated to be between 4 to 6 inches long.

Experimental programs were initiated to examine mitigation of SCC in the tanks with cracks and to prevent cracks from initiating in newly constructed tanks [6]. For the latter, post-weld stress relief operations were employed for the new tanks. This step eliminated residual stresses near welds, which provided the driving force for cracking. Mitigation of existing cracks, and prevention of the initiation of new cracks, in the tanks that were not stress-relieved required modification of the chemistry controls that were in place. One of the experimental techniques that was utilized to investigate the necessary inhibitor concentration for SCC was the slow strain rate testing (SSRT) [6]. A review of how this test was utilized and how it may be utilized in this program is presented in the next section.

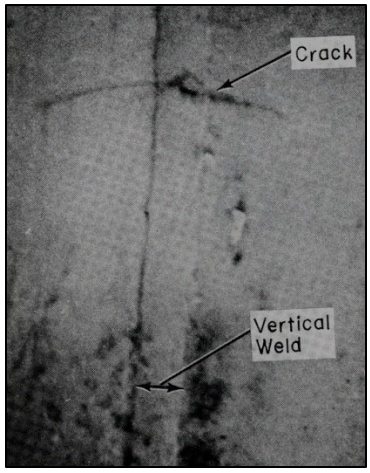

Figure 1-6 Dye-penetrant testing of stress corrosion crack on vertical weld in Tank 16 [12].

1.2 Use of the Slow Strain Rate Test in Literature and at SRS

The SSRT is an accelerated test that was developed to predict SCC susceptibility for a given material in an environment of interest [13], SSRT is performed per ASTM G129-21 [14]. The test involves a slow (compared to conventional tensile tests) dynamic strain applied at a constant extension rate (e.g., 10^{-6} inch/sec). SSRTs are typically run until total failure of the specimen, which typically take days or weeks depending on the extension rate selected. After failure, the test specimen is examined for SCC and the mechanical properties measured during the test (e.g., elongation, ultimate strength, cross-sectional area) are compared to similar data for an inert environment (e.g., air, mineral oil, etc.). SSRT has been the primary test method for defining SCC inhibitor requirements at the Savannah River Site and Hanford [15].

Important parameters for the test are the strain rate and the electrode potential. In some situations, there is a range of strain rates above and below which there is reduced or no susceptibility to SCC. That is, there are zones for the strain rate where susceptibility is detected. For carbon steel materials, a strain rate of 10^{-6} sec^{-1} has typically been satisfactory for demonstrating SCC susceptibility [16].

The test specimen electrode potential during an SSRT can greatly influence SCC susceptibility. In many situations, the OCP is often close to but not quite inside zones of maximum SCC susceptibility [17, 18]. The critical cracking potential (CCP), the minimum potential that is necessary to induce SCC, appears to be a complex function of waste composition and temperature. Early investigations indicated that increasing potentials, either from applied potential or through the use of redox species, such as $KMnO_4$, increased cracking susceptibility, although in the case of applied potentials, there appears to be a critical range of potentials [19]. Parkins et. al., noted that nitrate induced SCC occurs most readily in the potential range from -0.3 V to 1.1 V vs. SCE [20].

Gui, et. al. evaluated the effects of NO_2^-/NO_3^- ratio, pH and the applied potential on SCC of carbon steel in a Hanford waste simulant. They showed that for a simulant with a NO_2^-/NO_3^- ratio of 0.32, pH 11, and temperature of 50 °C, SCC did not occur at potentials more negative than -0.1 V vs. SCE [21]. Concurrently, Beavers et. al. showed that SCC generally did not

occur below -0.27 V vs. SCE for various NO_2^-/NO_3^- ratios and in most cases SCC occurred above -0.1 V vs. SCE (Figure 1-7) [22]. Mickalonis investigated the effect of applied potential for waste simulants with high nitrate concentrations (5.5 M to 9.7 M), high temperatures (50 to 95 °C), and low NO_2^-/NO_3^- ratios (0 – 0.09) [17, 23]. His investigation also showed that SCC susceptibility initiated at an applied potential of -0.1 V vs. Ag/AgCl (-0.144 V vs. SCE). Thus, CCPs in these nitrate rich waste simulants seem to initiate above this value if the waste is susceptible to SCC. Mickalonis also performed companion tests at the OCP. He noted that the OCP for these waste simulants ranged between -0.4 to -0.2 V vs. Ag/AgCl (-0.444 to -0.244 V vs. SCE). Additionally, SCC susceptibility was not observed at the OCP. Boerstler, in earlier tests for this program, also observed similar OCPs and critical cracking potentials [24]. Similar observations on SCC susceptibility at the OCP were also indicated.

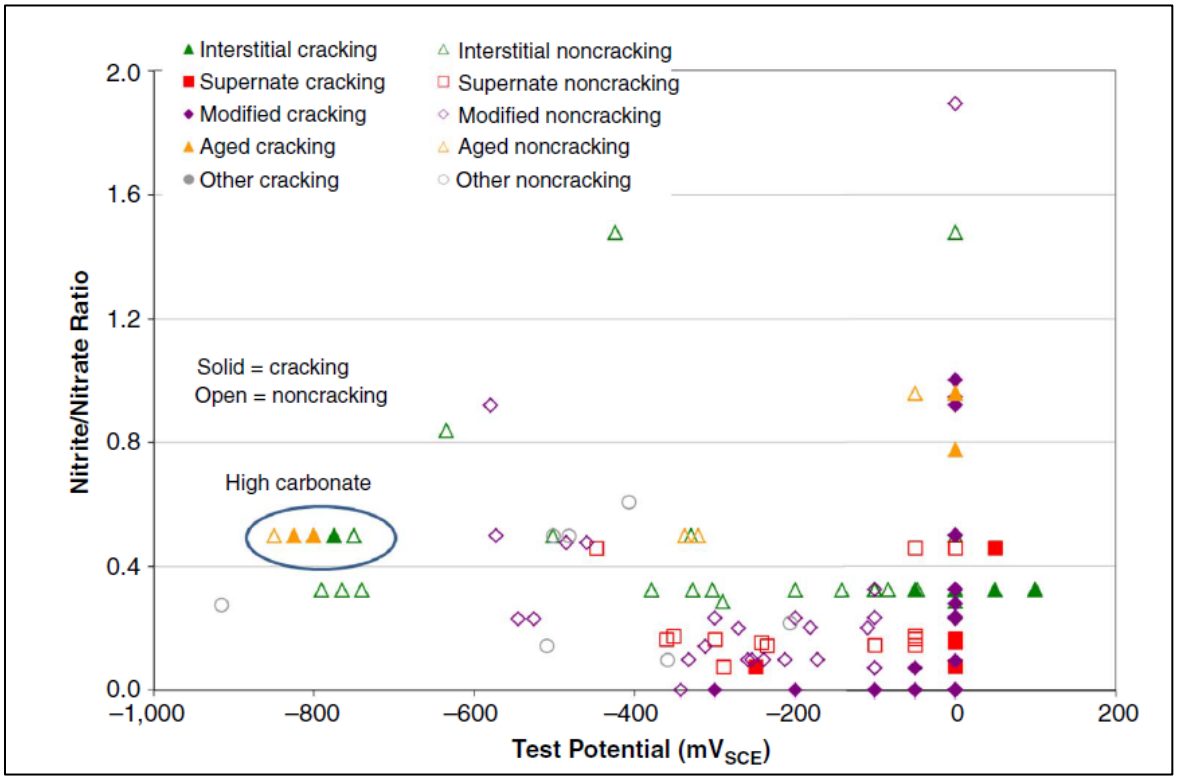

Figure 1-7 Relationship between NO2-/NO3- ratio, applied potential, and susceptibility for SCC as determined by SSRTs in waste simulant at 50 °C and 77 °C [21, 22]

1.3 Historical Open Circuit Potential in Lab and in Field

The waste tanks in the field are not at an applied potential, but rather at the OCP. A connection between the potentials measured in the laboratory and that of the actual tanks is needed. The fundamental basis for predicting long-term performance using the tank OCP is illustrated schematically in Figure 1-8 [25]. The onset of SCC occurs when the OCP exceeds the CCP for SCC in the same tank waste. Furthermore, the onset of localized corrosion (e.g., pitting) may also occur once the OCP exceeds the repassivation potential (E_{rp}). The E_{rp} is the potential

below which a pit passivates and cease to grow. This approach ignores the gestation time for initiation and stable growth of SCC and localized corrosion, and thus is a conservative estimate for the occurrence of these failure mode. Although not directly correlated with the tank, if the OCP in a laboratory simulant exceeded the CCP or the E_{rp} the risk of susceptibility would be greater.

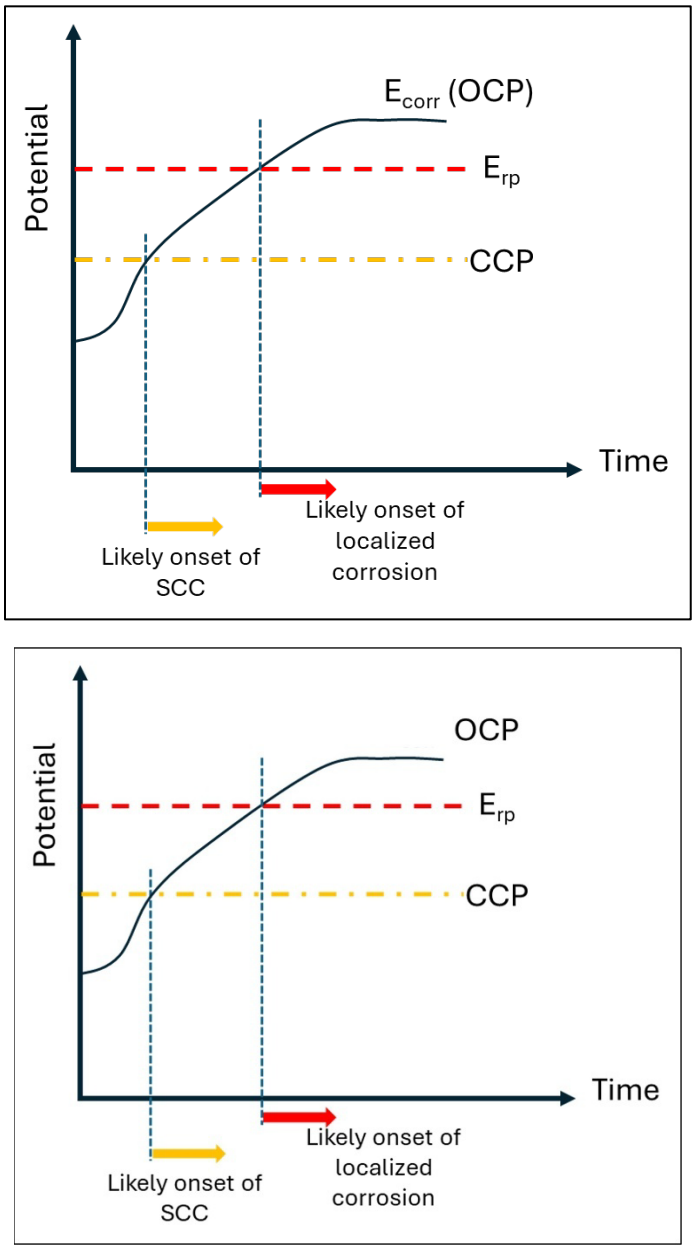

Figure 1-8. Schematic illustration of conditions for the onset of localized corrosion and SCC and their use in tank integrity prediction [25]

Long-term laboratory tests were conducted with carbon steel in several waste simulants to measure the evolution of the OCP with time [19]. Figure 1-9 shows that the OCP increases considerably, sometimes as much as 0.4 V before achieving a plateau. The increase in potential

indicates an enhancement of the oxide film on the surface in terms of thickness, chemistry or electronic properties. In a waste tank, the potential may also increase due to a change in the oxide film at the metal surface or the presence of an oxidizing species in the waste.

Counts et. al., observed similar OCP behavior in high nitrate concentration solutions with a plateau value of between -0.30 to -0.240 V vs. SCE (Figure 1-10) after 7 months of exposure [26]. Although not a robust data set, tank potentials have been taken periodically throughout the service life of several double shell tanks at Hanford [27]. In general, for concentrated nitrate wastes, the long-term tank potential is less than -0.2 V vs. SCE. This coincides well with the laboratory measurements of the OCP. These long-term OCP values, along with the 24-hour OCP values measured during the tests will be utilized to assess the conservatism of the inhibitor requirements.

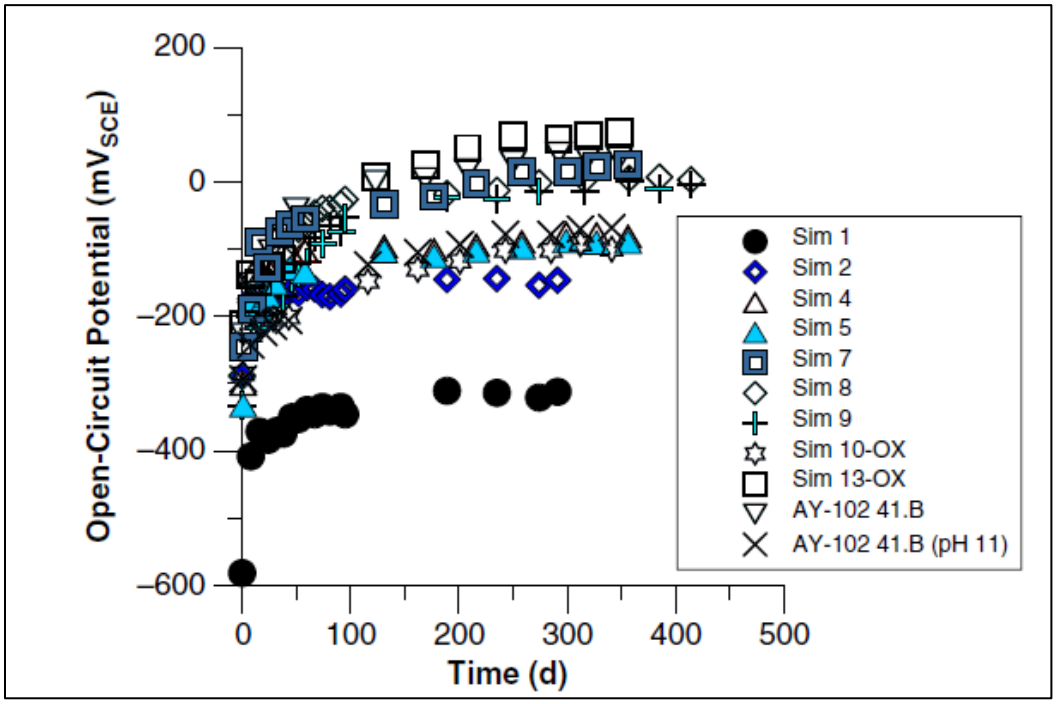

Figure 1-9 Evolution of OCP with time for several nitrate-nitrite waste simulants [19]

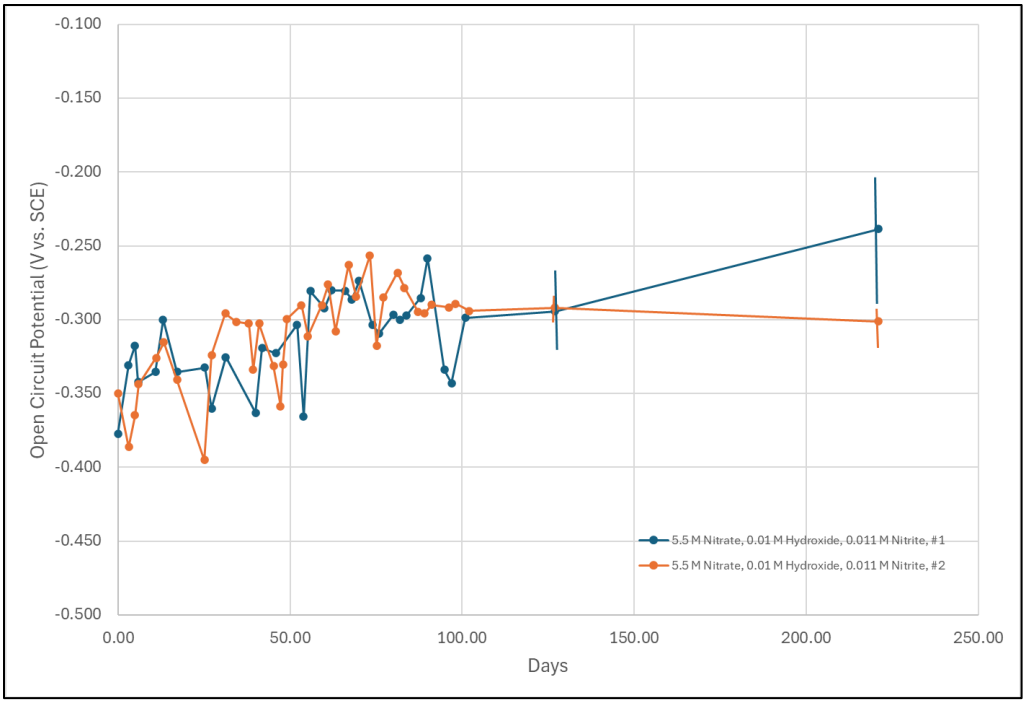

Figure 1-10 OCP data in 5.5 M nitrate salt simulants at 50 °C. Data taken during the first 100 days are shown to demonstrate increase in potential with time. After 100 days, the potential begins to stabilize. Data were averaged and the standard deviation is shown by the error bars [26].

1.4 Background on Corrosion Control Program for SCC

Controls for supernate waste chemistry were instituted in the late 1970's to preclude the initiation and propagation of SCC in tanks constructed from A285 Grade B carbon steel [5]. The controls were in response to the observations of through-wall cracks, and subsequent waste leakage, from the Type I and II waste tanks. The basis for these chemistry controls were electrochemically controlled (i.e., either applied current or applied potential) SSRTs. The first series of tests investigated an envelope of anticipated nitrate, nitrite, and hydroxide concentrations and temperature that would be expected for the waste tanks during interim storage of fresh waste from the canyons. In this case, current SSRTs were performed. Table 1-1 shows the corrosion control requirements adopted based on the results.

Table 1-1 Corrosion control requirements [5]

Required Minimum OH^- and NO_2^- Concentrations in SRP Wastes

Concentration, M		
NO_3^-	OH^-	$OH^- + NO_2^-$
3-5.5	0.3	1.2
1-3	0.1 [NO_3]	0.4 [NO_3]
<1	0.01	-

During the 1980s retrieval of salt cake waste was initiated from these original tanks. Sample data obtained during retrieval indicated that the nitrate concentration exceeded the maximum nitrate concentration (i.e., 5.5 M) tested previously [28]. Applied potential SSRT were performed on A285 carbon steel to extend the maximum nitrate concentration up to 8.5 M [29]. Since salt dissolution operations were typically at low temperatures, the testing covered a range up to 75 °C. Table 1-2 shows the chemistry controls that were added [30].

Table 1-2 Chemistry controls [30]

Applicability	Limit	Parameter	Minimum Needed	Units
$5.5M < [NO_3^-] \leq 8.5M$	1	$[OH^-]$	0.6	Molar
		$[OH^-] + [NO_2^-]$	1.1	Molar
$2.75M < [NO_3^-] \leq 5.5M$	2	$[OH^-]$	0.3	Molar
		$[OH^-] + [NO_2^-]$	1.1	Molar
$1.0M \leq [NO_3^-] \leq 2.75M$	3	$[OH^-]$	$0.1[NO_3^-]$	Molar
		$[OH^-] + [NO_2^-]$	$0.4[NO_3^-]$	Molar

It should be noted that although testing was performed on A285 carbon steel, the chemistry controls were also applied to the new tanks (referred to as the Type III and IIIA tanks) that were constructed of A516 and A537 carbon steel. Testing showed that in general that these latter two materials had superior SCC resistance as compared to A285 carbon steel [31]. Furthermore, these new tanks received a post-weld stress relief procedure that mitigated the residual stresses near welds (i.e., the largest tensile stress in the tank). The combination of stress relief and chemistry controls result in a low probability of failure due to SCC for the Type III and IIIA tanks. Similar chemistry controls were implemented at Hanford [32].

In the mid-1990s waste removal personnel calculated that the expected temperature during salt removal may be as high as 90 °C due to heat dissipated by the use of slurry pumps [33]. Solubility testing was performed to determine the maximum nitrate concentration at a temperature of 95 °C [34]. A maximum nitrate concentration of 9.7 M was determined, which exceeded the nitrate concentration range specified in the corrosion control program. A test program was conducted to investigate whether the current SRS requirements at the time were adequate [17, 23]. The compositional and temperature range for the tests is shown in Table 1-3 below. Many of these simulants have nitrite and hydroxide concentrations (i.e., inhibitor species) that were at the boundary of the limits at that time. Two series of SSRTs were undertaken to investigate: 1) OCP, and 2) applied potential. The OCP tests showed that the initial 30-minute OCP for these simulants is between -0.4 to -0.2 V vs. Ag/AgCl (-0.444 to -0.244 V vs. SCE) Secondly, neither A285 nor A537 carbon steel were susceptible to SCC at the OCP. On the contrary, severe cracking of these grades of carbon steel was observed at applied potentials. The range of potentials where cracking was first observed was -0.1 to 0.0 V vs. Ag/AgCl. Given the margin between the 30-minute OCP and the CCP, it was determined that no changes in the inhibitor level were warranted.

Table 1-3 Simulant concentrations for potential controlled SSRT in 1997 [17, 23]

	Constituent Concentrations (M)			
Solution	Nitrate	Hydroxide	Nitrite	Temperature (C)
A	5.5	0.6	0.5	95
A2	5.5	1.2	0.5	95
A3	5.5	2.0	0.5	95
F	8.7	0.6	0.5	75
G	8.7	1.0	0.5	75
J	9.7	0.6	0.5	95
K	9.7	1.0	0.5	95
W	6.0	0.1	0.0	50

In 2009, SSRTs were performed to determine if the inhibitor concentrations required in Table 1-2 could be reduced [35]. Tests were conducted with A537 carbon steel at 50 °C, with a nitrate concentration of 7 M, hydroxide concentrations between 0.01 M and 0.6 M, and nitrite concentrations between 0.01 and 0.2 M. Tests were performed at the OCP and at applied potentials. No susceptibility to SCC was observed at the OCP even at the lowest inhibitor concentration. However, at applied potentials approximately -0.15 to -0.3 V vs. SCE greater than OCP, SCC was observed. Thus, lowering the chemistry control standards was not pursued at the time. It is important to note that the acceptance criteria for SSRT did not include consideration of the difference between the CCP and the OCP at that time.

In 2010, the Hanford tank farm facility reviewed the conservatism that was inherent in the chemistry control program for their waste tanks. Stock et.al. evaluated more than 400 SSRT tests performed on carbon steel in simulated waste tank environments found in the DOE complex [15]. The data investigated were taken at the OCP. The following changes were made to the chemistry control program at Hanford. The maximum storage temperature that the limits applied to was 50 °C. The decrease in the temperature limit reflected the lower waste temperatures and that a decrease in temperature reduces the risk of SCC for carbon steel. The minimum nitrite concentration was increased from 0.011 M to 0.05 M. An increase in the minimum concentration was necessary to mitigate SCC susceptibility in dilute solutions. A new specification regarding the NO_2^-/NO_3^- ratio was added. Examination of the test results revealed that no test solutions with a NO_2^-/NO_3^- ratio greater than 0.08 cracked within the boundaries of the new specifications. The new chemistry specification for mitigation of the SCC mechanism set this parameter conservatively at 0.15. Finally, the adoption of the specifications for the absolute and relative compositions of nitrite ions enabled relaxation of the hydroxide ion concentration to pH 11. These changes are summarized in Table 1-4 below. The OCP was not specifically included in the specifications. However, the Hanford tank farm monitors the potential in several tanks that contain nitrate bearing waste [27]. In each case the tank potential was well below the CCP (i.e., a low propensity for SCC). It was, however, acknowledged that neither actual tank potentials with wastes at temperatures greater than 50 °C, nor the CCP at these conditions was known.

Table 1-4 Chemistry Control Requirements for the Prevention of SCC in Hanford Double Shell Tanks [15].

DST Specification Criteria For Waste At ≤ 50 °C	Limit
Maximum Temperature	50 °C
Maximum Concentration of Nitrate Ion	6.0 M
Maximum Concentration of Hydroxide Ion	6.0 M
Minimum pH	11
Minimum Concentration of Nitrite Ion	0.05 M
Minimum Nitrite Ion/Nitrate Ion Ratio	0.15

Pitting corrosion is also a concern for the waste tanks [30]. Chemistry control limits for pitting have been in place at SRS since the early 1990s, however, Hanford had not implemented similar controls for waste in their tank farm facility, particularly with respect to the halide ions, chloride and fluoride. In 2019, Wiersma et.al., performed corrosion testing that defined a limit known as the pitting factor (PF) that provided chemistry control for pitting corrosion [36]. The limits are shown in Table 1-5 below and include the anions that are a part of the PF calculation. The NO_2^-/NO_3^- ratio was maintained as a limit for SCC mitigation, while the absolute concentration for nitrite was increased to 0.2 M to prevent pitting corrosion. The 75 °C temperature limit was valid for pitting corrosion and several SSRT tests at OCP also validated its effectiveness for SCC mitigation at the higher temperature. However, no testing was performed to assess the CCP at the higher temperatures.

Table 1-5 Chemistry Control Limits for Pitting and SCC in the Hanford Double Shell Tanks [31].

Quantity	Minimum	Maximum
Temperature, °C		75
Hydroxide, M	0.01	6.0
Nitrite, M	0.20	
Nitrate, M		5.5
Nitrite/Nitrate Ratio	0.15	
Pitting Factor	1.2	

Boerstler in 2021 [24] and 2023 [37], adapted the PF approach to the SRS tank farm chemistry envelope. The testing performed evaluated the effect of higher sulfate concentrations (up to 0.6 M), dissolved salt solution compositions (e.g., Hydroxide > 4 M), and lower chloride concentrations (less than 0.1 M). These tests showed that the PF may be utilized for corrosion control of pitting corrosion up to temperatures of 75 °C. No significant effect of sulfate concentration up to 0.6 M was observed. The approach has been subsequently applied during retrieval operations [2]. A question still remained as to whether the NO_2^-/NO_3^- ratio was adequate to mitigate SCC at temperatures up to 75 °C.

Boerstler in 2021 began to investigate this question by performing SSRT tests on both A285 carbon steel and A537 carbon steel [24]. The test matrix, which shows the key constituents of the test simulants, and the PF, is shown below in Table 1-6. The tests were performed at 75 °C. The ranges for PF and NO_2^-/NO_3^- ratio were 0.55-2.88 and 0.0025-0.3, respectively. The tests were predominantly performed at the OCP. In all cases, the tests performed at the OCP did not show any indications of SCC. However, 2 of the 3 tests performed at an applied potential of approximately -0.1 V vs. SCE exhibited SCC. In the cases that exhibited SCC, the PF was less than 0.86 and the NO_2^-/NO_3^- ratio was 0.0025. For the case where no SCC was observed, the PF was 2.88 and the NO_2^-/NO_3^- ratio was 0.3. While the information from these tests was informative, they did not fully investigate SCC mitigation at the boundaries of the NO_2^-/NO_3^- ratio and PF limits.

Table 1-6 Test matrix for 2021 SSRT tests in dissolved salt solutions [24]

Trial	Nitrate [M]	Hydroxide [M]	Nitrite [M]	Sulfate [M]	Chloride [M]	Pitting Factor
2	4	0.6	0.01	0.3	0.1	0.86
5	4	0.6	0.01	0	0.1	0.86
9	5.5	0.6	0.01	0	0	0.88
10	5.5	0.6	0.5	0	0	1.02
11	4	0.6	0.5	0.3	0	1.40
16	2.75	0.3	0.6	0.1	0.2	0.55
17	0.94	1.2	0.2	0.01	0.24	2.02
34	5.5	0.3	0.6	0.3	0	0.61
35	1	0.3	0.3	0.3	0	2.88

Figure 1-11 and Figure 1-12 were designed to illustrate the results of these tests and current gaps in the data near the boundaries of the NO_2^-/NO_3^- ratio and PF limits. The concentration ranges considered were nitrate greater than 3.5 M, nitrite from 0.01 to 3.5 M, and hydroxide from 0.001 to 0.6 M. The temperatures ranged from 50 to 95°C. In Figure 1-11, the area shaded in red shows the boundary for the NO_2^-/NO_3^- ratio as a function of the potential. The various SSRTs described previously are plotted in the figure with closed symbols representing SCC susceptibility and open symbols representing no SCC susceptibility. Also shown, is the typical range for the OCP for this composition and temperature range. This illustrates the margin between the OCP and the CCP. A difference of greater than 0.2 V between a 24-hour OCP measurement and the CCP has been defined as an indication of relatively low susceptibility to SCC. As shown in the figure, below a NO_2^-/NO_3^- ratio of 0.08, the difference between the 24-hour OCP and the CCP appears to be less than 0.2 V, while there is some indication that above a NO_2^-/NO_3^- ratio of 0.15 the difference may be greater than 0.2 V. However, the dashed oval shape in the figure that outlines the NO_2^-/NO_3^- ratio of 0.15 indicates a gap in the data. Data showing no susceptibility in the range of the OCP exist, however, CCP data are absent at these NO_2^-/NO_3^- ratios (0.08-0.15).

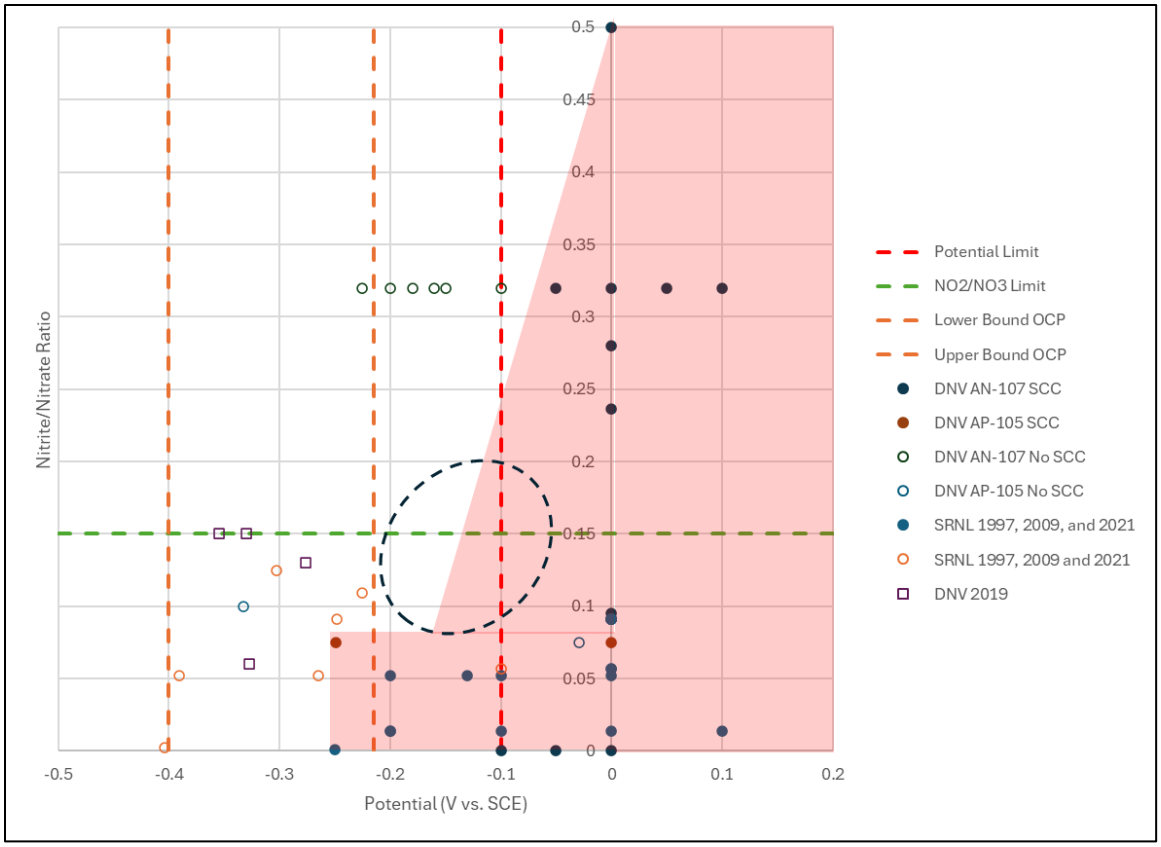

Figure 1-11 Graph showing Potential vs Nitrate/Nitrite ratio for historical SSRT. An estimate of the critical cracking potential of -0.1 V is shown. The historical OCP range for dissolved salt solutions is also shown [17, 18, 21, 23, 24, 37].

In Figure 1-12, the area shaded in red shows the boundary for the PF as a function of the potential. The various SSRTs described previously are plotted in the figure with closed symbols representing SCC susceptibility and open symbols representing no SCC susceptibility. Also shown, is the typical range for the OCP for this composition and temperature range. This illustrates the margin between the OCP and the CCP. A difference of greater than 0.2 V between a 24-hour OCP measurement and the CCP has been defined as an indication of relatively low susceptibility to SCC. As shown in the figure, below a PF of 0.9, the difference between the 24-hour OCP and the CCP appears to be less than 0.2 V, while there is some indication that above a PF of 1 the difference may be greater than 0.2 V. However, the dashed circle shape in the figure that outlines the PF of 1.2 indicates a gap in the data. Data showing no susceptibility in the range of the OCP exist, however, CCP data are absent at these PF (0.9-1.5).

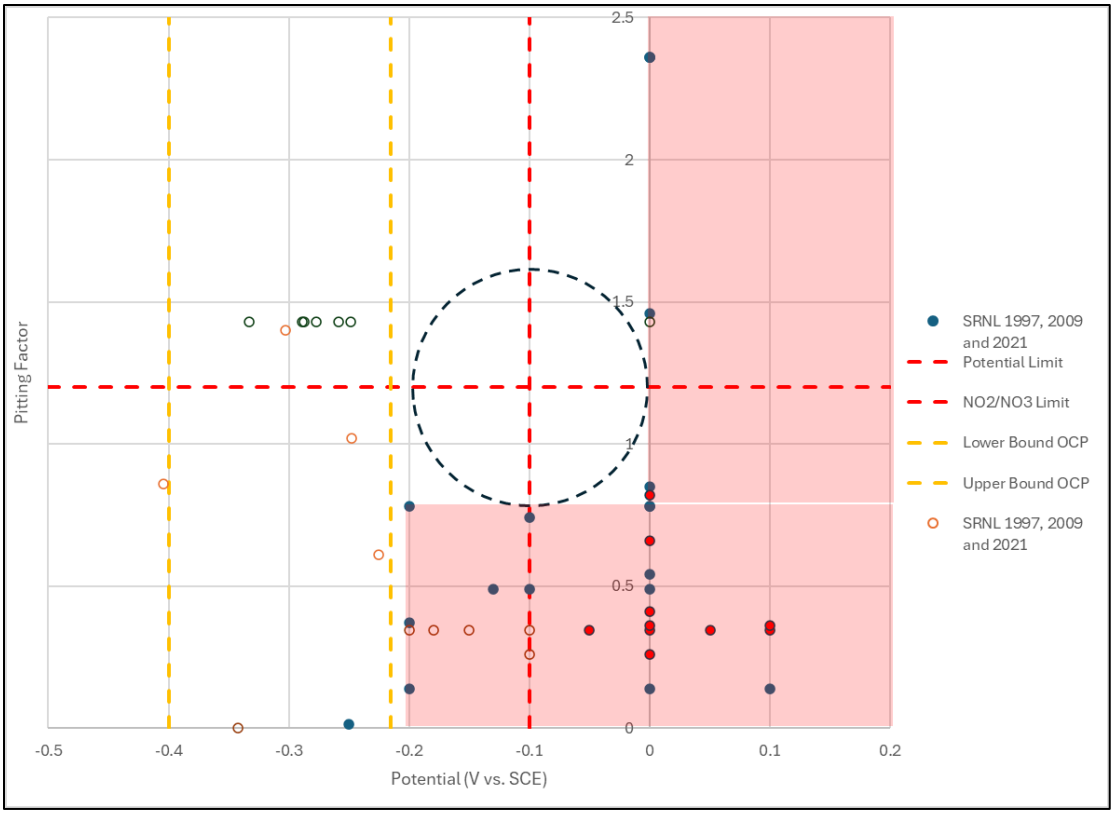

Figure 1-12 Graph showing Potential vs Pitting Factor for historical SSRT. An estimate of the CCP of -0.1 V is shown. The historical OCP range for dissolved salt solutions is also shown [17, 18, 21, 23, 24, 37].

The objective for these tests was threefold:

1. *Determine if the PF and NO_2^-/NO_3^- ratio limits as currently expressed mitigate SCC at 75 °C.* Figures 1-8 and 1-9 indicate that there is a region near the chemistry limit border that needs to be examined more closely to determine the effectiveness of these limits for SCC. Note that the testing may show that the PF and NO_2^-/NO_3^- ratio are restricted due to mitigation of pitting corrosion (e.g., PF is lower for SCC mitigation than for pitting mitigation).
2. *Using applied potential tests, assess the margin for these limits.* Tests were performed to determine the CCP for a given environment. For the first criteria, if the CCP is 0.2 V more positive than the 24-hour OCP, this indicates that the propensity for SCC is low. This assertion was tested by comparing long-term laboratory OCP data with the CCP. Although comparison with actual tank potential data would be preferable, this approach provides some assurances of being able to predict SCC propensity.
3. *Make recommendations for retrieval operations at the high temperature limits.* Based on the results of SSRT testing, the current limits for waste chemistry were assessed and recommendations for revisions to the Corrosion Control Program Description Document (PDD were considered.

2.0 Experimental

2.1 Materials Utilized

Round tensile test bars per ASTM E8 [38] were fabricated out of A537 [39] material and used for SSRT per ASTM G129 [14]. Table 2-1 and Table 2-2 highlight the chemical composition and mechanical properties of A537 for heat number AH730 with comparison to the ASTM A537 requirements.

Table 2-1 Composition of A537

Element	wt% for AH370	ASTM A537 Requirement
C	0.14	0.24 max
Mn	1.38	1.00-1.60
P	0.013	0.025 max
S	0.005	0.025 max
Si	0.288	0.15-0.50
Cu	0.022	0.35 max
Ni	0.01	0.25 max
Cr	0.09	0.25 max
Mo	0.056	0.08 max
V	0.001	-
Ti	0.002	-
Al	0.03	-
B	0.0002	-
Nb	0.032	-
N	0.006	-
Sn	0.005	-
Fe	balance	-

Table 2-2 Material Properties of A537

	Yield Strength (MPa)	Tensile Strength (MPa)	Elongation %
AH370	319	529	30.6
ASTM A537 Requirement	310	450	22

One A537 sample was sectioned, mounted, ground and polished and is shown in the as polished condition for Inclusion Rating (Figure 2-1). Inclusions were rated per ASTM E45-25

[40] as Type D Globular inclusions severity level 2.5. The mounted sample was then etched using 10% Nital to reveal a mostly ferritic microstructure with bands of pearlite (Figure 2-2).

Elemental analysis using EDS was performed to confirm the major constituents in the steel. As shown in Figure 2-3 the major peak of iron and minor peaks of silicon, manganese and carbon consistent with an A537 alloy.

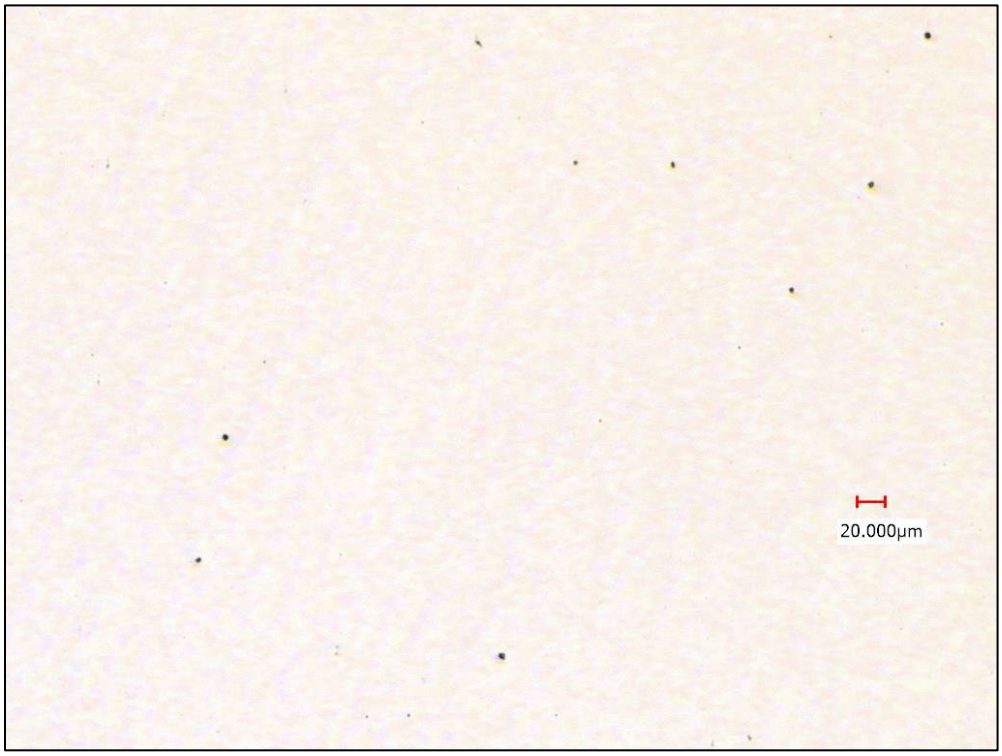

Figure 2-1 As polished A537 Sample

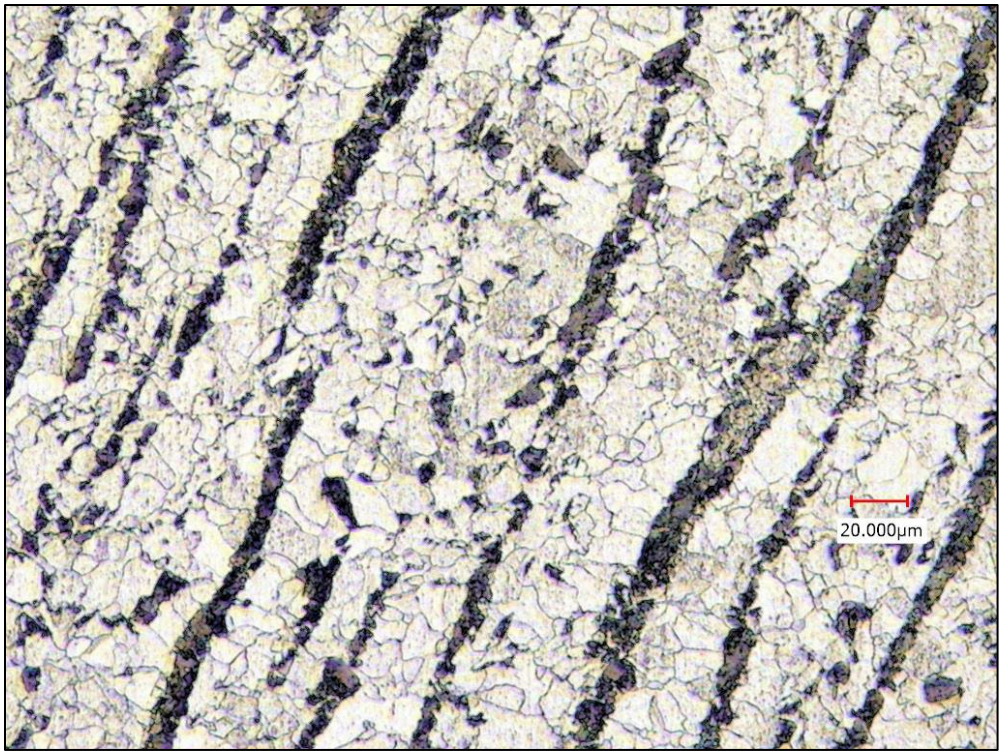

Figure 2-2 As etched (10% Nital) A537 Sample

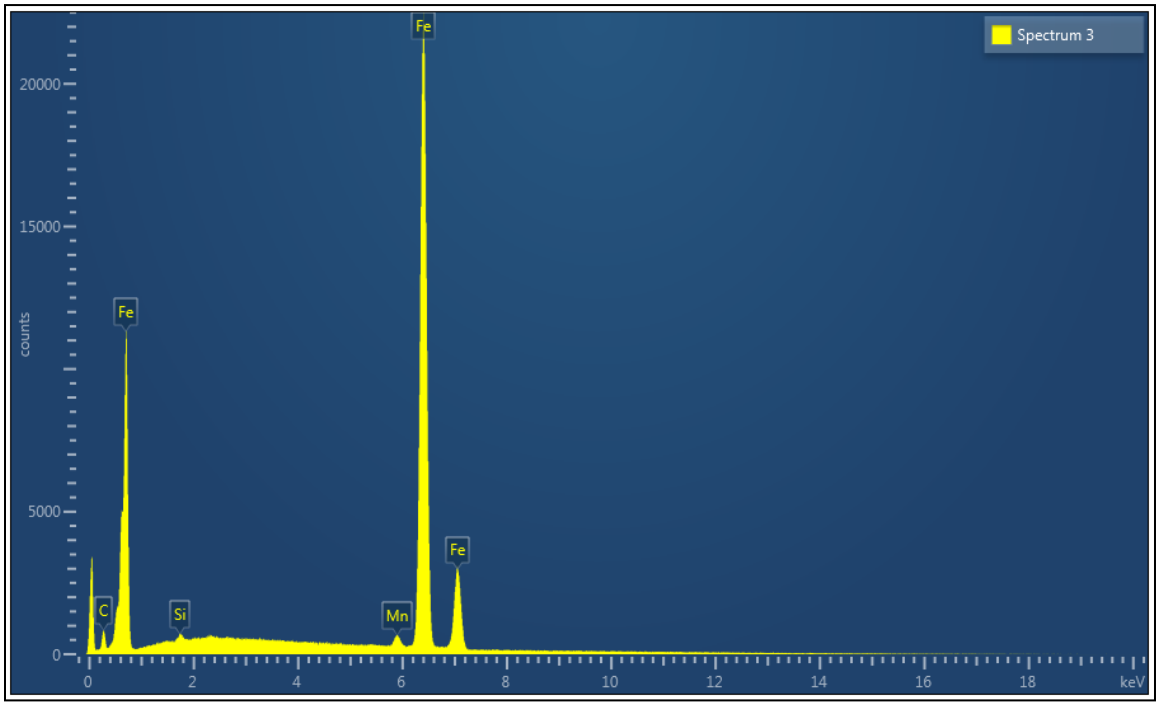

Figure 2-3 A537 EDS elemental analysis

The tensile bar samples that were used for the SSRT were measured prior to testing (See Table 2-3), The measurements confirmed that the specifications required by the purchase order were met. Knowing the gage length of the sample allows for calculation of the strain that occurs during the test. Knowing the diameter of the diameter of the sample allows for calculation of the stress that occurs during the test. The Trial names for each sample follow the nomenclature of "Simulant" letter (A through J), "Simulant Run" (number) and "Sample ID" (A through Z).

Table 2-3 Dimensions of A537 test samples

Simulant	Trial	Gage Length (mm)	Dia 1 (mm)	Dia 2 (mm)	Dia 3 (mm)	Dia Ave (mm)
A	A4Q	27.44	6.38	6.37	6.38	6.38
	A5R	27.32	6.36	6.37	6.37	6.37
B	B1K	27.37	6.38	6.38	6.41	6.39
C	C1L	27.50	6.39	6.41	6.39	6.40
D	D1M	27.11	6.38	6.42	6.39	6.40
	D2W	27.04	6.33	6.37	6.39	6.36
	D3T	27.19	6.33	6.34	6.37	6.35
E	E1J	27.20	6.39	6.39	6.37	6.38
	E2S	27.07	6.34	6.36	6.36	6.35
F	F1D	26.72	6.38	6.39	6.35	6.37
	F3B	27.11	6.30	6.34	6.29	6.31
G	G1N	27.40	6.38	6.39	6.39	6.39
	G2U	27.19	6.39	6.40	6.40	6.40
	G3Z	27.00	6.41	6.39	6.41	6.40
H	H2H	27.13	6.31	6.29	6.33	6.31
I	I1P	27.43	6.35	6.35	6.37	6.36
J	J1F	27.02	6.33	6.35	6.33	6.34
	J2I	27.69	6.35	6.37	6.32	6.35
	J3V	27.09	6.38	6.38	6.41	6.39
Mineral Oil	-	26.72	6.38	6.34	6.35	6.36

Dia - Diameter

2.2 Test Simulants

Table 2-4 shows the 10 simulant compositions that were utilized in this test program. Eight of the 10 simulants had high nitrate concentrations (i.e., greater than 4 M) which is typical of dissolved salt solutions. The PF and NO_2^-/NO_3^- ratios were chosen to examine the data gaps shown in Figure 1-11 and Figure 1-12. Two tests (B and F) were performed to verify the efficacy of PF and NO_2^-/NO_3^- ratio limits at low nitrate concentrations (i.e., less than or equal to 1 M).

For reference, Equation 1 for the PF is:

$$Pitting\ Factor = \frac{8.06 * [Hydroxide] + 1.55 * [Nitrite]}{[Nitrate] + 16.7 * [Chloride] + 5.7 * [Fluoride]} \quad 1$$

Table 2-4 Simulant Compositions

Simulant	Nitrate [M]	Hydroxide [M]	Nitrite [M]	Chloride [M]	NO_2/NO_3	Pitting Factor
A	4	0.6	0.5	0	0.125	1.403
B	0.94	1.2	0.2	0.24	0.2128	2.017
C	5.5	0.6	0.5	0	0.0909	1.02
D	5.5	0.67	0.825	0	0.15	1.214
E	5.5	0.53	0.825	0	0.15	1.009
F	1	0.1	0.1	0	0.1	0.961
G	5.5	0.72	0.55	0	0.1	1.21
H	5.5	0.4	0.825	0	0.15	0.819
I	4	0.5	0.6	0	0.15	1.24
J	4	0.4	0.6	0	0.15	1.039

2.3 Test Procedure

SSRT was performed at a crosshead speed of 10^{-6} inch/sec until failure [17, 23] according to ASTM G129 on a computer-controlled Instron 8862 load frame (Figure 2-4 and Figure 2-5). A Cortest vessel made of Hastelloy C276 with a glass wall and silicone heat tape plugged into a temperature controller to maintain the set temperature of 75 °C for all the tests (Figure 2-6). A Gamry Reference 600 Potentiostat was used to monitor and control the potential of the sample (screen shot shown in Figure 2-7).

The vessel was assembled with the desired sample (electrically insulated with silicone), a salt bridge (0.1M sodium nitrate) with a SCE reference electrode, a graphite counter electrode and approximately 250 mL of chosen simulant from Table 2-4 above. The simulant with the tensile specimen present was maintained at a temperature of 75 °C for 24 hours prior to mechanical testing, with the OCP being monitored in some cases during the delay. After the 24-hour delay was completed, tension was applied by manually adjusting the position of the test specimen until a force increase was observed. Once the test preparation was completed, the mechanical test would begin. A constant extension rate of 10^{-6} inch/sec was used. Elongation of the specimen continued until failure occurred (i.e., a fracture of the specimen into two pieces). Position and force were recorded throughout the duration of the mechanical testing. A potentiostat was used to apply a potential to the working electrode, the tensile specimen. The potentiostatic polarization would last for the duration of the tensile test, with potential and

current being measured throughout. At the conclusion of the test, the sample was removed, rinsed and dried. The vessel was cleaned in preparation for the next test.

Figure 2-4 Instron 8862

Figure 2-5 Instron computer screen

Figure 2-6 Test vessel

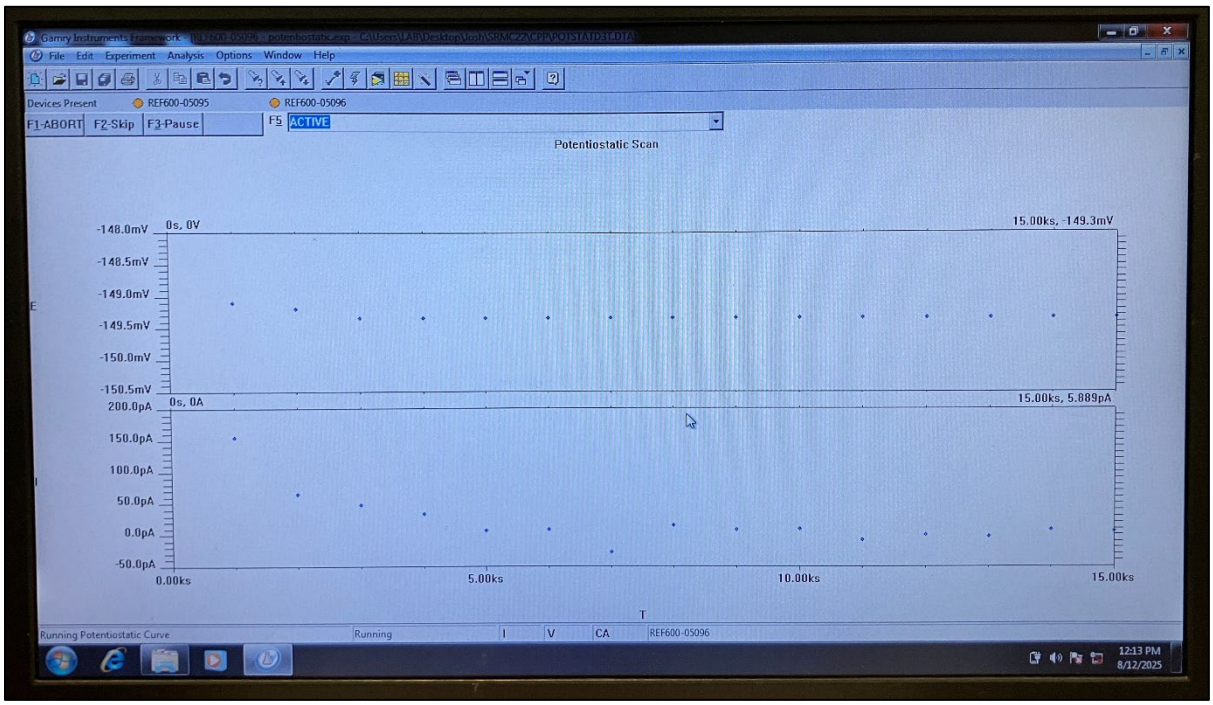

Figure 2-7 Gamry potential data screen

2.4 Stress-Position Curve Data

An example of a stress-position curve is shown in Figure 2-8. This curve was produced from an A537 sample that was exposed to mineral oil, an inert environment, at 75 °C. The extension rate for the sample was the same as for the tests in the various simulants, 10^{-6} inch/sec. The key mechanical property parameters that are evaluated from the curve are the ultimate tensile strength (UTS) and the elongation. The UTS is the maximum stress measured and is the point on the curve where uniform elongation ceases and reduction in the sample area ("necking") initiates. Elongation is a measure of the ductility of the sample and in this case will be determined as the length at which the sample fractures. A reduction of these parameters due to exposure to an aggressive environment is typically related, although not always, to SCC susceptibility. In the example shown in Figure 2-8, the UTS is approximately 500 MPa and the elongation at fracture is approximately 0.38 inches. These values generally correlate with the mechanical property data for the as-received samples and the ASTM requirements for A537 carbon steel (see Table 2-2). The UTS of the material is slightly lower likely due to the higher temperature of the test, which results in decreased atomic bond and increased dislocation mobility. For the same reasons, the material elongation is typically longer at the higher temperature. Stress-position curves from the tests in the simulants will be overlayed upon this stress-position curve in the inert environment to assess SCC susceptibility.

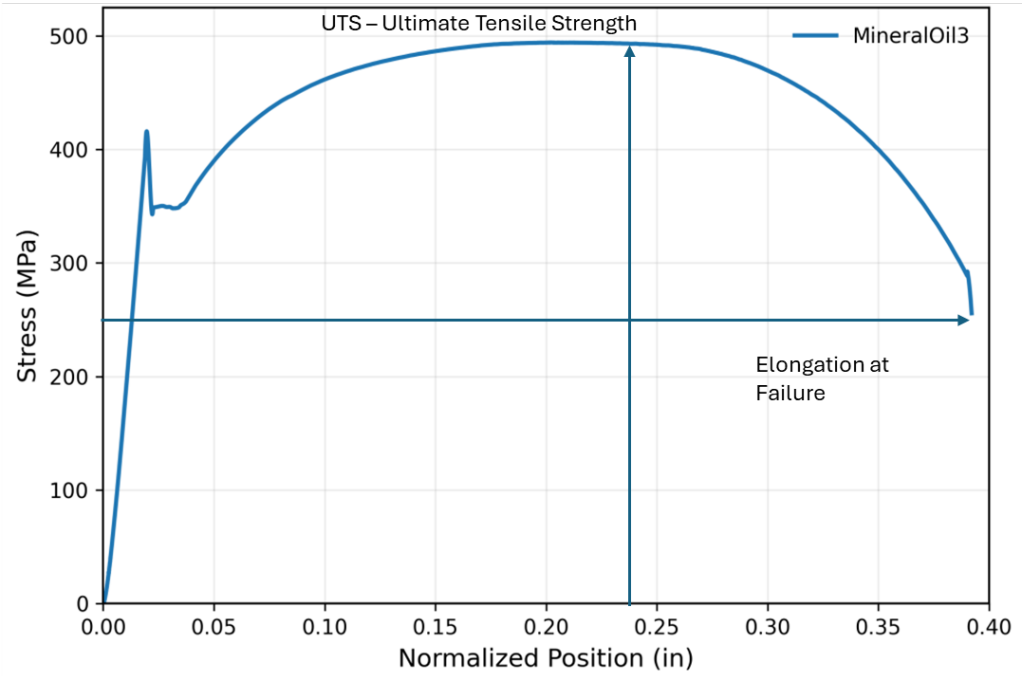

Figure 2-8 UTS of Mineral Oil 3 test (Stress vs. Normalized Position)

2.5 Fracture Surface Evaluation

The fracture surface was evaluated three ways to confirm SCC. First, post-test photographs of the tensile sample were taken (shown in Appendix A.1). A sample that shows little reduction in the sample cross-sectional area and secondary cracking on the gage length is indicative of SCC (see Figure 2-9). In contrast, a sample that shows a significant reduction in area indicates no SCC susceptibility.

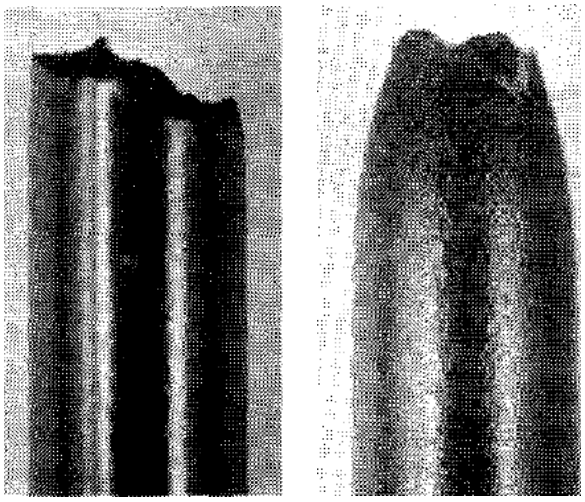

(a) (b)

Figure 2-9 Examples of SSRT fracture surface showing (a) SCC susceptibility and (b) no SCC susceptibility [6]

Secondly, SEM micrographs of the fracture surface as seen from the top view were taken. Examples of ductile and intergranular fractures are shown in Figure 2-10 and Figure 2-11, respectively [41]. The dimpled rupture appearance is characteristic of ductile failure and no SCC. Alternately, grain boundary attack leaves a blocky structure of outlined grain boundaries and occasionally a crack. This appearance is indicative of SCC.

Finally, the tensile bar was sectioned axially to reveal cracks on the side. Serial metallography was performed to reveal the intergranular nature of the cracks. An example of this feature is shown in Figure 3-12.

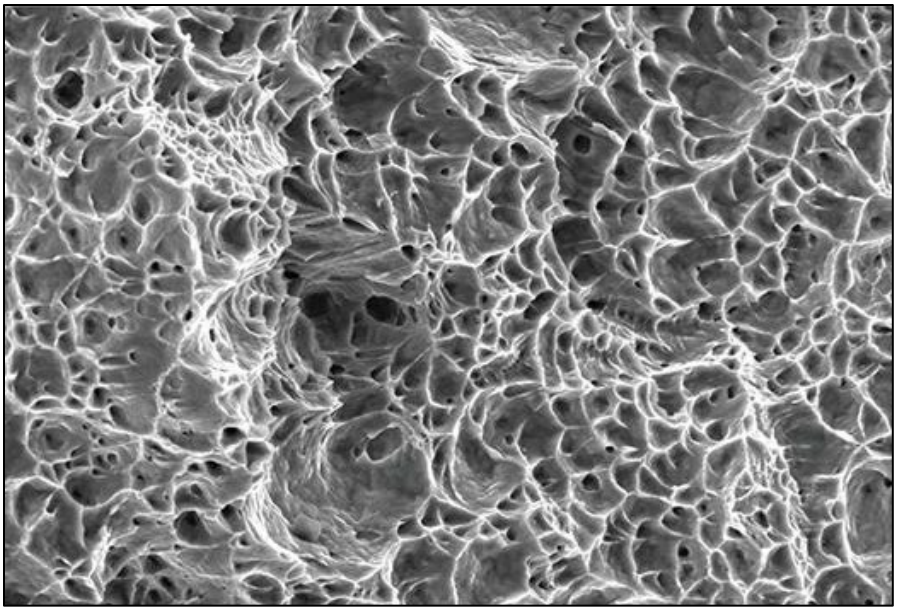

Figure 2-10 Ductile fracture surface example [41]

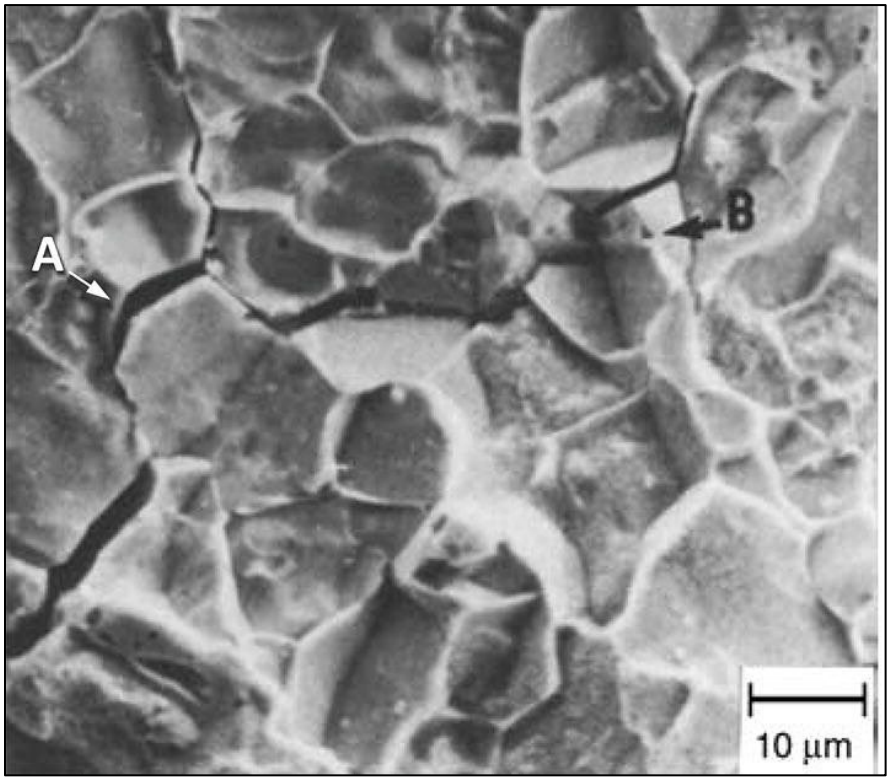

Figure 2-11 SCC fracture surface example [41]

2.6 Electrochemical Measurements

Figure 2-12 illustrates the electrochemical part of the SSRT. The sample was allowed to equilibrate in the simulant for 24 hours before the test was initiated. During that time, the OCP was monitored. The potential frequently increased with time before beginning to plateau and stabilize. After 24 hours, the sample was polarized to a constant potential of -0.1 V vs. SCE. The potential was constant until the sample fractured. If SCC is observed at that potential, the next test was performed at a potential more negative, in this case -0.2 V vs. SCE. If no SCC is observed at this potential, the CCP is between -0.2 V and -0.1 V vs. SCE. To further define the CCP, a test at -0.15 V vs. SCE was performed. If no SCC is observed in this case the CCP is between -0.15 and -0.1 V vs. SCE. On the other hand, if SCC is observed, the CCP is between -0.2 V and -0.15 V vs. SCE. The potential at 24 hours will be compared with the CCP to assess margin on SCC susceptivity.

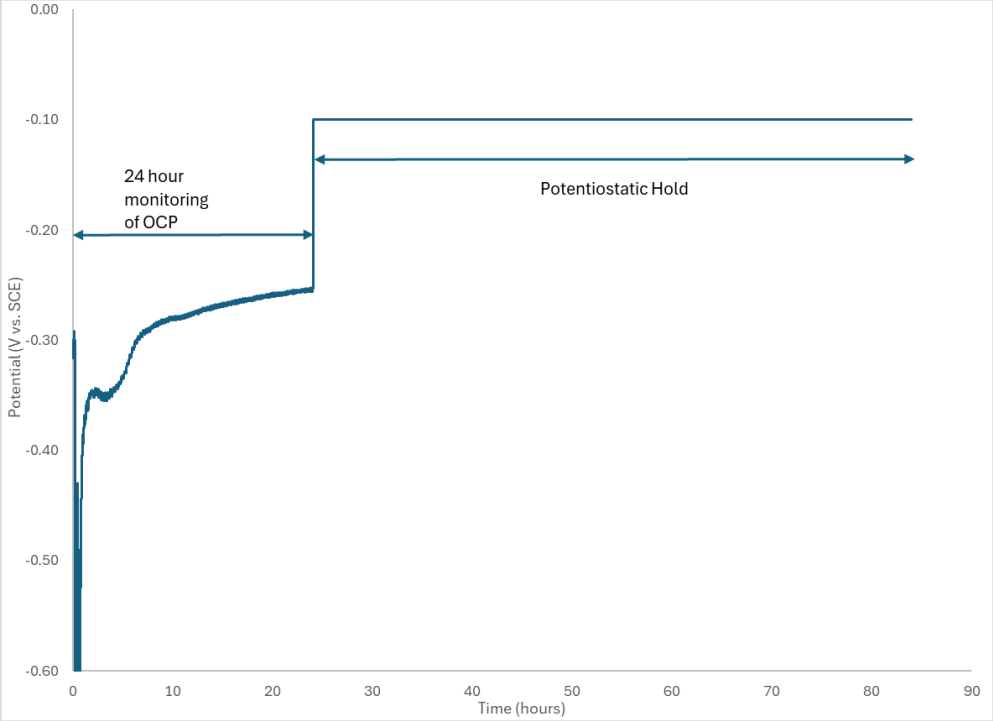

Figure 2-12 The 24-hour OCP and the Potentiostatic Hold are illustrated

2.7 Lab Notebook Information

Requirements for performing reviews of technical reports and the extent of review are established in manual E7 2.60. SRNL documents the extent and type of review using the SRNL Technical Report Design Checklist contained in WSRC-IM-2002-00011, Rev. 2 [42]. All work was documented in Electronic Lab Notebook K9637-00509-20.

3.0 Results and Discussion

Three metrics were utilized to confirm or deny SCC susceptibility for the test. First, the stress vs. position plot was made to investigate if there was a reduction in the mechanical properties of the material as a result of exposure to the environment. Secondly, the fracture surface was examined for evidence of intergranular cracking. This evaluation was the most critical as it provides physical evidence for SCC. Finally, an assessment of the difference between the 24-hour OCP and the CCP for each simulant was made.

3.1 Stress-Position Curves

The test results were grouped based on whether a brittle fracture was observed or not. The first comparison is between samples that showed a significant reduction in the UTS, and elongation as compared with the inert environment (see Figure 3-1). All these tests were conducted at -0.1 V vs. SCE. The ratio of the UTS in these environments relative to the UTS inert environment ranged between 0.79-0.95. The elongation ratio ranged between 0.33-0.51. The fracture surface for each sample was examined. In each case SCC was observed and photographs of the attack are shown in Appendix A.1. Thus, even at conditions that meet the PF and NO_2^-/NO_3^- ratio requirements SCC can be observed at applied potentials. Stress Position Curves and Stress Strain Curves for all samples tested are in Appendix A.2.

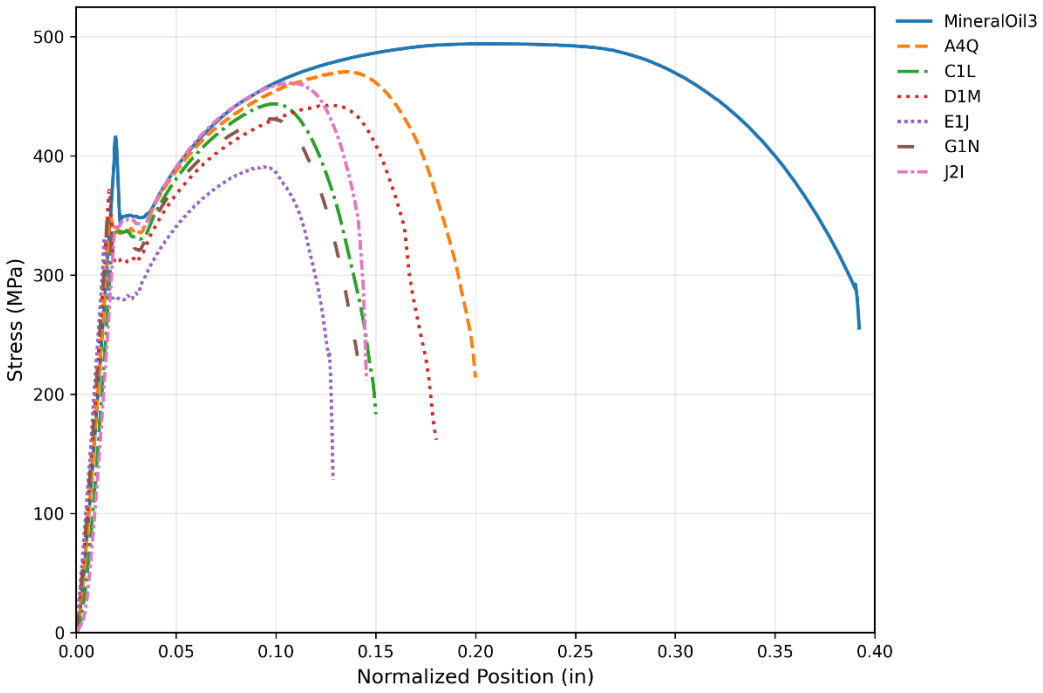

Figure 3-1 Mineral Oil Test vs. select samples with excessive SCC

Another group of tests performed at -0.1 V vs. SCE exhibited a more modest reduction in the ratio parameters (see Figure 3-2). The UTS ratio ranged between 0.97 and 1.01, while the elongation ratio ranged between 0.63-0.86. In fact, the tests in Simulants H and J resulted in curves that were fairly similar to the inert environment. These ratios are significantly higher than what was observed for the other tests at -0.1 V vs. SCE (Figure 3-1). The result in Simulant J (with sample F) was different than what was observed for a duplicate test (with sample I). There was a significant difference in the elongation ratio (Sample I: 0.5 and Sample F: 0.8). Photographs are shown in Appendix A.1. The samples typically exhibited more ductility; however, they did exhibit secondary cracking along the gage length of the sample, which is characteristic of SCC.

These tests were also of interest given that the NO_2^-/NO_3^- ratio was constant at 0.15, while the PF ranged from 0.82 to 1.24. This NO_2^-/NO_3^- ratio is at the boundary of the limits. Thus, the higher NO_2^-/NO_3^- ratio appears to be beneficial. However, there was no correlation with the PF value, as the lowest UTS and elongation ratios (Simulant I) were both in the simulant with the highest PF of the three.

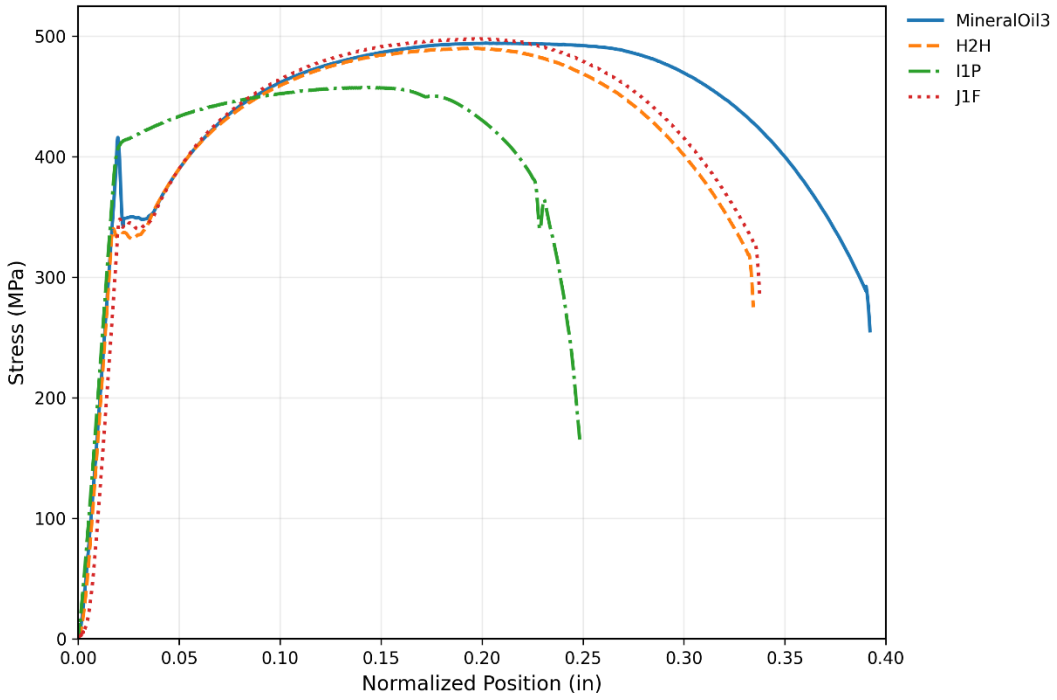

Figure 3-2 Mineral Oil Test vs. select samples with some SCC

The next comparison that was made was between samples that showed a similar UTS, and elongation as compared with the inert environment (see Figure 3-3). All these tests were conducted at -0.2 V vs. SCE. The ratio of the UTS in these environments relative to the UTS inert environment ranged between 0.93-1.00. The elongation ratio was even closer to the inert environment as it ranged between 0.91-0.94. The fracture surface for these samples did not exhibit SCC as observed in the photographs shown in Appendix A.1. Four of the five simulants in this set of tests are at a PF less than 1.2 (E and J) or at a NO_2^-/NO_3^- ratio less than 0.15 (A and G). Given that this behavior suggests that carbon steel is not susceptible to SCC in these environments and that the CCP is greater than -0.2 V vs. SCE at the PF and NO_2^-/NO_3^- ratio limits (see Table 1-5).

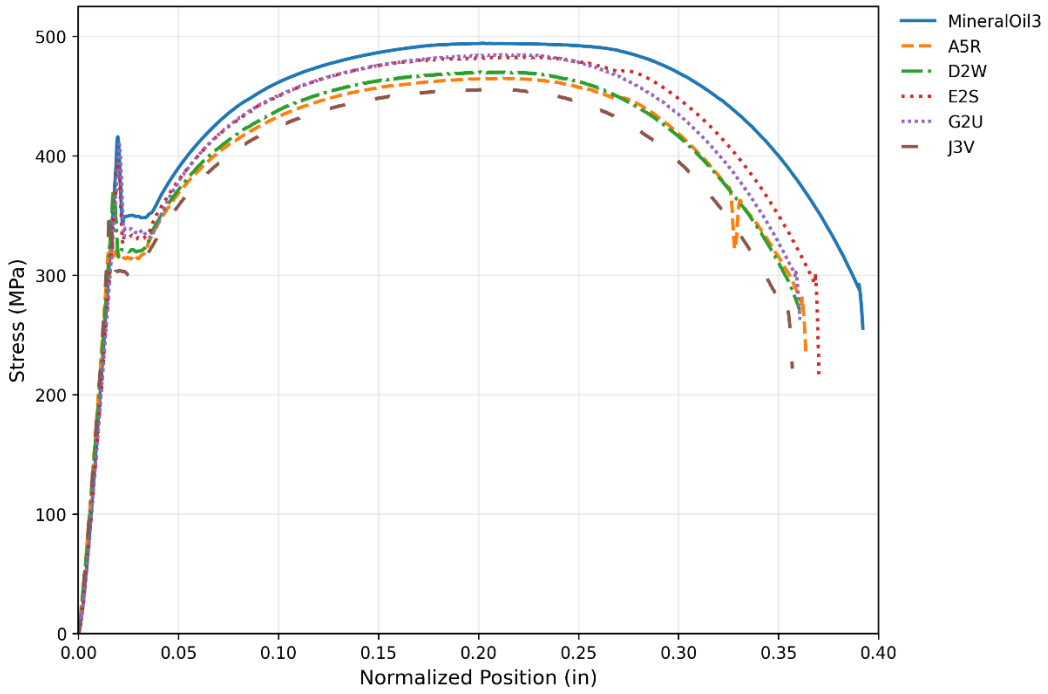

Figure 3-3 Mineral Oil tests vs. select samples that exhibit little to no SSC

In an attempt to further define the CCP, two simulants were chosen for testing at -0.15 V vs. SCE (see Figure 3-4). Both samples had exhibited major cracking at -0.1 V vs. SCE, while they had shown no evidence of cracking at -0.2 V vs. SCE. The ratio of the UTS in these environments relative to the UTS inert environment ranged between 0.87-0.98. The elongation ratio was also close to the inert environment as it ranged between 0.89-0.90. The results are very similar to those observed for the tests performed at -0.2 V vs. SCE (Figure 3-3). The fracture surface for these samples did not exhibit SCC as shown in Appendix A.1. Simulant D meets the PF and NO_2^-/NO_3^- ratio limits, while Simulant G meets the PF requirement only. Thus, it appears that the CCP at the PF and NO_2^-/NO_3^- ratio limits (see Table 1-5) is between -0.1 to -0.15 V vs. SCE .

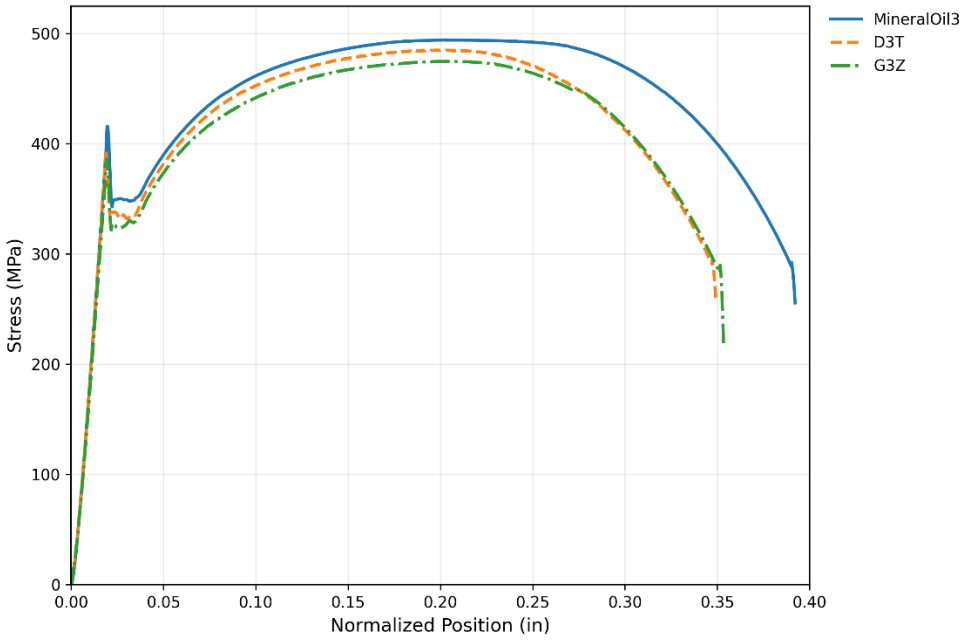

Figure 3-4 Mineral Oil tests vs. select samples with intermediate applied potential of -0.15 V vs. SCE

The effect of applied potential is best illustrated by reviewing the results (see Figure 3-5) from tests in Simulant D that were performed at potentials of -0.2, -0.15, and -0.1 V vs. SCE. Significant reduction in the mechanical property parameters compared with the inert environment was observed at the more positive potential. These results were corroborated by the fracture surface appearance. Simulant D is significant because PF and NO_2^-/NO_3^- ratio are at the limit values. The same results were observed for tests at the same potentials in Simulant G. Simulant G however, has a low NO_2^-/NO_3^- ratio (i.e., 0.1).

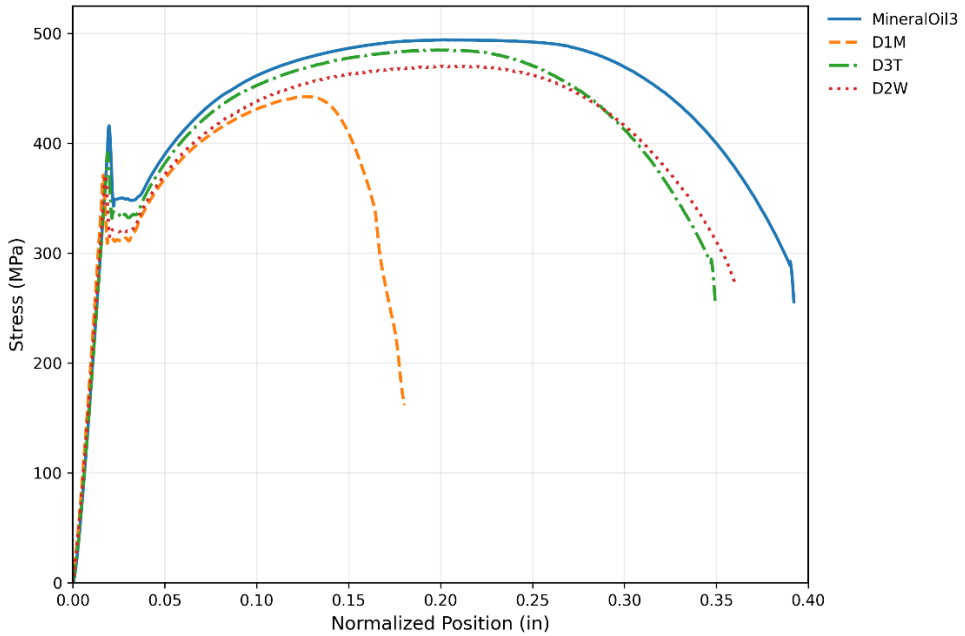

Figure 3-5 Mineral Oil tests vs. select samples with varying applied potentials and matching simulants

Two other tests were performed at low nitrate concentrations (i.e., less than or equal to 1 M) as seen in Figure 3-6. In one case, PF and NO_2^-/NO_3^- ratio exceeded the limit values (Simulant B), and in the second case PF and NO_2^-/NO_3^- ratio were less than the limit values (Simulant F). The tests were performed at -0.1 V vs. SCE. In both cases, the mechanical properties and the fracture surface indicated no SCC susceptibility. The CCP for the low nitrate concentration solution is obviously higher than those at higher nitrate concentrations (i.e., greater than 4 M) and thus these chemistry conditions are more benign.

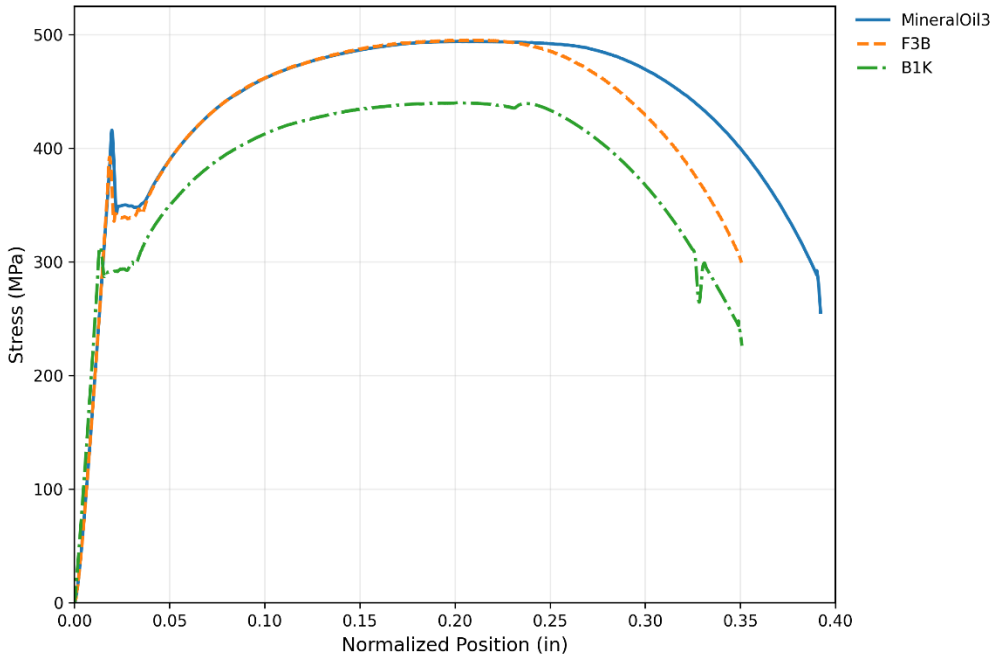

Figure 3-6 Mineral Oil tests vs. select samples with low nitrate concentrations

The UTS and Elongation ratio for each test is summarized in Table 3-1 below. The results were color coded to indicate which samples had indication of SCC. In general, the stress position plots provided good evidence that SCC had occurred. However, this was not universally true, as was observed for Simulants H, I and J. Thus, verification of SCC must always be confirmed by the condition of the fracture surface.

Table 3-1 Applied potential, Ultimate Tensile Strength Ratio and Elongation Ratio

Simulant	Trial	Sample	Applied Potential (V vs. SCE)	Max Stress (MPa)	Max Normalized Position (in)	UTS Ratio	Elongation Ratio
A	4	Q	-0.1	473.232	0.200	0.953	0.510
A	5	R	-0.2	468.951	0.364	0.944	0.928
B	1	K	-0.1	441.558	0.351	0.889	0.895
C	1	L	-0.1	445.078	0.150	0.896	0.383
D	1	M	-0.1	444.046	0.180	0.894	0.460
D	2	W	-0.2	473.847	0.361	0.954	0.920
D	3	T	-0.15	487.595	0.349	0.982	0.891
E	1	J	-0.1	392.086	0.129	0.790	0.328
E	2	S	-0.2	485.860	0.370	0.978	0.944
F	3	B	-0.1	497.573	0.351	1.018	0.894
G	1	N	-0.1	432.560	0.143	1.011	0.364
G	2	U	-0.2	487.947	0.362	1.002	0.923
G	3	Z	-0.15	479.005	0.353	0.871	0.901
H	2	H	-0.1	491.476	0.334	0.983	0.853
I	1	P	-0.1	459.426	0.248	0.965	0.633
J	1	F	-0.1	499.360	0.338	1.006	0.861
J	2	I	-0.1	462.458	0.145	0.931	0.371
J	3	V	-0.2	459.351	0.359	0.925	0.914
Mineral Oil	3		NA	496.540	0.392	NA	NA

Orange – Intergranular SCC features with severely reduced mechanical properties.

Yellow – Intergranular SCC features with moderately reduced mechanical properties.

No highlight – No SCC features and no significant reduction in mechanical properties.

NA – Not applicable

3.2 Fracture Surfaces

Photographs and scanning electron micrographs were utilized to confirm the observation of SCC. To illustrate the range of no SCC to SCC behavior, the results from tests in Simulant D were selected. Sample M was chosen to show SCC susceptibility at -0.1 V vs. SCE, while sample W, which was tested at -0.2 V vs. SCE exhibited no susceptibility. Other photographs of select samples are included in Appendix A.1.

Figure 3-7 is a photograph showing a side view of Sample D1M. SCC susceptibility is illustrated by the flat, jagged appearance of the sample where it fractured and the presence of secondary cracks on the gage length of the sample just beneath the fracture. Secondary cracks were even more evident on the gage length of Sample H2H in Figure 3-8, which was tested in Simulant H. Both samples also do not exhibit extensive “necking”, that is, a reduction in the cross-sectional

area at the fracture location. There is some indication of attack near the fracture location, however, the area beneath the fracture remains unaffected. This observation is characteristic of SCC in that most of the metal surface remains passive except for the area where cracking occurs. These observations are consistent with the stress-strain curve for this test shown Figure 3-1 and Figure 3-2 above.

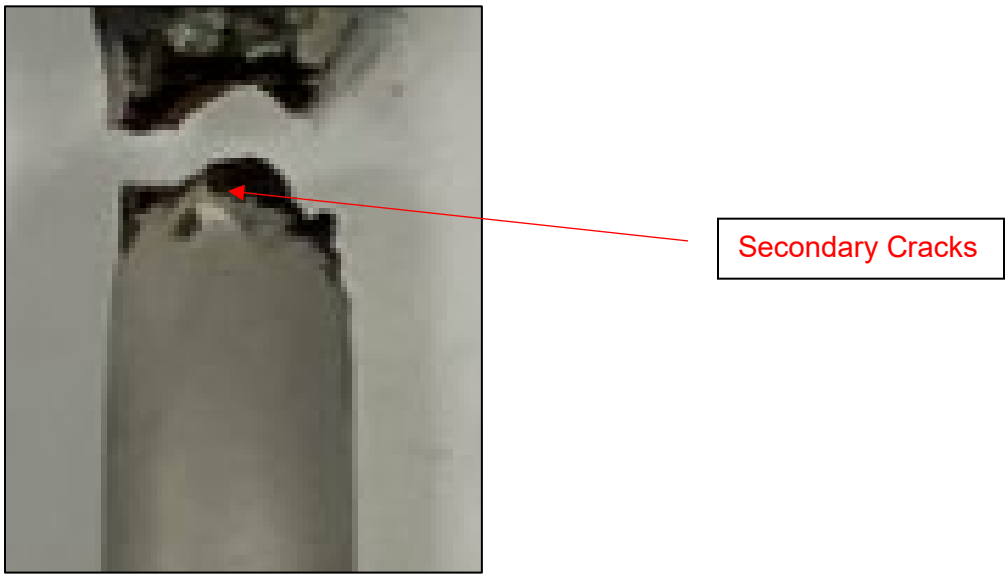

Figure 3-7 Side view of Sample D1M

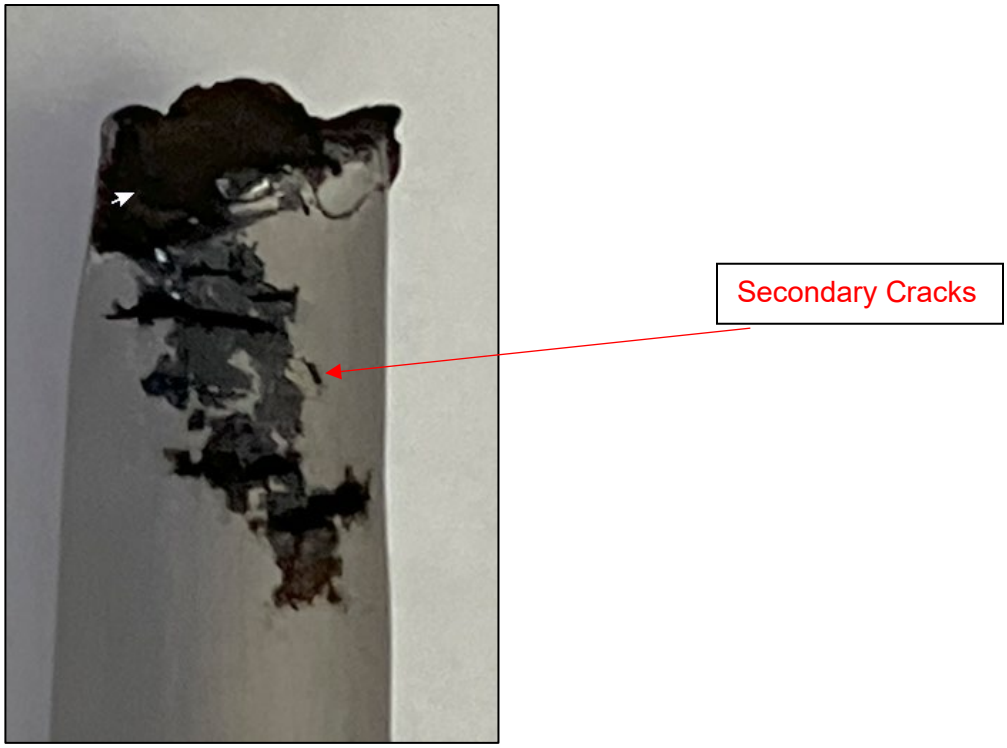

Figure 3-8 Side view of Sample H2H

Figure 3-9 is a photograph showing a side view of Sample D2W. In contrast to Sample D1M, the location of the fracture is characterized by a “cup-cone” appearance, that is, there is a significant reduction in the cross-sectional area of the sample. There were no secondary cracks along the gage and no indication of corrosion. There is essentially no difference between the appearance of this sample and one that is tested in air or an inert environment. These observations are consistent with the stress-strain curve for this test shown in Figure 3-6 above.

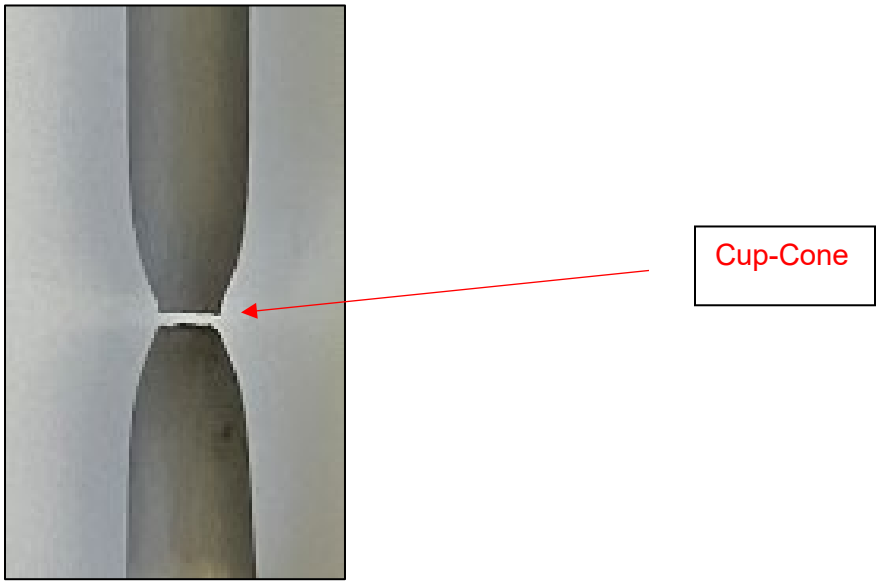

Figure 3-9 Side view of sample D2W

A view of the cross-sectional area from the top of the fracture surface was obtained for both samples tested in Simulant D as well. Samples D1M and D2W were selected for fracture examination using a Zeiss Sigma VP Scanning Electron Microscope (SEM) and Oxford Instruments Energy Dispersive Spectroscopy (EDS) to determine major elements present in the A537 alloy.

Figure 3-10 shows a high magnification SEM micrograph of sample D1M that was tested in Simulant D at -0.1 V vs. SCE. The surface is characterized by blocky, etched grains and indications of cracks in the surface. The surface clearly indicates intergranular attack, which is a characteristic of nitrate SCC.

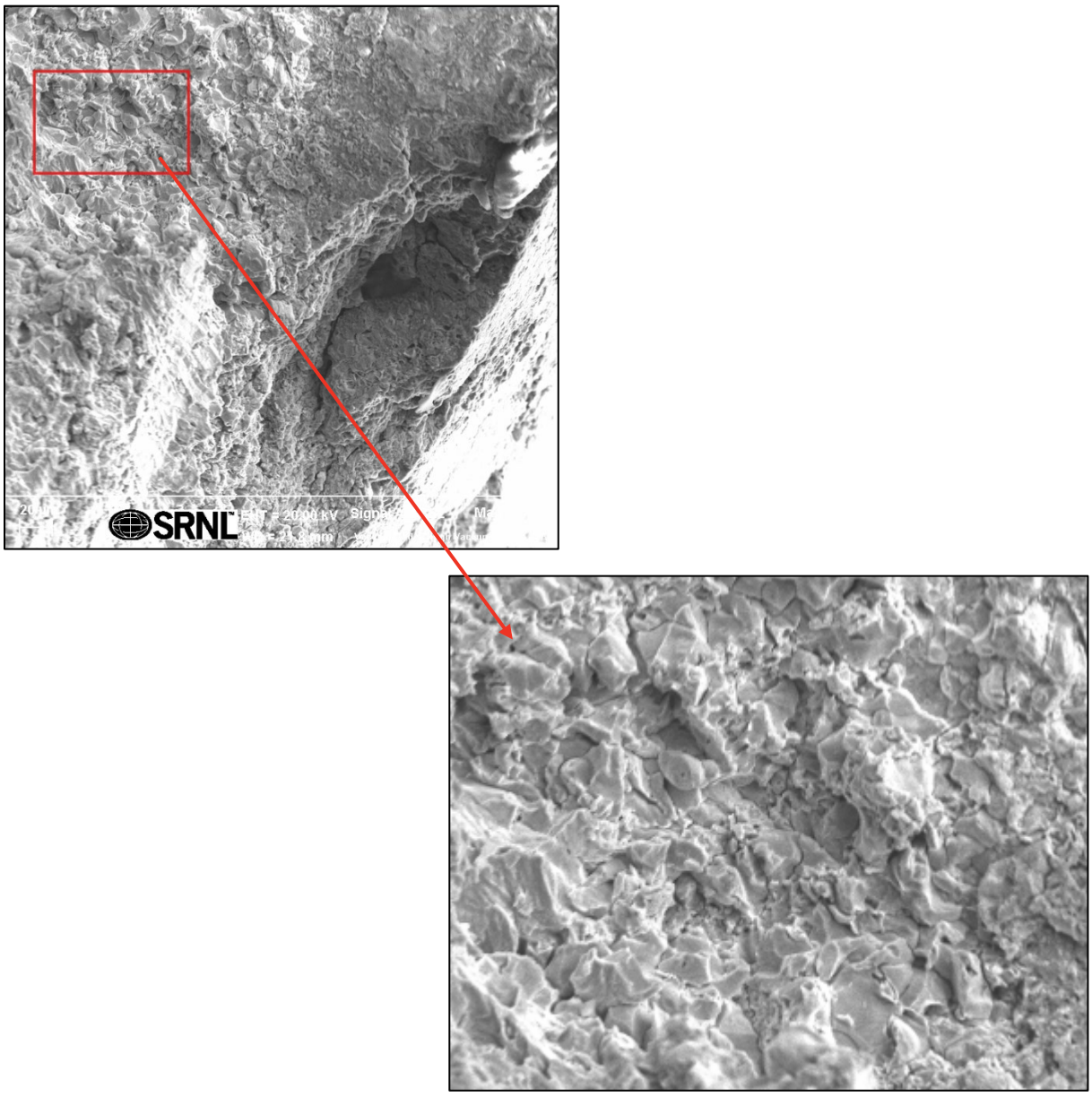

Figure 3-10 SEM image of Sample D1M at low and high magnifications.

Figure 3-11 shows the cross-sectional area from the top of the fracture surface for Sample D2W that was tested in Simulant D at -0.2 V vs. SCE. The fracture surface is characterized by ductile, dimpled rupture, which is indicative of no SCC susceptibility. There is essentially no difference between the appearance of this sample and one that is tested in air or an inert environment. These observations are also consistent with the stress-strain curve for this test shown above.

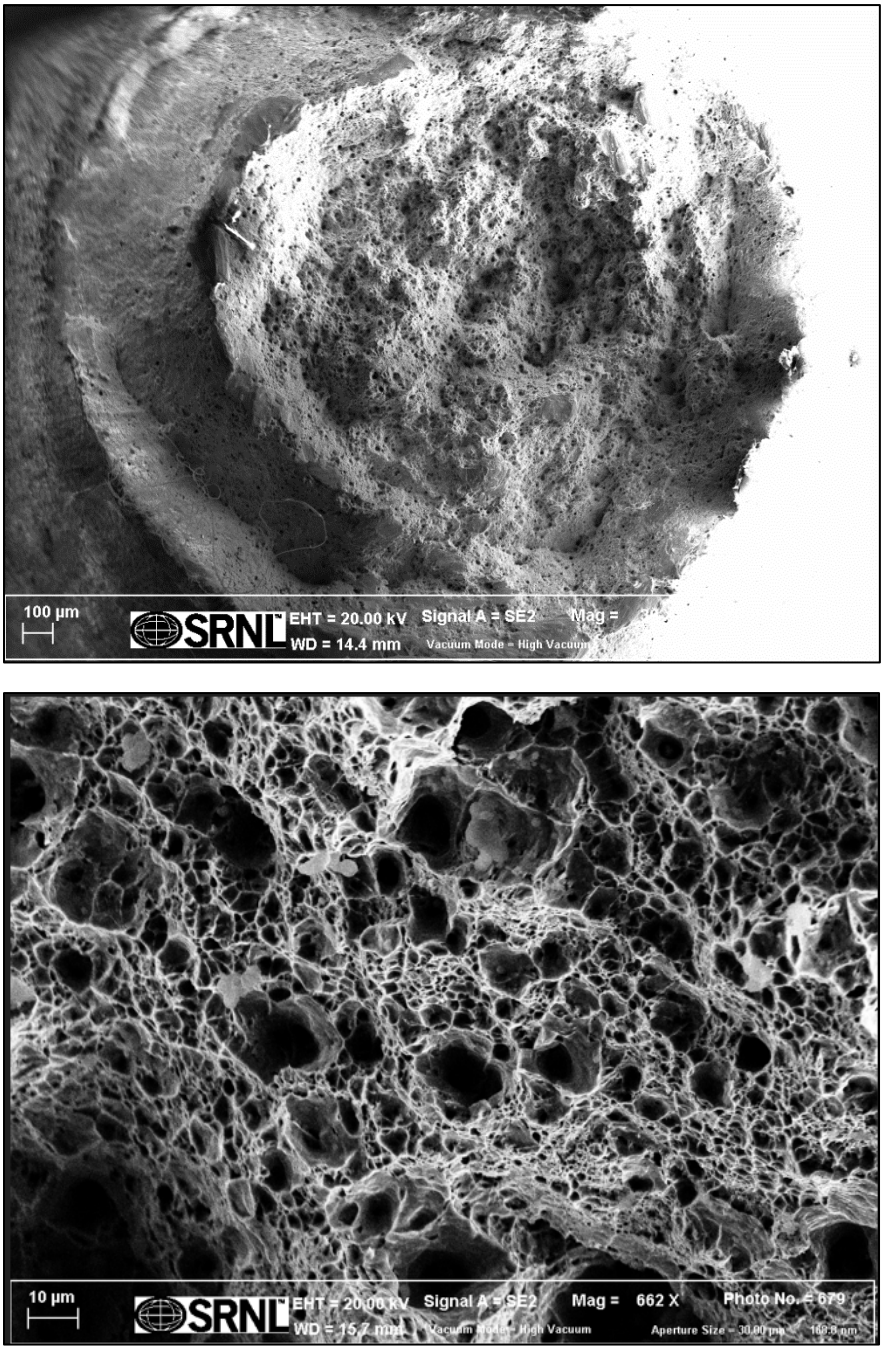

Figure 3-11 Ductile fracture surface of Sample D2W at low and high magnifications

Finally, a sample was sectioned longitudinally, along the axis, mounted and metallographically polished to reveal the cracks as they penetrate through the side of the sample. Figure 3-12 exhibits a section of Sample C1L, that was exposed to Simulant C. This figure shows extensive intergranular cracking through the cross-section of the sample. This confirmed the major cracking and correlates with the appearance of the sample and the stress-strain curve.

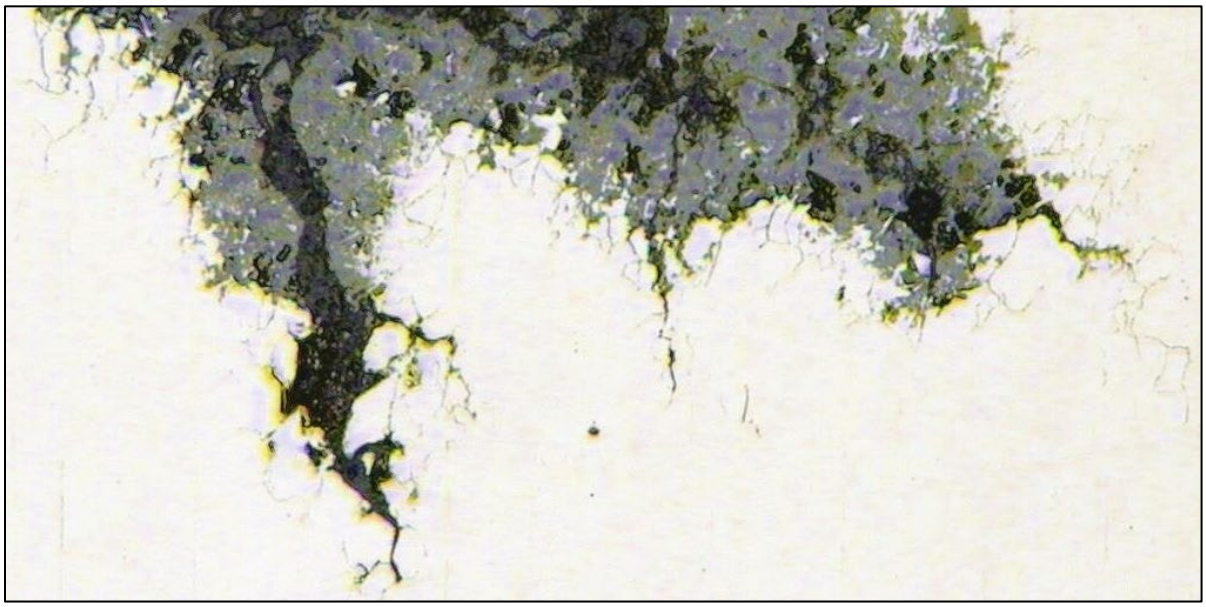

Figure 3-12 SCC fracture surface of sample L, Simulant C (C1L)

3.3 Electrochemical Potential Monitoring

The OCP was monitored for 24 hours before for the SSRT was initiated. An example of the OCP measurement that was made is shown in Figure 3-13 below. As with many laboratory OCP tests, the potential started at a negative potential, increased steadily due to oxide film growth during the first 5 hours, before becoming fairly stable. While the initial phase was not always evident, the potentials were fairly stable in most cases at the end of 24 hours (See Appendix A.3). The OCP for each test is shown in Table 3-2. The average OCP for the simulants was -0.330 V vs. SCE with a standard deviation of 0.076 V and the range was between -0.19 to -0.45 V vs. SCE. These values were consistent with OCPs measured during previous testing[35].

No SCC was observed at OCP values in this range in previous tests. However, as shown in previous sections, this testing indicates that a CCP near -0.1 V vs. SCE exists. This value is approximately 100 to 250 mV more positive than the typical OCP in dissolved salt simulants. This provides a relatively narrow margin between a region where the material is susceptible to SCC and where it is not. A major concern for tank operations is the risk that the tank potential could increase due to changes in the oxide film on the metal or the presence of an oxidizing species in the waste.

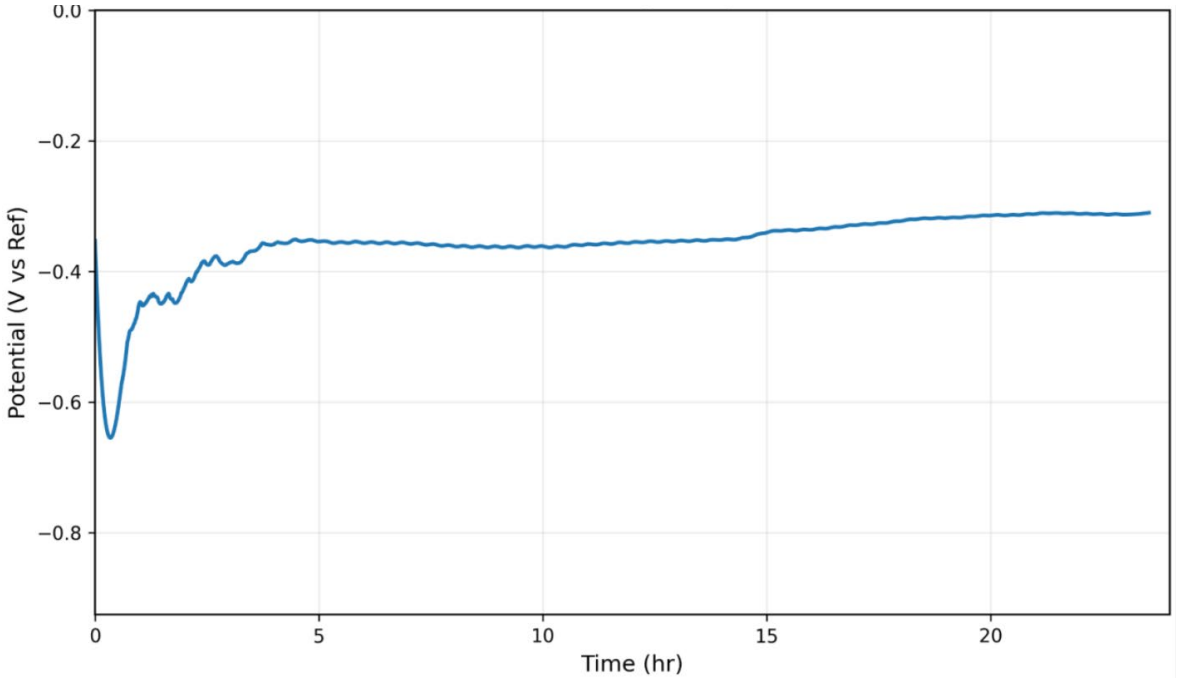

Figure 3-13 24 OCP curve example from this study

Table 3-2 24 hr. OCP for samples in this study

Simulant	Trial	Sample	24 hr. OCP (V vs. SCE)
A	4	Q	-0.19
A	5	R	-0.29
B	1	K	-0.44
C	1	L	-0.32
D	1	M	-0.39
D	2	W	-0.35
D	3	T	-0.295
E	1	J	-0.45
E	2	S	-0.305
F	3	B	-0.45
G	1	N	-0.405
G	2	U	-0.33
G	3	Z	-0.22
H	2	H	-0.26
I	1	P	-0.255
J	1	F	-0.37
J	2	I	-0.32
J	3	V	-0.315

4.0 Conclusions

This testing program was designed to examine the risk of SCC associated with utilizing the PF and NO_2^-/NO_3^- ratio limits for handling dissolved salt solutions at an elevated temperature in the carbon steel waste tanks. Figure 1-11 and Figure 1-12 showed that there was a gap in the data between SSRT that had been conducted at the OCP and those that had been performed at an applied potential. As shown in Figure 4-1 and Figure 4-2, the tests that were performed addressed that gap. The results indicate that if the NO_2^-/NO_3^- ratio is greater than 0.1 and the PF is greater than approximately 0.8 there is a margin between the OCP and the tests at applied potential. However, this margin is relatively small as defined by the difference between the OCP values and the CCP. This difference appears to be on the order of 0.1 to 0.25 V at the limits for PF and NO_2^-/NO_3^- ratio. It is not known whether changes in the waste chemistry during retrieval could result in the OCP evolving such that it would be greater than the CCP. These results confirm that dissolved salt solutions provide a potent chemistry that under certain conditions makes carbon steel susceptible to SCC.

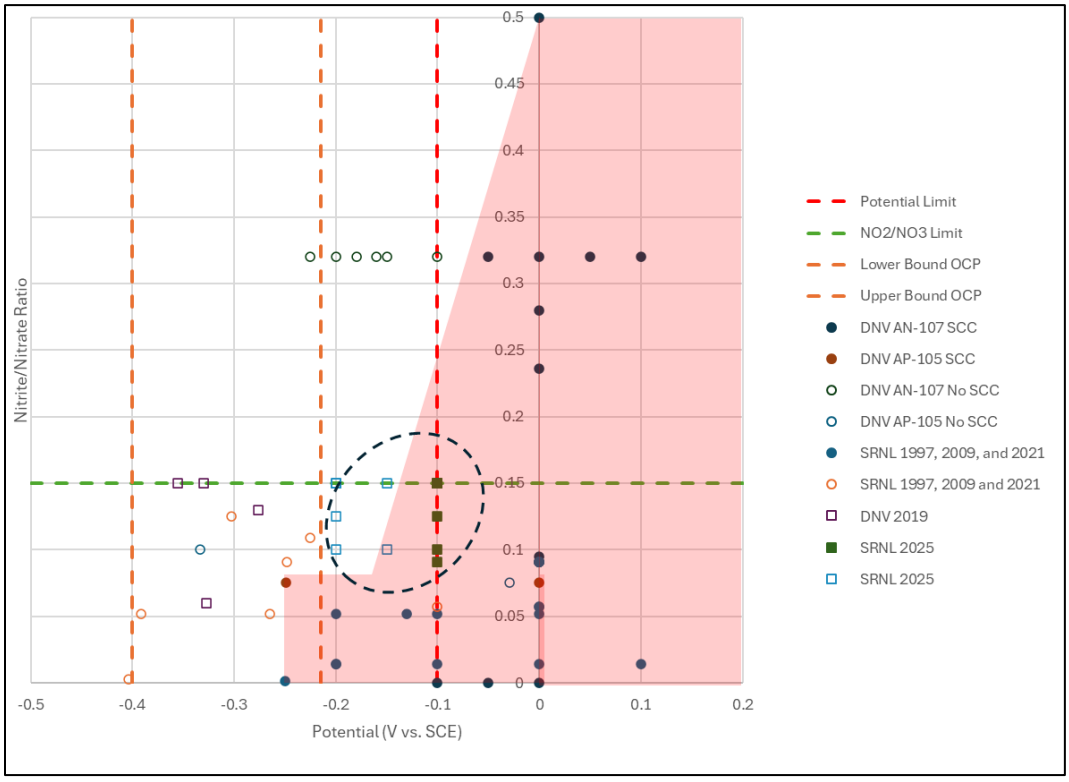

Figure 4-1 Graph showing Potential vs Nitrate/Nitrite ratio including this studies results

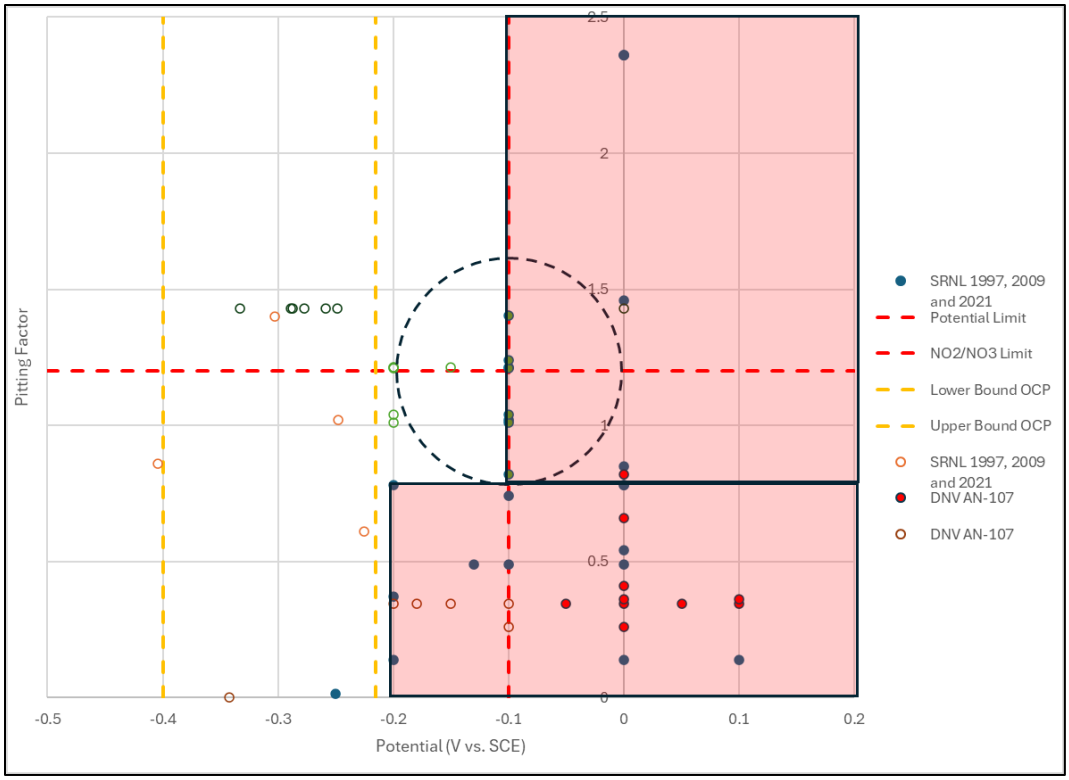

Figure 4-2 Graph showing Potential vs Pitting Factor including this studies results

The next question to consider is the influence these results will have on decisions for storage and retrieval of waste from the tanks. For Type III/IIIA waste tanks, the risk of SCC remains very low. First, and most importantly, the post-weld stress relief of the tanks has reduced the residual stress near the welds. Thus, without the stress component, SCC risk is minimized. The material of construction (A537 Carbon steel) for the Type III/IIIA tanks is superior to the steel in its resistance to SCC than the steel that was utilized for the Type I, II, and IV tanks (A285 carbon steel). From a chemistry control standpoint for a Type III/IIIA tank directly involved with handling dissolved salt solutions, the PF and NO_2^-/NO_3^- ratio limits may be utilized. Chemistry control provides an extra layer of defense against SCC. Chemistry control for a Type III/IIIA tank minimizes the risk for a tank that may receive the dissolved salt solution, particularly if that tank is a Type I, II, or IV waste tank.

On the other hand, if the dissolved salt solution is handled by a Type I, II, or IV waste tank the risk of SCC is real. Potent chemistry, lack of stress relief and inferior material result in a condition that is very likely to produce cracking. Efforts should be made to either avoid transferring waste that may not meet the PF and NO_2^-/NO_3^- ratio criteria to one of these tanks or if it is unavoidable, take measures to minimize the consequences of a leak. As shown by these tests, even if the PF and NO_2^-/NO_3^- ratio criteria are met, there is a risk that the tank potential may be disturbed in the positive direction and the risk of SCC increase.

5.0 Recommendations

The following recommendations are made if the tank farm operator desires to investigate the risk of SCC to the tanks further.

1. Perform additional SSRT to further define the CCP for the PF and NO_2^-/NO_3^- ratio. These tests confirmed that dissolved salt solutions are potent SCC contributors. A larger matrix of simulant chemistry and applied potentials would further define the critical potential.
2. Rather than applying a potential, during the test add oxidizing species to the simulant and perform the same tests. This approach would determine which species could influence the tank potential and how much of that species is necessary to increase the tank potential above the CCP. If a species is discovered limits on this species could be developed.
3. Perform long-term OCP measurements to determine if the potential has stabilized after 24 hours at a value below the CCP. An envelope of dissolved salt solution chemistry would be investigated.
4. Perform electrochemical polarization studies in the tank simulants to define the range of the passive region or if there is an active-passive transition that may indicate susceptibility to SCC. An envelope of dissolved salt solution chemistry would be investigated.

Finally, if the tank farm facility desires more information on the SCC susceptibility of an actual tank, consideration should be given to the installation of a reference electrode to measure the actual tank potential. This tank potential may be compared with the CCP. Tank potential monitoring is currently performed for the Hanford tanks and has been done periodically in the SRS waste tanks. However, risk for SCC at the anticipated storage and retrieval conditions, the materials of construction, tank fabrication procedures, and expected service life should be considered prior to installation of a reference electrode.

6.0 References

1. Wiersma, B.J., *The Performance of Underground Radioactive Waste Storage Tanks at the Savannah River Site: A 60-Year Historical Perspective.* JOM, 2014. **66**(3).
2. Martin, K.B., *U-PDDEV-H-00005 Deviation from Corrosion Control Program Description Document for Tank 41*. 2020.
3. Boerstler, J.T., *Task Technical and Quality Assurance Plan for Refinement of Pitting Factor Basis in Support of Corrosion Control Program Implementation*: SRNL-RP-2022-00106, 2022.
4. Parkins, R. N., *Stress Corrosion Cracking of Low Carbon Steels*. in *Conference on Fundamental Aspects of Stress Corrosion Cracking*, ed. R.W.Staehle., A. J. Forty, and D. Van Rooyen. 1969. Houston: NACE, p. 361.
5. Donovan, J.A., *Materials Aspects of SRP Waste Storage -Corrosion and Mechanical Failure*. *DP-1476,* 1977.
6. Ondrejcin, R.S., *Prediction of Stress Corrosion of Carbon Steel by Nuclear Process Liquid Wastes*, *DP-1478,* 1978.
7. Holzworth, M. L., L.P.Costas, and W. C. Rion, *Stress Corrosion Cracking of Carbon Steel in Simulated Waste Solutions*, *DP-1023,* 1966.
8. Wiersma, B. J. and R.L.Sindelar, *SRS High Level Waste Tank and Piping Systems - Structural Integrity Program and Topical Report*, *WSRC-TR-95-0076,* 1995.
9. Girdler, R.M., *Leaks in Radioactive-Waste Tanks, DP-990*. December 1965.
10. Poe, W.L., *Leakage from Waste Tank 16: Amount, Fate, and Impact*, *DP-1358,* 1974.
11. *Investigation of Waste Tank Leakage Savannah River Plant – Interim Report, DPE-2207*. April 1962.
12. Davis, T. L., D.W.Tharin, D. W. Jones, and D. R. Lohr, *"History of Waste Tank 16: 1959 through 1974", DPSPU-77-11-17*. July 1977.
13. Henthorne, M., *The Slow Strain Rate Stress Corrosion Cracking Test - A 50 Year Retrospective.* Corrosion, 2013. **72**(12).
14. ASTM International *G129-21 Standard Practice for Slow Strain Rate Testing to Evaluate Susceptibility of Metallic Materials to Environmentally Assisted Cracking*.
15. Stock, L. M., A.J. Feero, J. R. Follett, *Specifications for the Minimization of the Stress Corrosion Cracking Threat in Double Shell Tank Wastes*, *RPP-RPT-47337,* 2011.
16. Koch, G. H. and J.A.Beavers, *Limitations of the Slow Strain Rate Test for Stress Corrosion Cracking Testing.* Materials Technology Instituite of the Chemical Process Industries, Inc. MTI Publication No. 39, NACE International, 1995, p. 62..
17. Mickalonis, J.I., *Temperature Effects During Salt Dissolution: Susceptibility To Stress Corrosion Cracking*, *WSRC-TR-97-0177,* 1997.
18. Brossia, C. S., F. Gui., and C. Scott, *Hanford Tanks 241-AN-107 and AN-102: Effect of Chemistry and Other Variables on Corrosion and Stress Corrosion Cracking*, 2006.
19. Sridhar, N., J.A.Beavers, B. Rollins, S. Chawla, K. Evans, and X. Li, *Stress Corrosion Cracking and Localized Corrosion of Carbon Steel in Nitrate Solutions.* Corrosion, **72**(7), 2016.
20. Parkins, R. N. and M.J. Humphries in *Fundamental Aspects of Stress Corrosion Cracking*, in *National Association of Corrosion Engineers*, ed. R.W.Staehle., A. J. Forty, and D. Van Rooyen,1969: Houston, TX. p. 389.
21. Gui, F. and C.S. Brossia, Final Report - Effect of Chemistry and other Variables on Corrosion and Stress Corrosion Cracking of Hanford Tanks*, RPP-RPT-42703, Rev. A*. 2009.
22. Beavers, J. A., C.S.Brossia, F. Gui, C. Scott, H. Cong, N. Sridhar, B. J. Wiersma, G. S. Frankel, K. D. Boomer, *Stress Corrosion Cracking of Carbon Steel in Nitrate-Based Hanford Waste Simulants*, in *CORROSION 2014*. 2014.

23. Mickalonis, J.I., *Temperature Effects During Salt Dissolution: Slow Strain Rate Testing*, *WSRC-TR-96-0063,* 1996.
24. Boerstler, J.T., *Refinement of Salt Dissolution Inhibitor Requirements - Final Report*. 2021: SRNL-STI-2021-00116, 2021
25. Sykes, K. S., J.Jiang, B. J. Wiersma, S. Chawla, N. Sridhar, K. Evans, and J.A. Beavers, *Design and Materials of Reference Electrodes for Radioactive Waste Tank Service - A Literature Review*, *SRNL-STI-2024-00539,* 2024.
26. Counts, K. M., B.J. Wiersma, and J. I. Mickalonis, *Determination of Corrosion Inhibitor Criteria for Type III/IIIA Tanks During Salt Dissolution Operations-Interim Report*, *WSRC-STI-2007-00552,* 2007.
27. Crosswhite, R. J. and M.M. Dahl, *Corrosion Probe Monitoring Systems: January through March 2024 Quarterly Report*. *RPP-RPT-51766, Rev. 4*12024.
28. Ondrejcin, R.S., *Salt Removal from Waste Tanks: Nitrate-Induced Stress Corrosion Cracking*, *DPST-80-419,* 1980.
29. Ondrejcin, R.S., *Salt Removal Compositional Limits - Suggested Technical Standard for Types I, II, and IV Nuclear Waste Tanks*, *DPST-83-533,* 1983.
30. Martin, K.B., *CSTF Corrosion Control Program: Program Description Document*, *WSRC-TR-2002-00327,* 2002.
31. Ondrejcin, R.S. and J. A. Donovan, *Relative Resistance to Nitrate Cracking of A537 Class I and A516 Grade 70 Normalized Steels*, *WSRC-RP-2004-00198,* 2004.
32. *Operating Specifications for the 241-AN, AP, AW, AY, AZ and SY Tank Farms. OSD-T-151-00007*. 1998.
33. Barnes, D.M. and K.C. Kwon, *Tank 29 During Salt Removal Operations*, *WSRC-TR-94-00477,* 1994.
34. Mickalonis, J.I., *Maximum Solubilities of Sodium Nitrate In Simulated Waste*, *SRT-MTS-94-2043,* 1994.
35. Garcia-Diaz, B. L., J.I.Mickalonis and B. J. Wiersma, *Determination of Corrosion Inhibitor Criteria for Type III/IIIA Tanks During Salt Dissolution Operations-Summary Document*, *SRNL-STI-2009-00600,* 2009.
36. Wiersma, B. J., R.E.Fuentes, L.M. Stock, *Chemistry Envelope for Pitting and Stress Corrosion Cracking Mitigation, SRNL-STI-2019-0021,7* 2019.
37. Boerstler, J.T., *Refinement of Pitting Factor Basis to Support the Corrosion Control Program- Interim Report*, *SRNL-STI-2023-00061,* 2023.
38. ASTM International, *E8-E8M Standard Test Methods for Tension Testing of Metallic Materials*.
39. ASTM International, *A537/A537M020 Standard Specification for Pressure Vessel Plates, Heat-Treated, Carbon-Manganese-Silicon Steel*.
40. ASTM International, *E45-25 Standard Test Methods for Determining the Inclusion Content of Steel*.
41. ASM International *Failure Analysis and Prevention*. Vol. 11. 2021.
42. *WSRC-IM-2002-00011, Rev. 2 SRNL Technical Report Design Checklist* 2002.

Appendix A.

A.1 Tested Samples

Photographs of each sample after test in as tested orientation.

A4Q

A5R

B1K

C1L

D1M

D2W

D3T

E1J

E2S

F1D

F3B

G1N

G2U

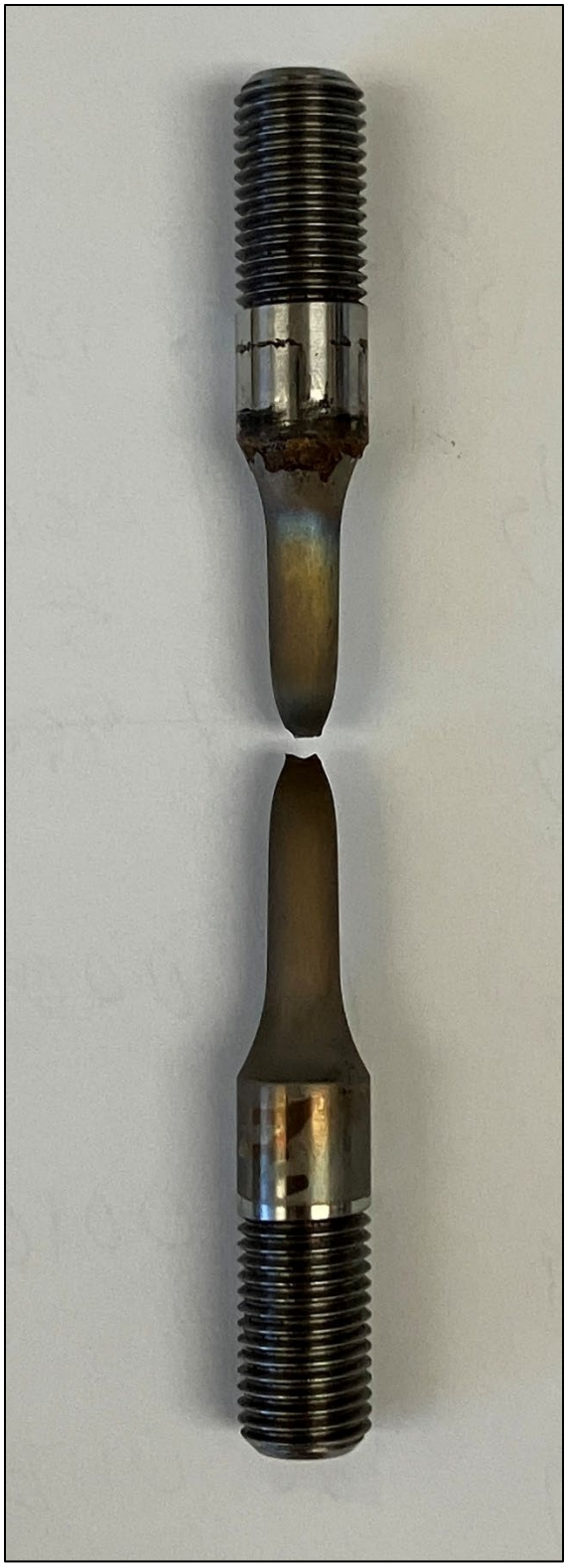

G3Z

H2H

I1P

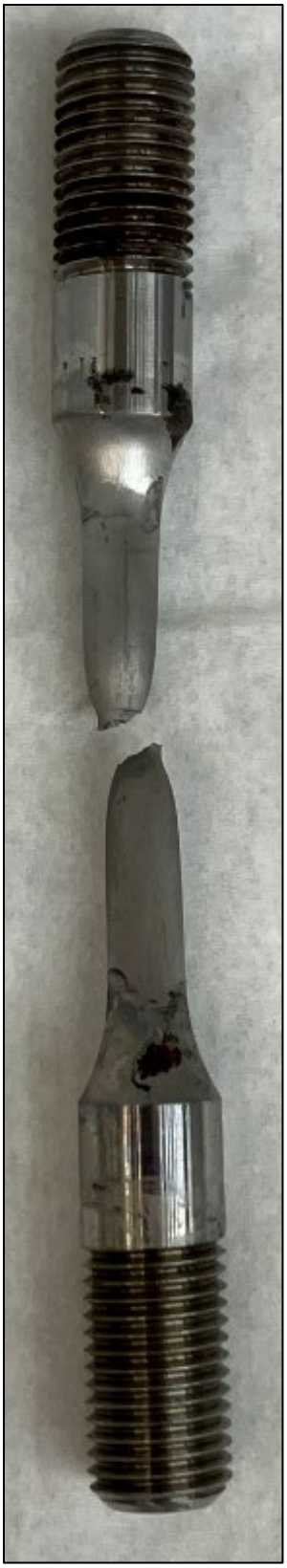

J1F

J2I

J3V

Mineral Oil Test 2

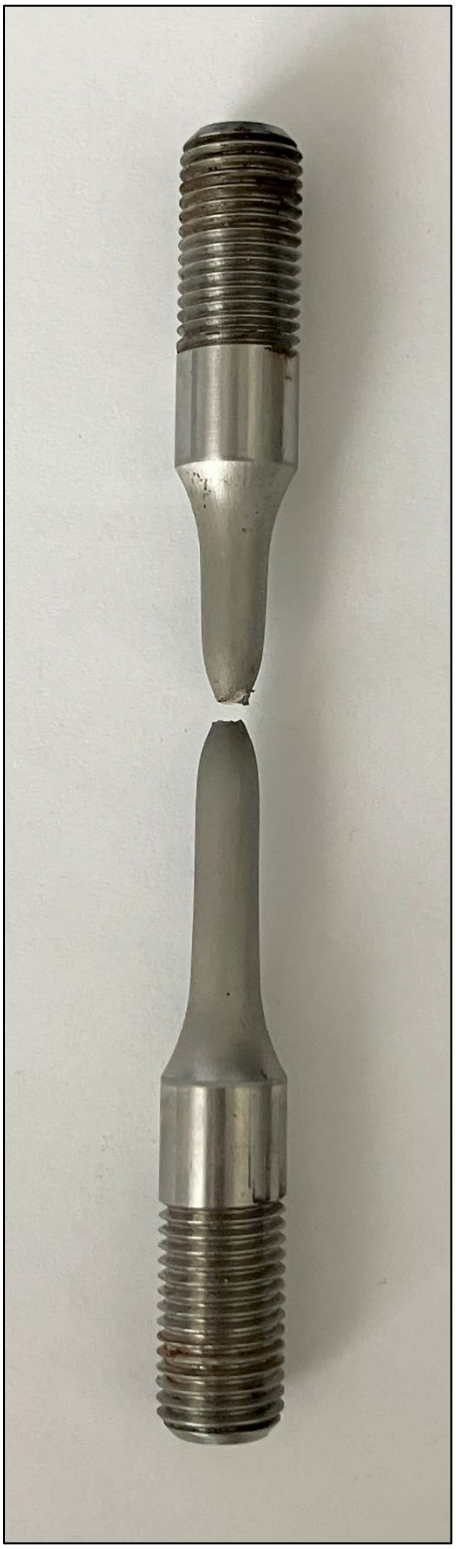

Mineral Oil Test 3

A.2 Stress vs. Position and Stress vs. Strain Curves

Stress vs Position plots and Stress vs Strain plots for A537 samples tested in this study. The position is “normalized” to account for machine position zeroing. The position at failure in this study is used as an analogous measurement to elongation, giving a model of ductility in different conditions. While engineering strain would be a more accurate measure, the in-situ electrochemical cell prevented the use and an extensometer and the strain values are not compliance correct. Strain curves are included for thoroughness.

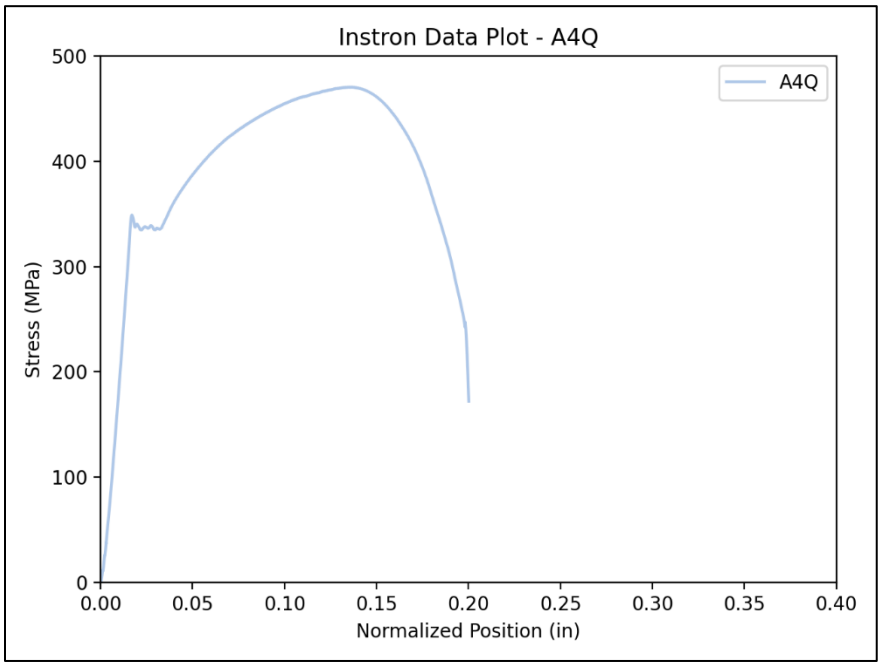

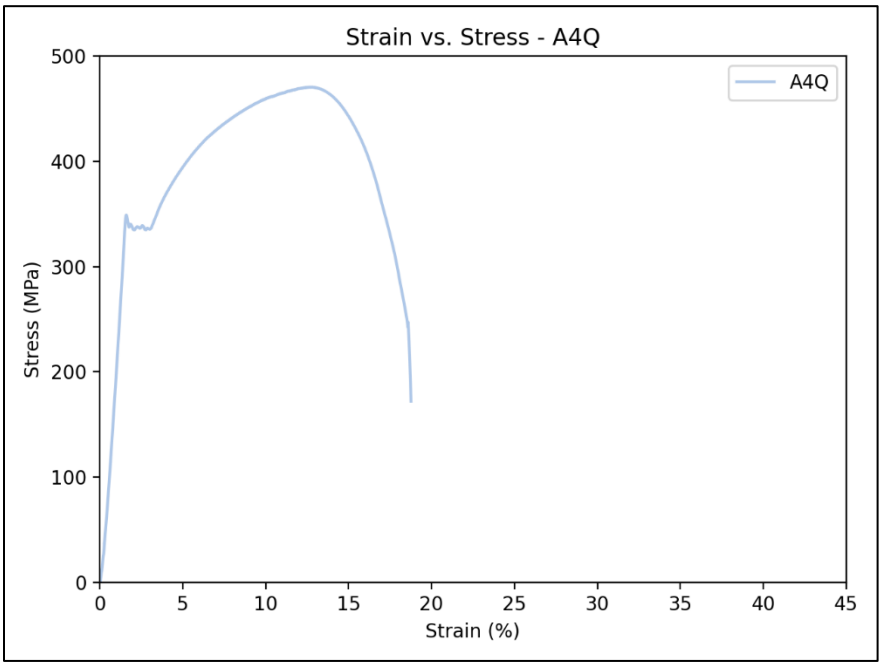

AQ4

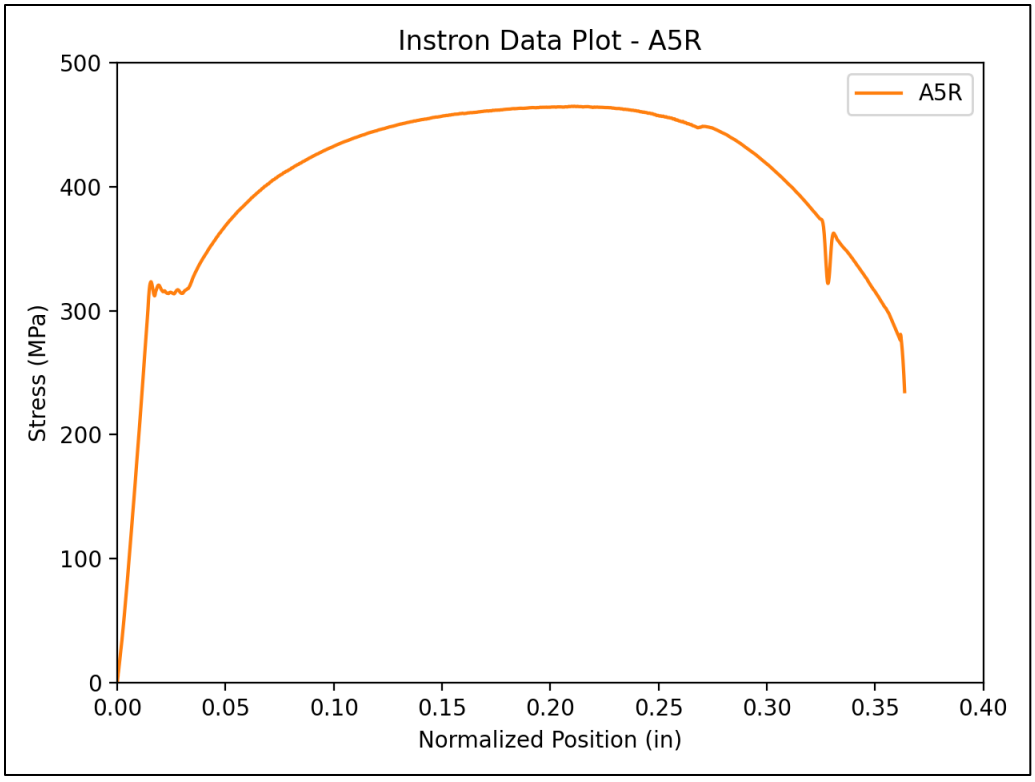
Instron Data Plot - A5R
A5R
Stress (MPa)
Normalized Position (in)
0
100
200
300
400
500
0.00
0.05
0.10
0.15
0.20
0.25
0.30
0.35
0.40

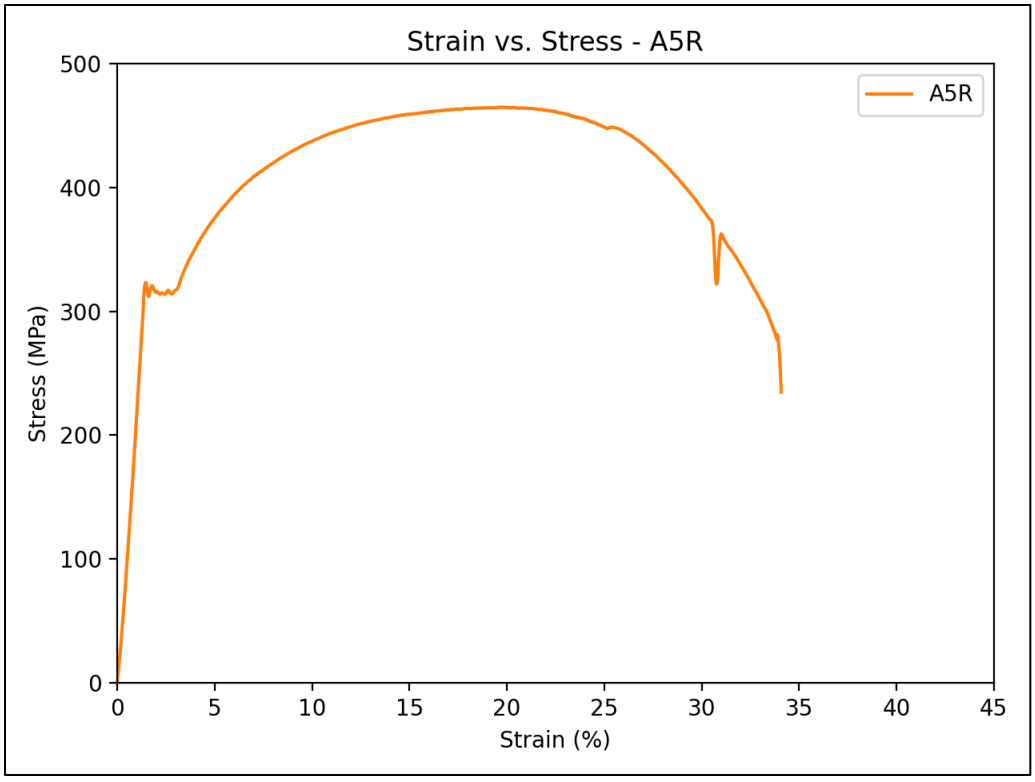
Strain vs. Stress - A5R
A5R
Stress (MPa)
Strain (%)
0
100
200
300
400
500
0
5
10
15
20
25
30
35
40
45

A5R

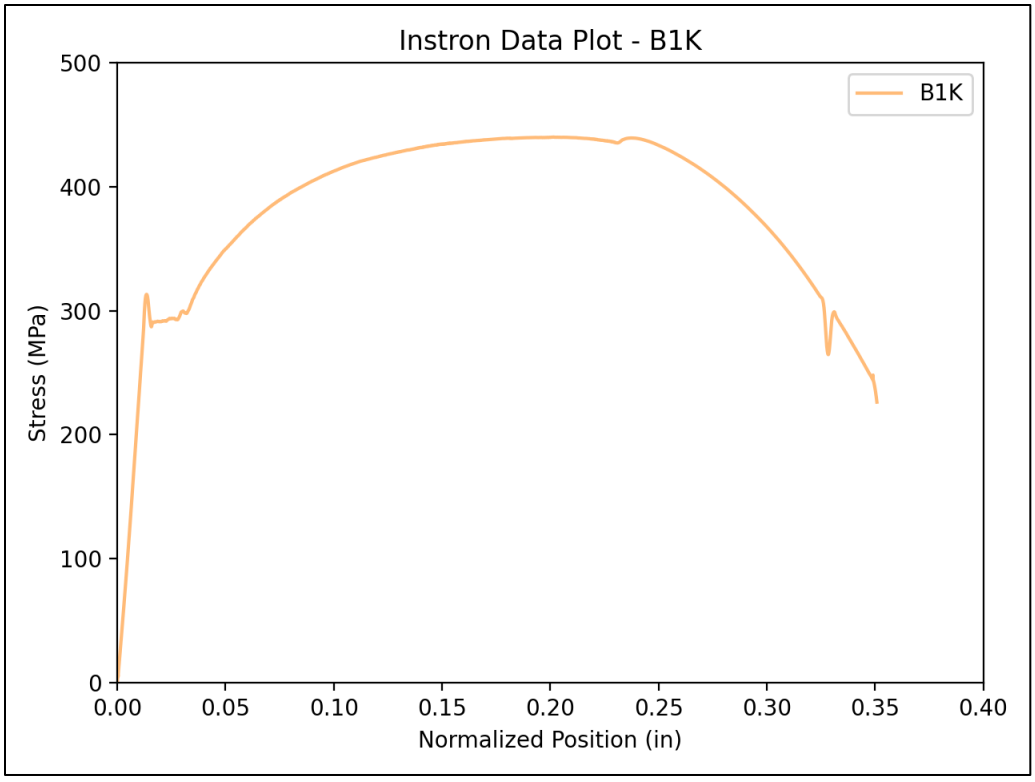
Instron Data Plot - B1K
B1K
Stress (MPa)
Normalized Position (in)
0
100
200
300
400
500
0.00
0.05
0.10
0.15
0.20
0.25
0.30
0.35
0.40

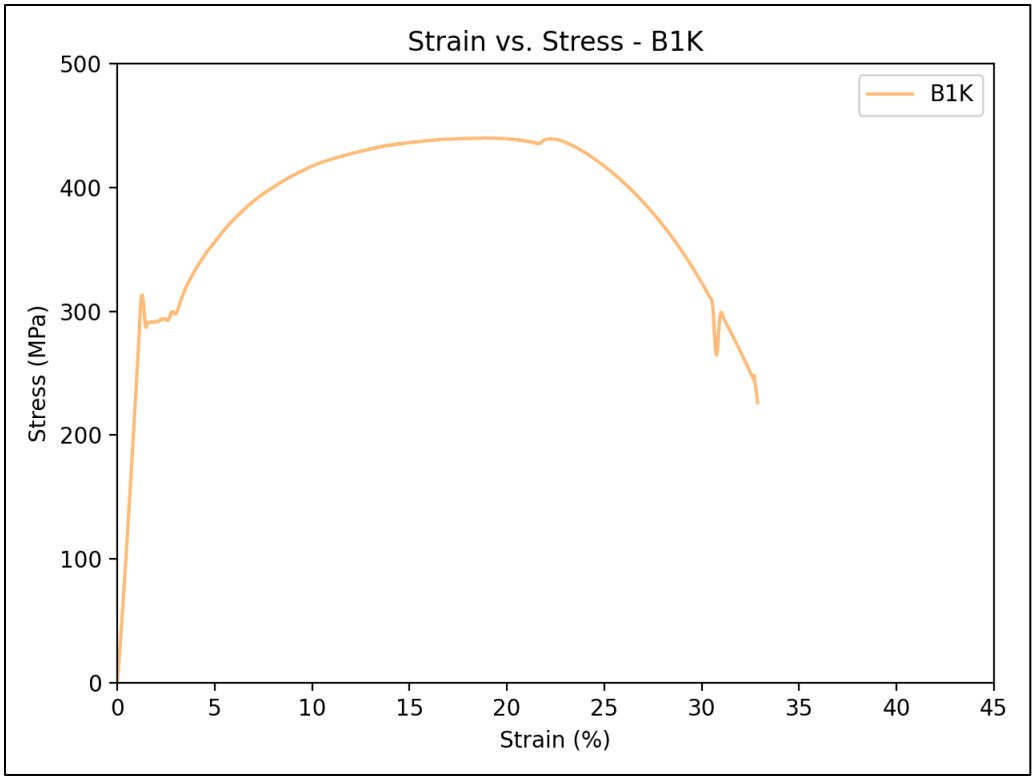
Strain vs. Stress - B1K
B1K
Stress (MPa)
Strain (%)
0
100
200
300
400
500
0
5
10
15
20
25
30
35
40
45

B1K

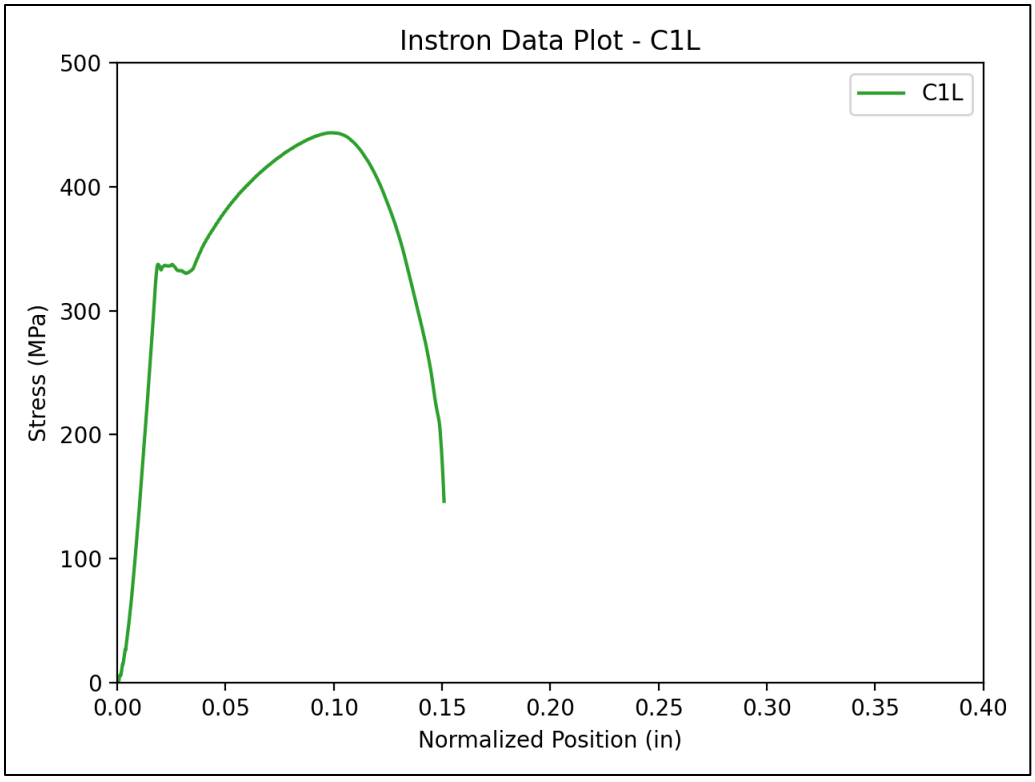
Instron Data Plot - C1L
C1L
Stress (MPa)
Normalized Position (in)
0
100
200
300
400
500
0.00
0.05
0.10
0.15
0.20
0.25
0.30
0.35
0.40

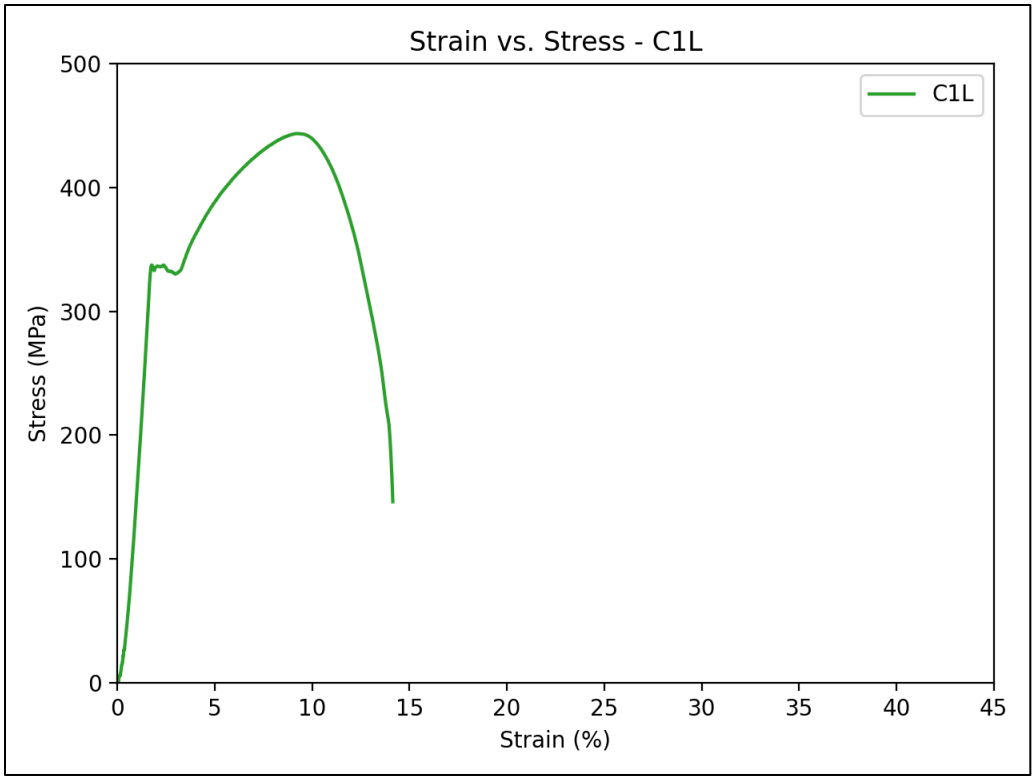
Strain vs. Stress - C1L
C1L
Stress (MPa)
Strain (%)
0
100
200
300
400
500
0
5
10
15
20
25
30
35
40
45

C1L

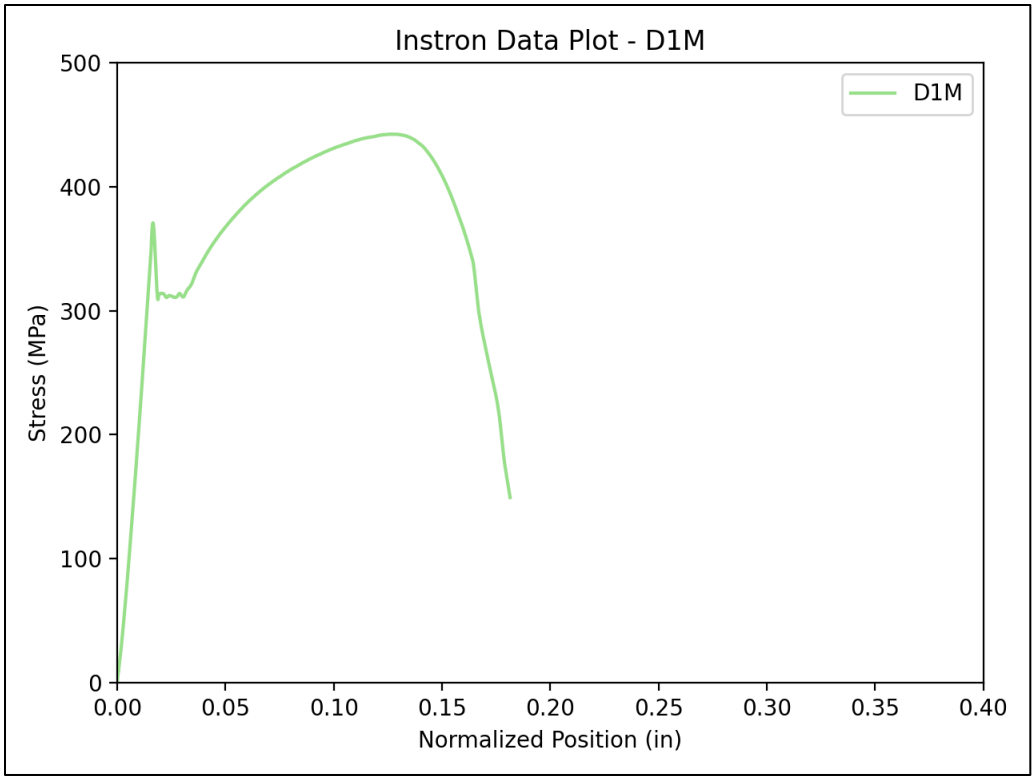
Instron Data Plot - D1M
D1M
Stress (MPa)
Normalized Position (in)
0
100
200
300
400
500
0.00
0.05
0.10
0.15
0.20
0.25
0.30
0.35
0.40

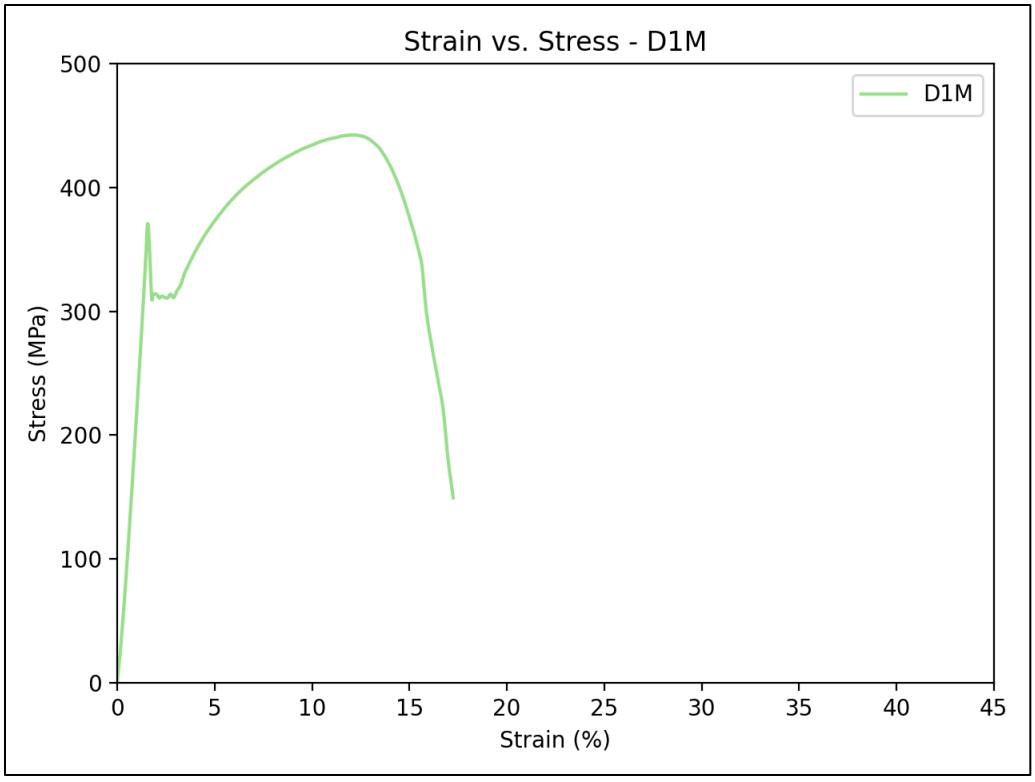
Strain vs. Stress - D1M
D1M
Stress (MPa)
Strain (%)
0
100
200
300
400
500
0
5
10
15
20
25
30
35
40
45

D1M

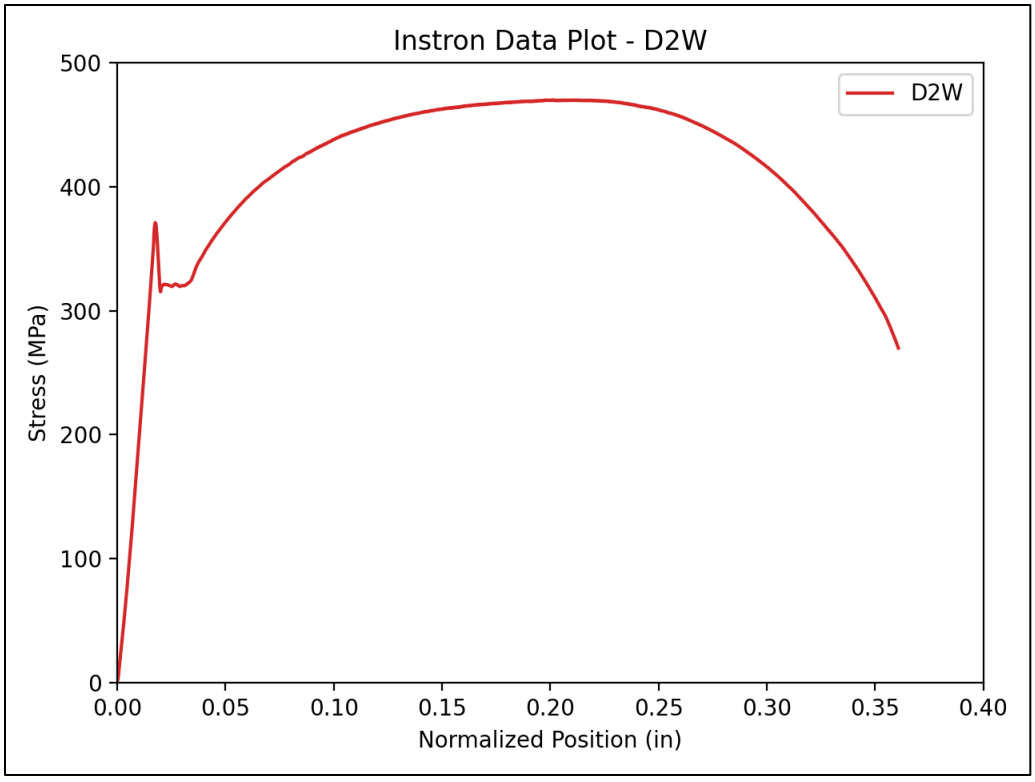
Instron Data Plot - D2W
D2W
Stress (MPa)
Normalized Position (in)
0
100
200
300
400
500
0.00
0.05
0.10
0.15
0.20
0.25
0.30
0.35
0.40

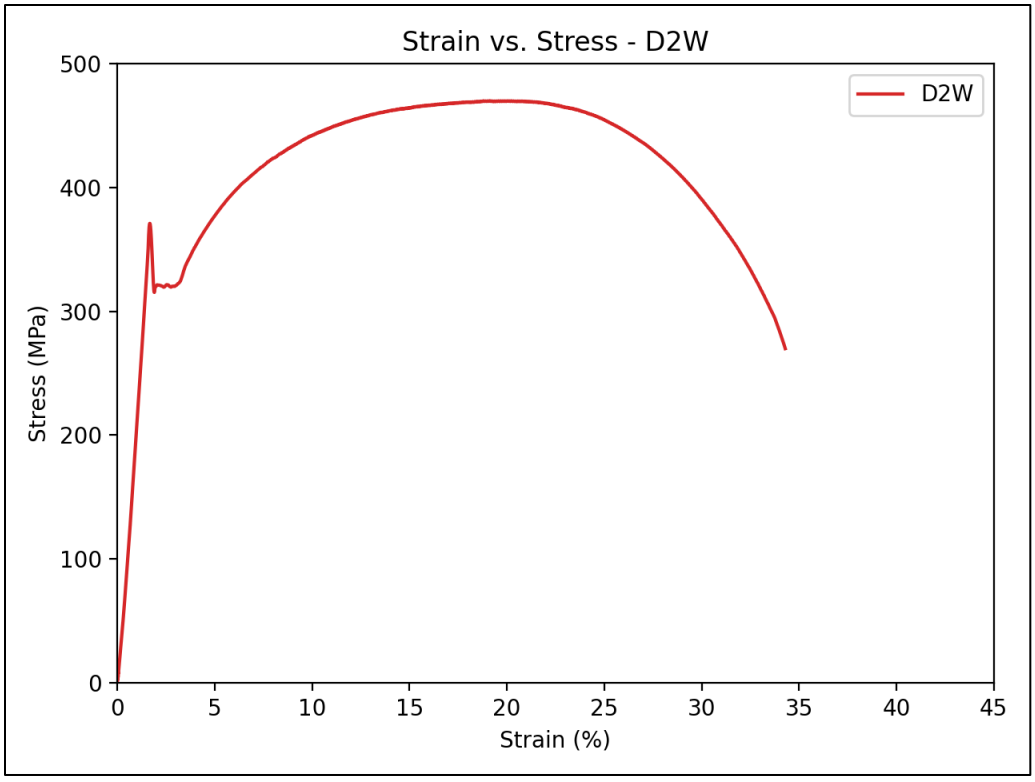
Strain vs. Stress - D2W
D2W
Stress (MPa)
Strain (%)
0
100
200
300
400
500
0
5
10
15
20
25
30
35
40
45

D2W

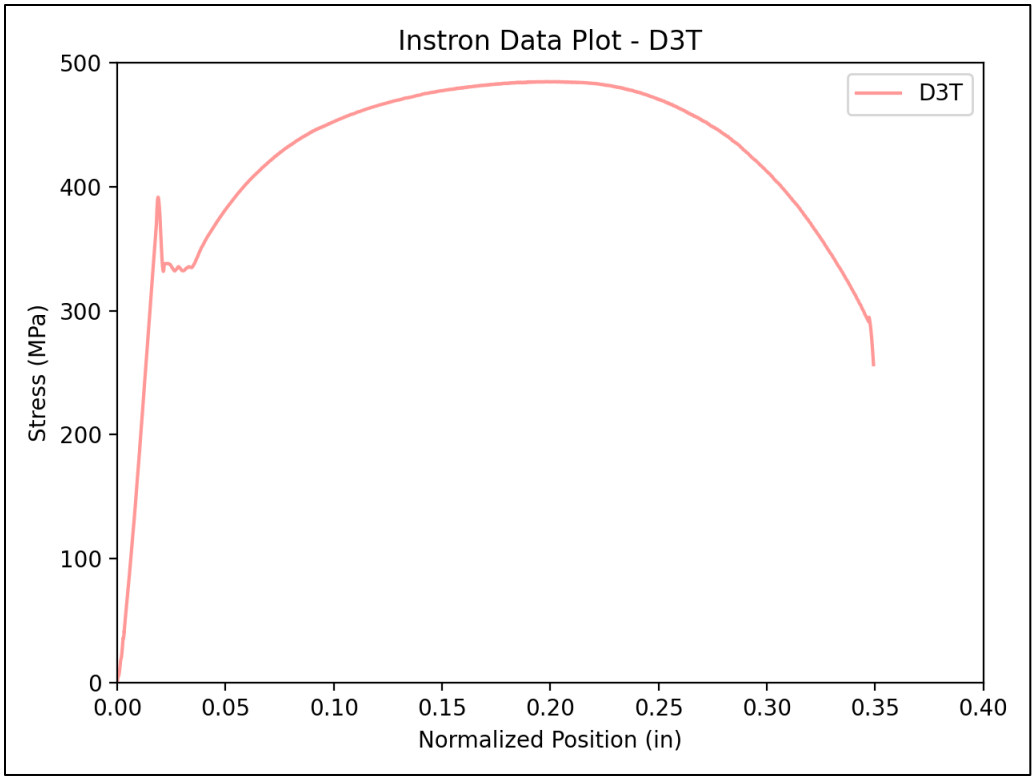
Instron Data Plot - D3T
D3T
Stress (MPa)
Normalized Position (in)
0
100
200
300
400
500
0.00
0.05
0.10
0.15
0.20
0.25
0.30
0.35
0.40

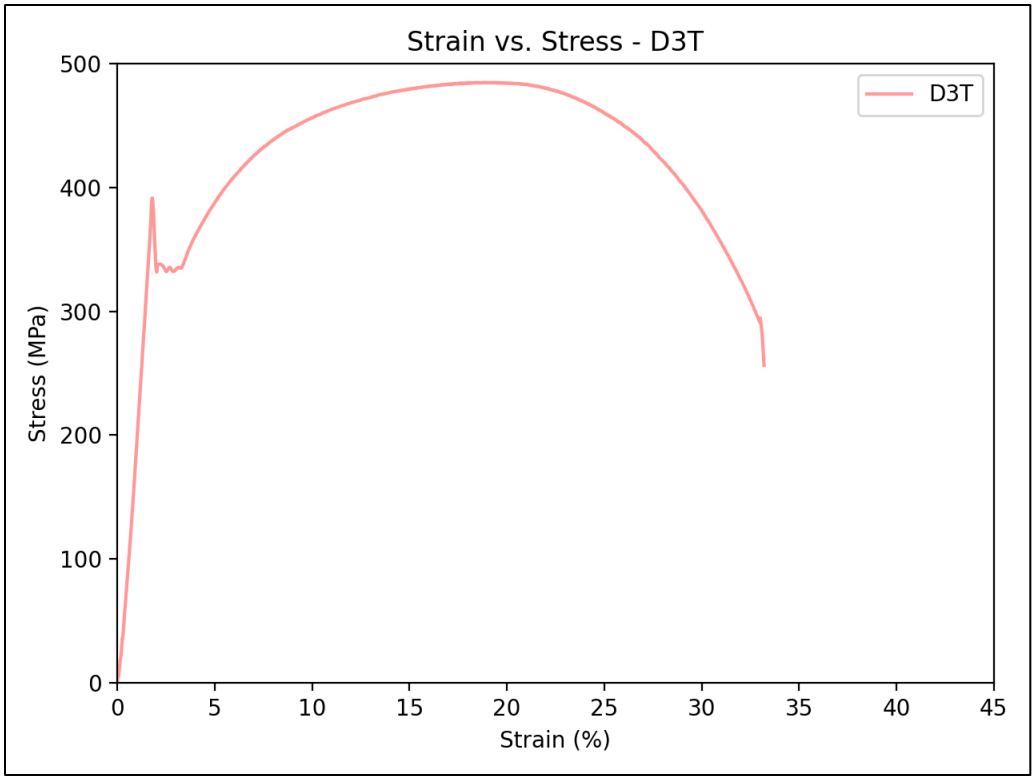
Strain vs. Stress - D3T
D3T
Stress (MPa)
Strain (%)
0
100
200
300
400
500
0
5
10
15
20
25
30
35
40
45

D3T

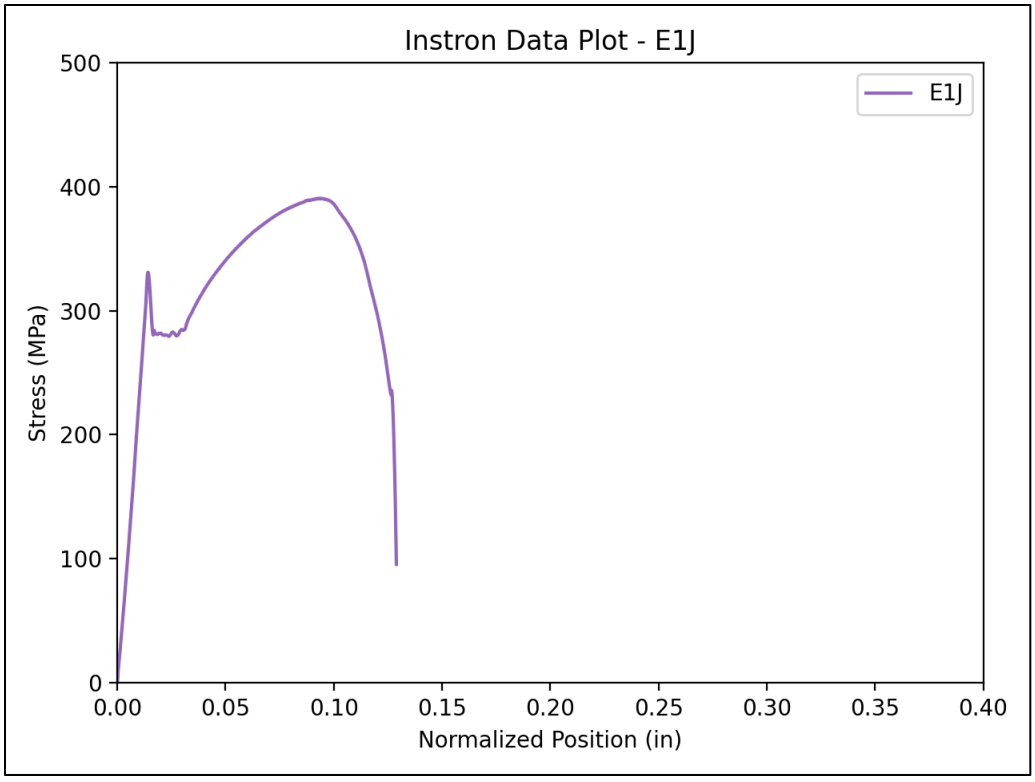
Instron Data Plot - E1J
E1J
Stress (MPa)
Normalized Position (in)
0
100
200
300
400
500
0.00
0.05
0.10
0.15
0.20
0.25
0.30
0.35
0.40

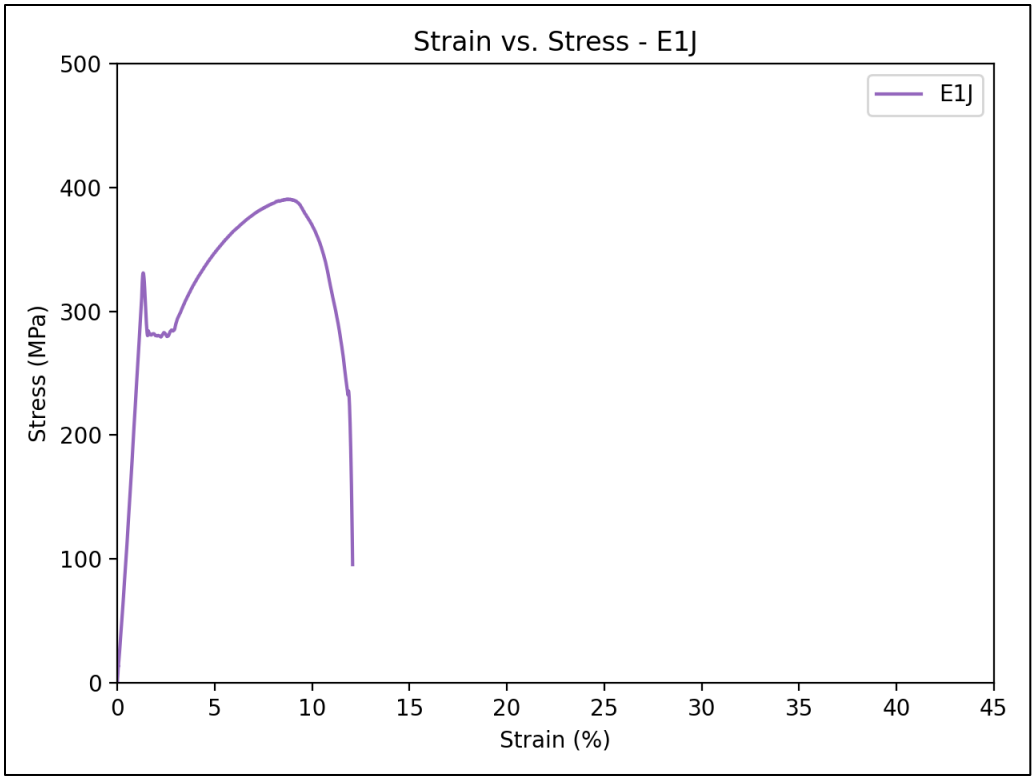
Strain vs. Stress - E1J
E1J
Stress (MPa)
Strain (%)
0
100
200
300
400
500
0
5
10
15
20
25
30
35
40
45

E1J

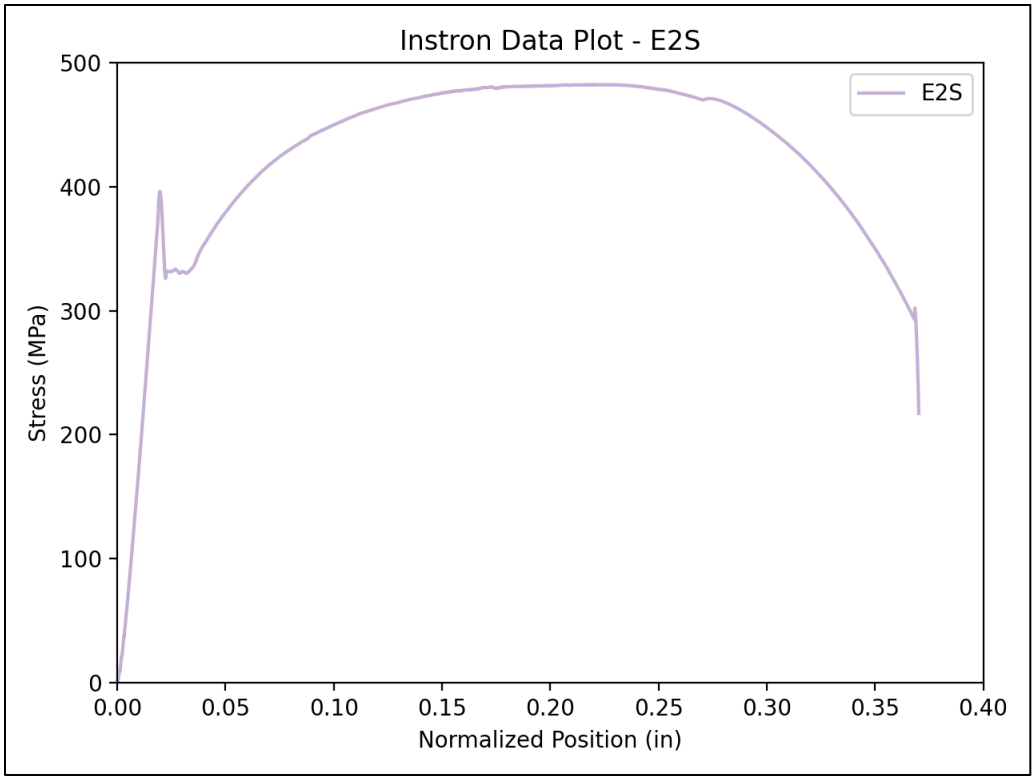
Instron Data Plot - E2S
E2S
Stress (MPa)
Normalized Position (in)
0
100
200
300
400
500
0.00
0.05
0.10
0.15
0.20
0.25
0.30
0.35
0.40

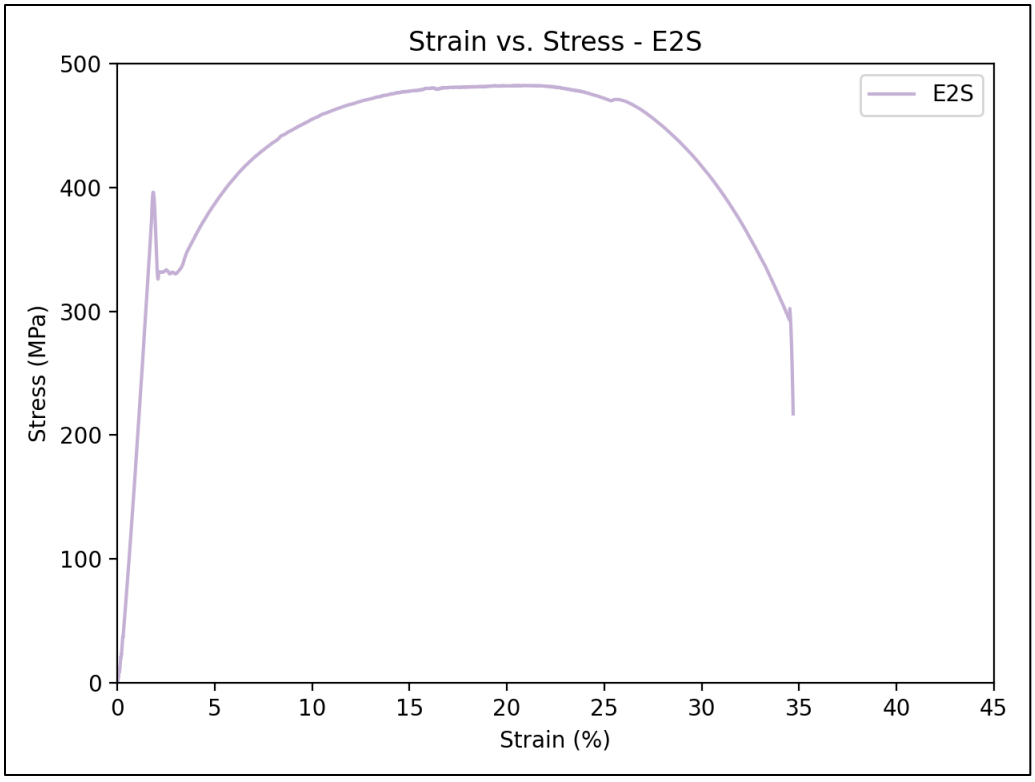
Strain vs. Stress - E2S
E2S
Stress (MPa)
Strain (%)
0
100
200
300
400
500
0
5
10
15
20
25
30
35
40
45

E2S

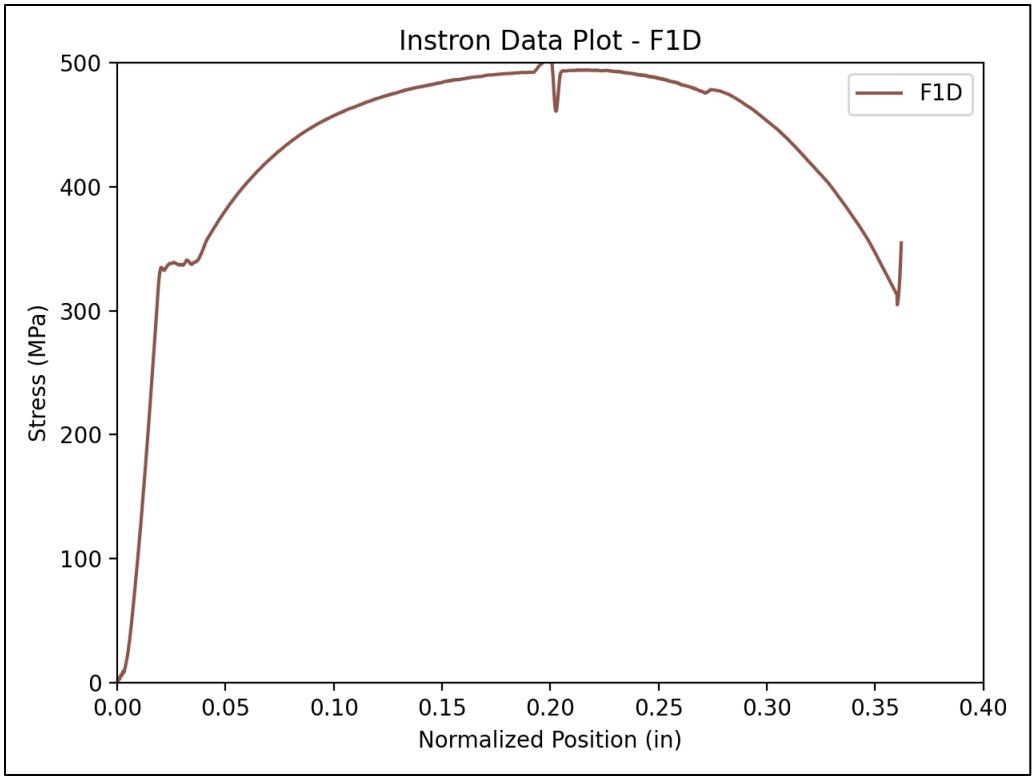
Instron Data Plot - F1D
F1D
Stress (MPa)
Normalized Position (in)
0
100
200
300
400
500
0.00
0.05
0.10
0.15
0.20
0.25
0.30
0.35
0.40

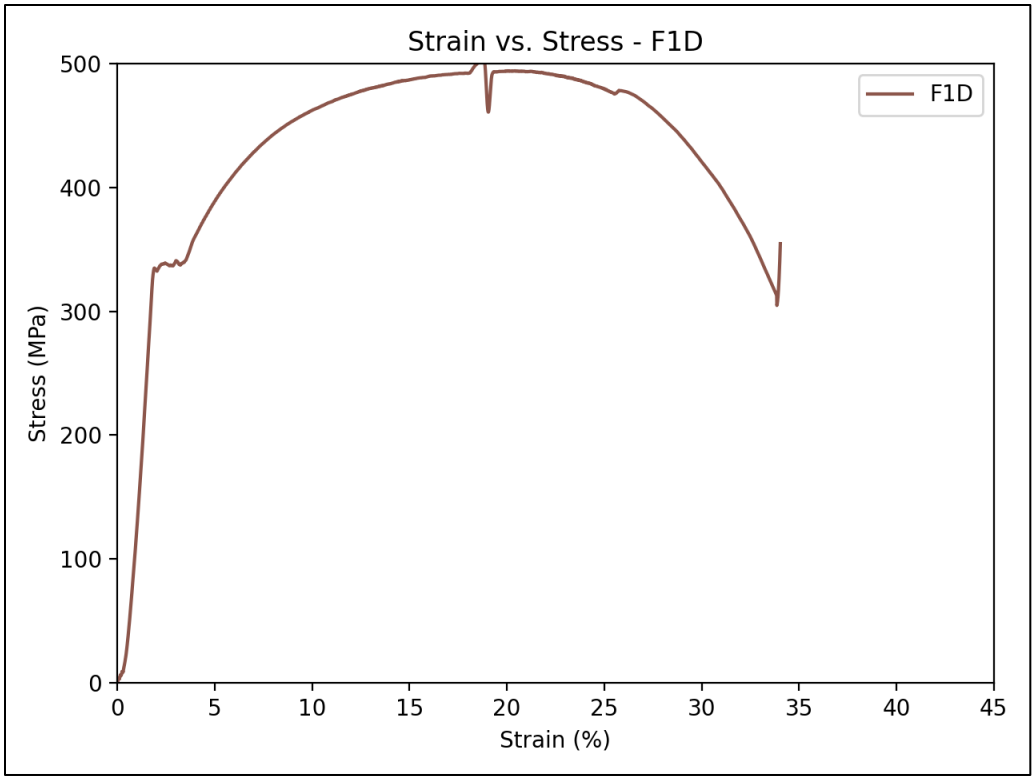
Strain vs. Stress - F1D
F1D
Stress (MPa)
Strain (%)
0
100
200
300
400
500
0
5
10
15
20
25
30
35
40
45

F1D

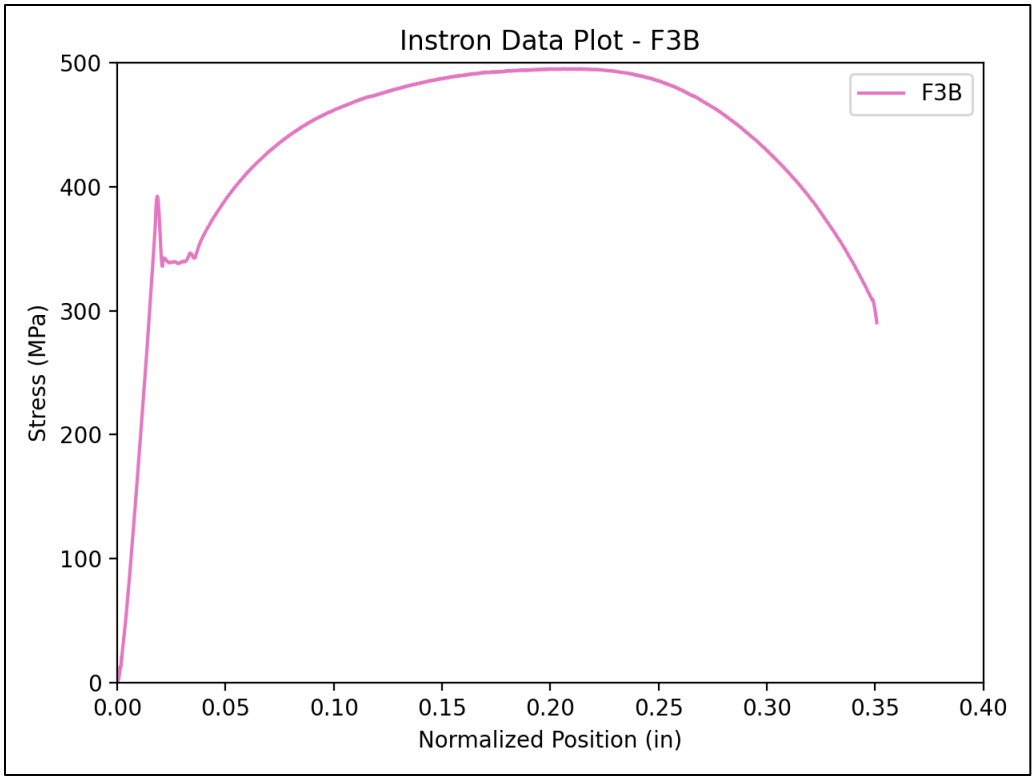
Instron Data Plot - F3B
F3B
Stress (MPa)
Normalized Position (in)
0
100
200
300
400
500
0.00
0.05
0.10
0.15
0.20
0.25
0.30
0.35
0.40

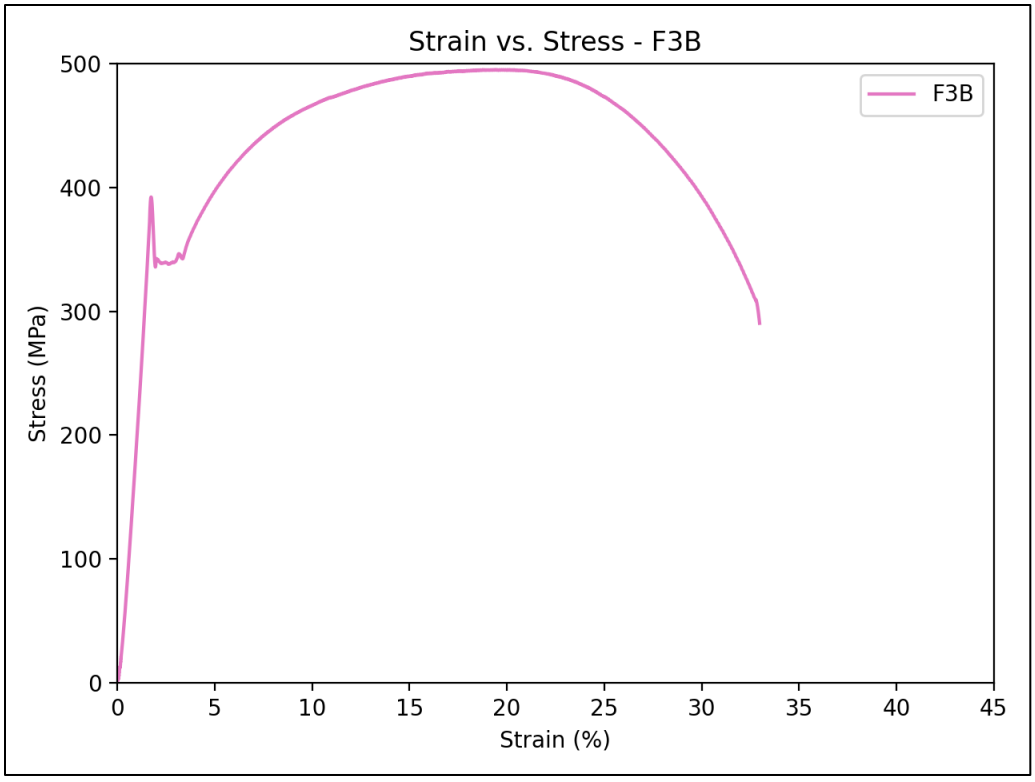
Strain vs. Stress - F3B
F3B
Stress (MPa)
Strain (%)
0
100
200
300
400
500
0
5
10
15
20
25
30
35
40
45

F3B

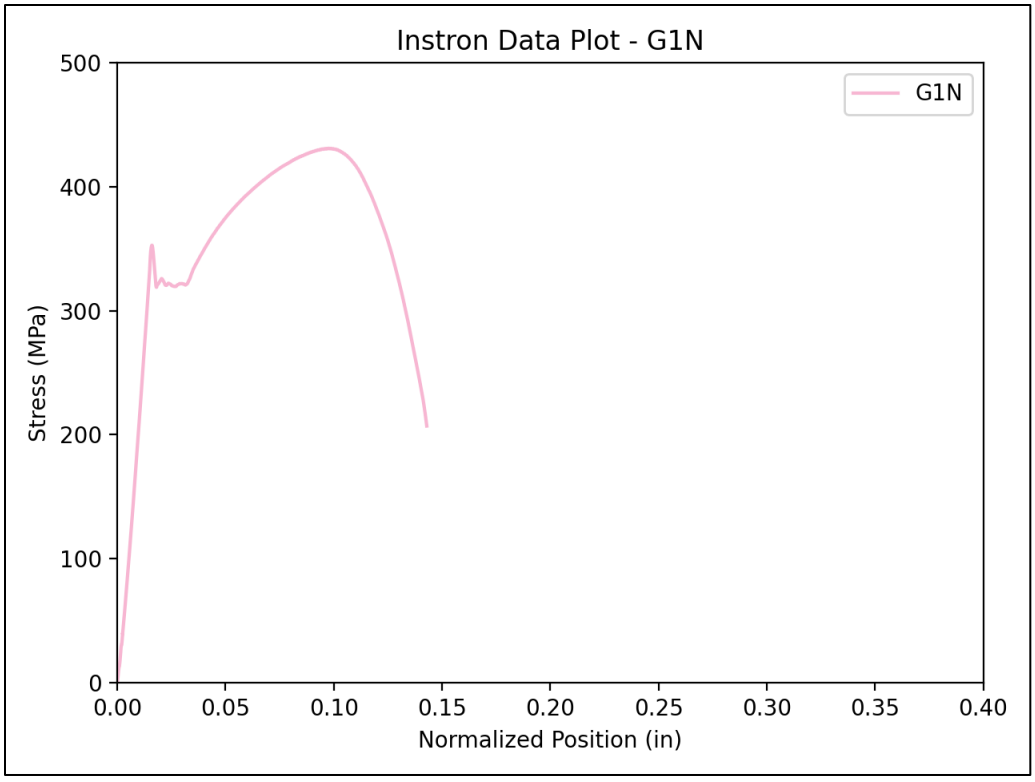
Instron Data Plot - G1N
G1N
Stress (MPa)
Normalized Position (in)
0
100
200
300
400
500
0.00
0.05
0.10
0.15
0.20
0.25
0.30
0.35
0.40

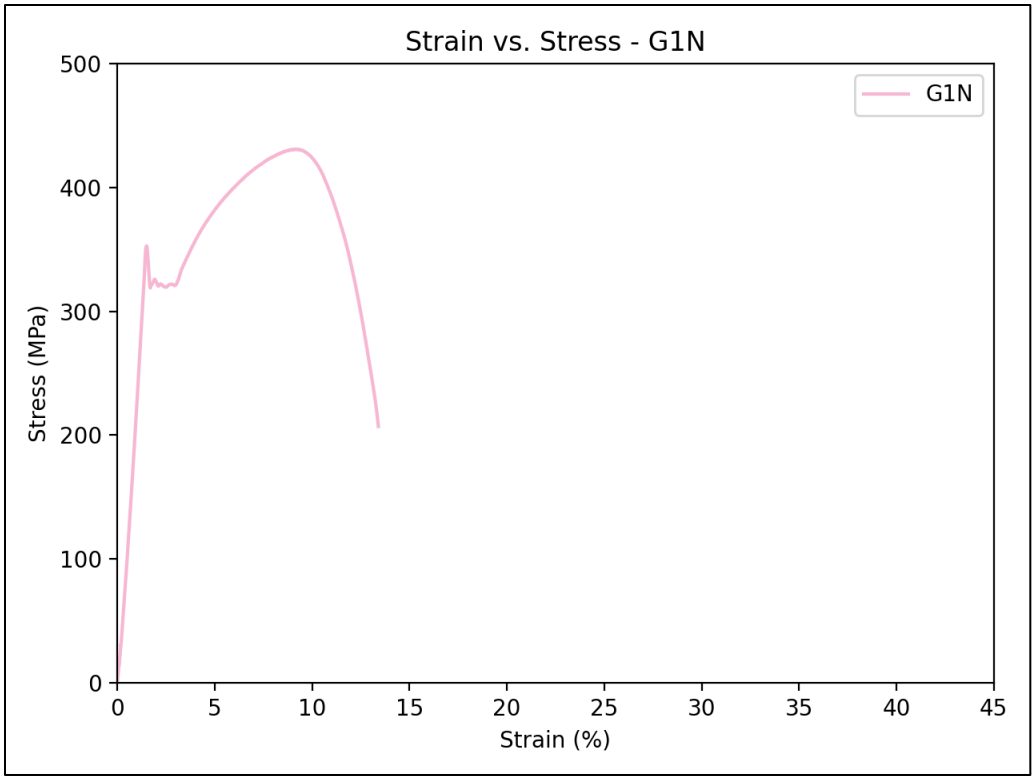
Strain vs. Stress - G1N
G1N
Stress (MPa)
Strain (%)
0
100
200
300
400
500
0
5
10
15
20
25
30
35
40
45

G1N

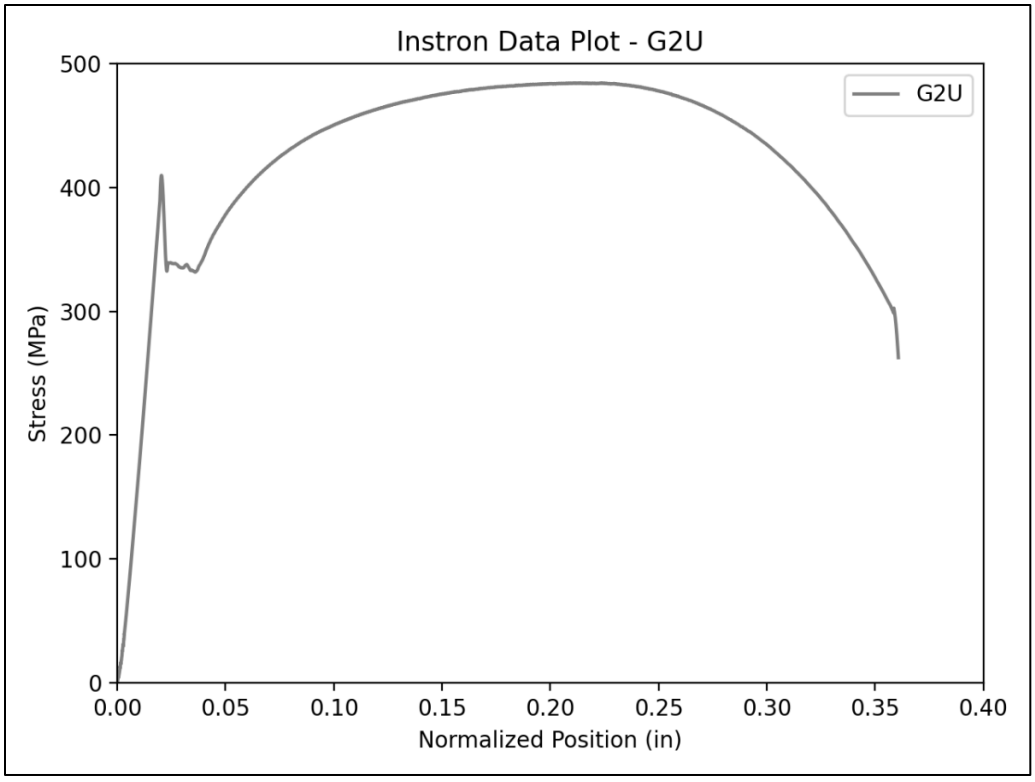
Instron Data Plot - G2U
G2U
Stress (MPa)
Normalized Position (in)
0
100
200
300
400
500
0.00
0.05
0.10
0.15
0.20
0.25
0.30
0.35
0.40

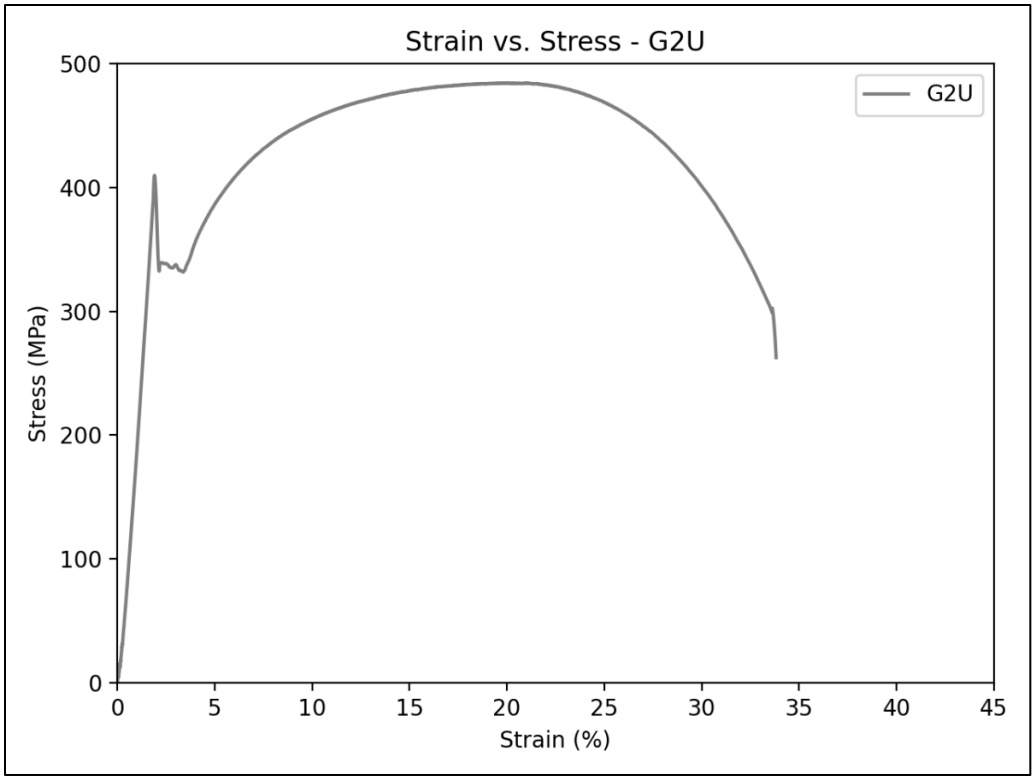
Strain vs. Stress - G2U
G2U
Stress (MPa)
Strain (%)
0
100
200
300
400
500
0
5
10
15
20
25
30
35
40
45

G2U

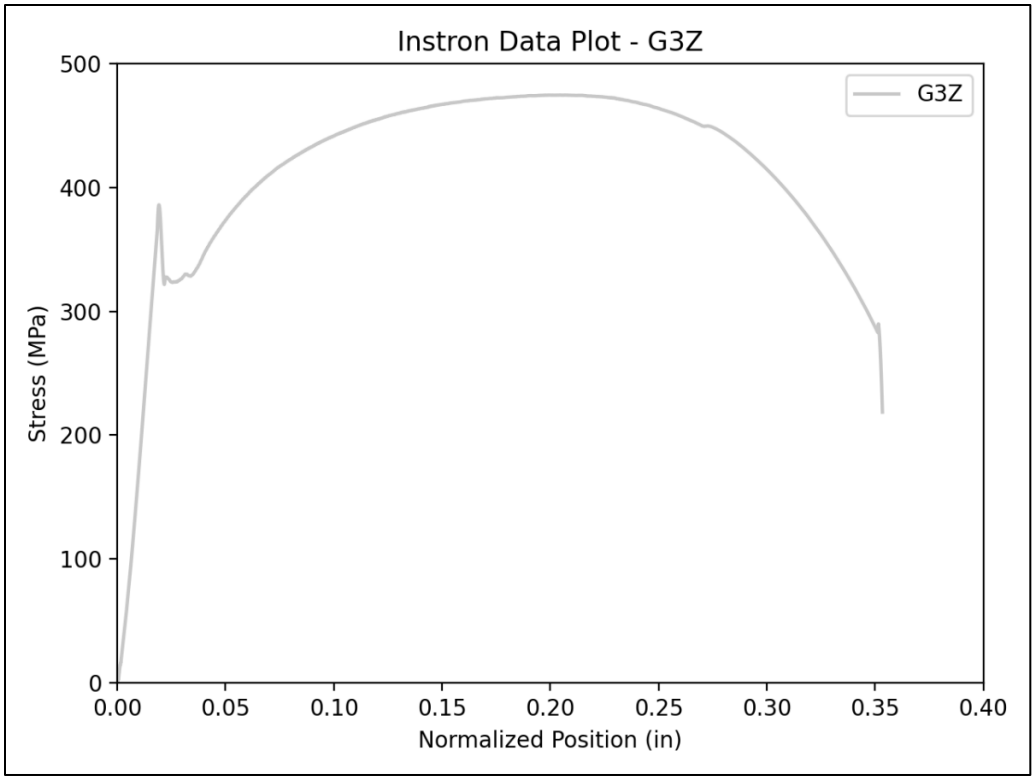
Instron Data Plot - G3Z
G3Z
Stress (MPa)
Normalized Position (in)
0
100
200
300
400
500
0.00
0.05
0.10
0.15
0.20
0.25
0.30
0.35
0.40

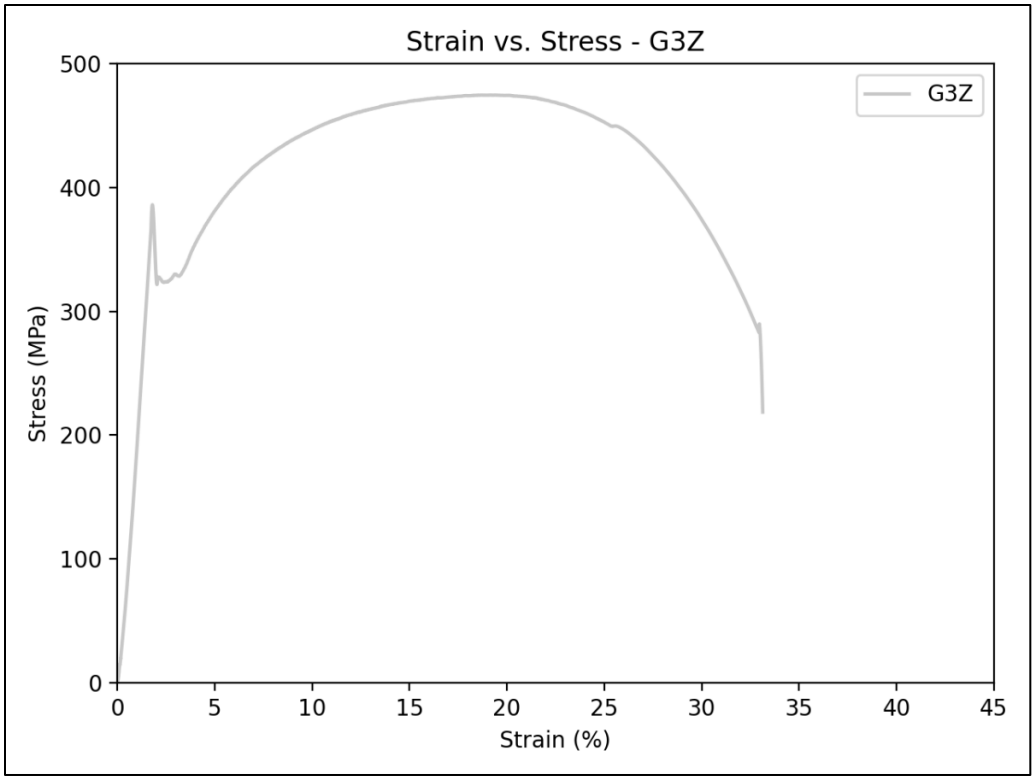
Strain vs. Stress - G3Z
G3Z
Stress (MPa)
Strain (%)
0
100
200
300
400
500
0
5
10
15
20
25
30
35
40
45

G3Z

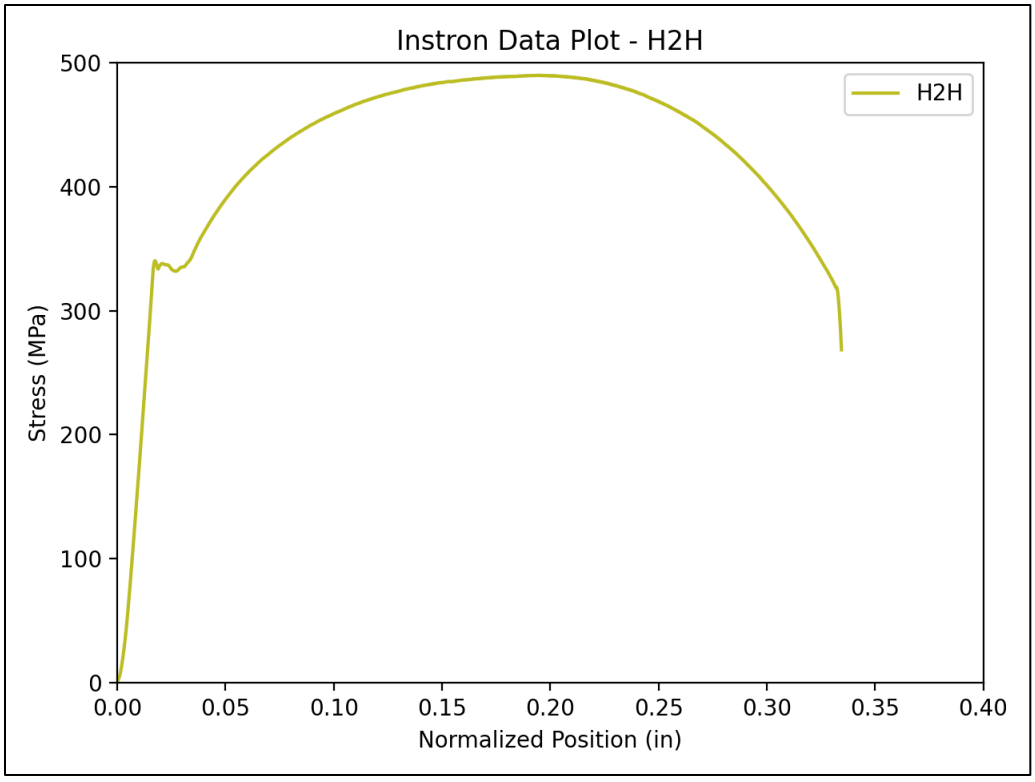
Instron Data Plot - H2H
H2H
Stress (MPa)
Normalized Position (in)
0
100
200
300
400
500
0.00
0.05
0.10
0.15
0.20
0.25
0.30
0.35
0.40

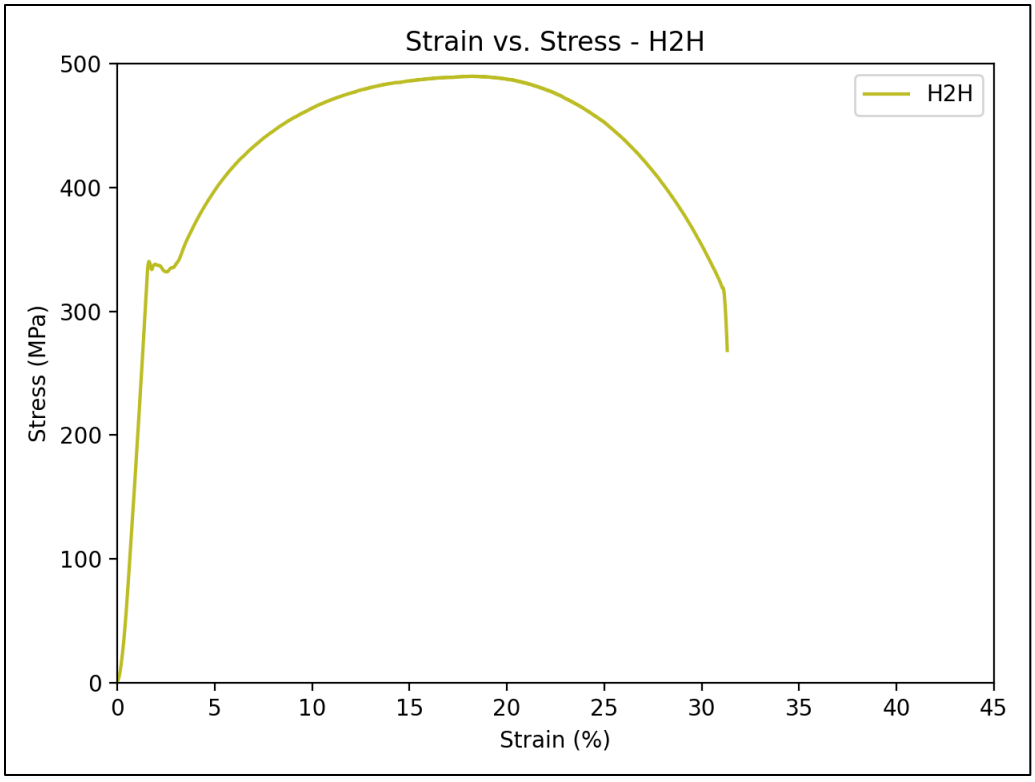
Strain vs. Stress - H2H
H2H
Stress (MPa)
Strain (%)
0
100
200
300
400
500
0
5
10
15
20
25
30
35
40
45

H2H

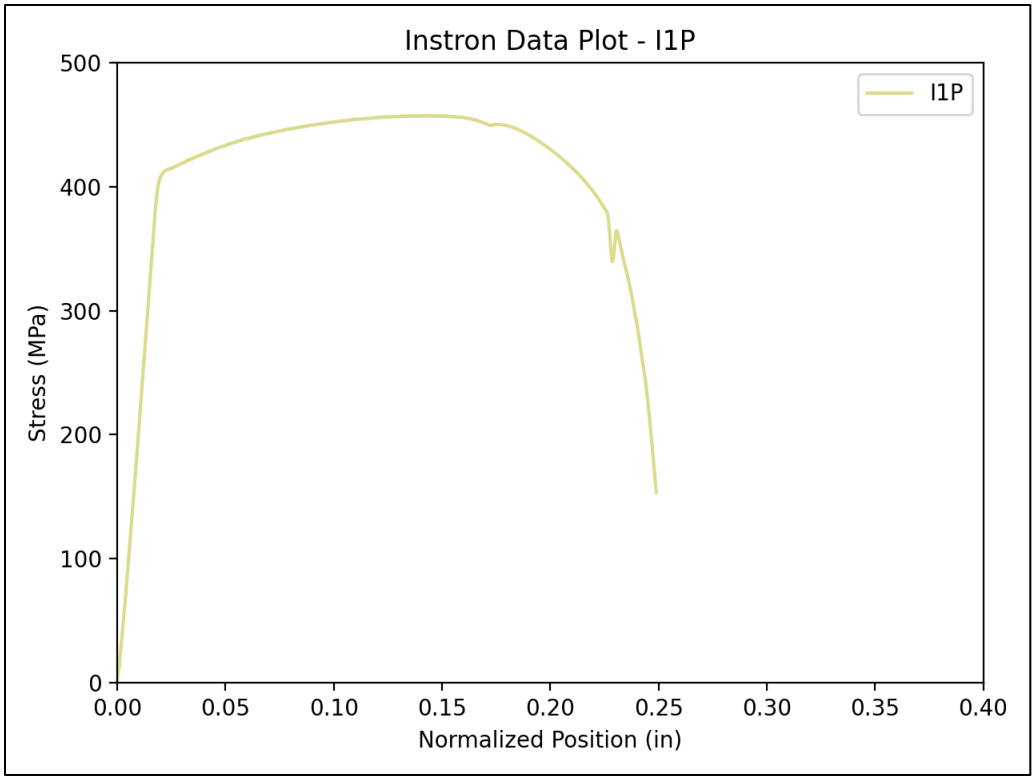
Instron Data Plot - I1P
I1P
Stress (MPa)
Normalized Position (in)
0
100
200
300
400
500
0.00
0.05
0.10
0.15
0.20
0.25
0.30
0.35
0.40

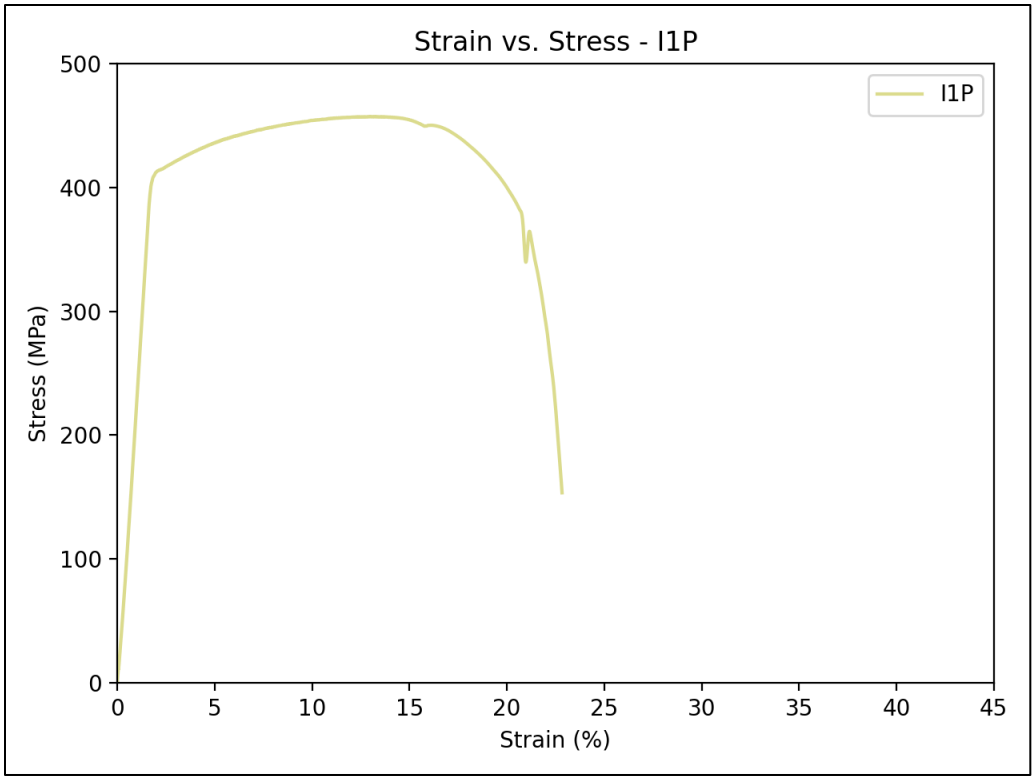
Strain vs. Stress - I1P
I1P
Stress (MPa)
Strain (%)
0
100
200
300
400
500
0
5
10
15
20
25
30
35
40
45

I1P

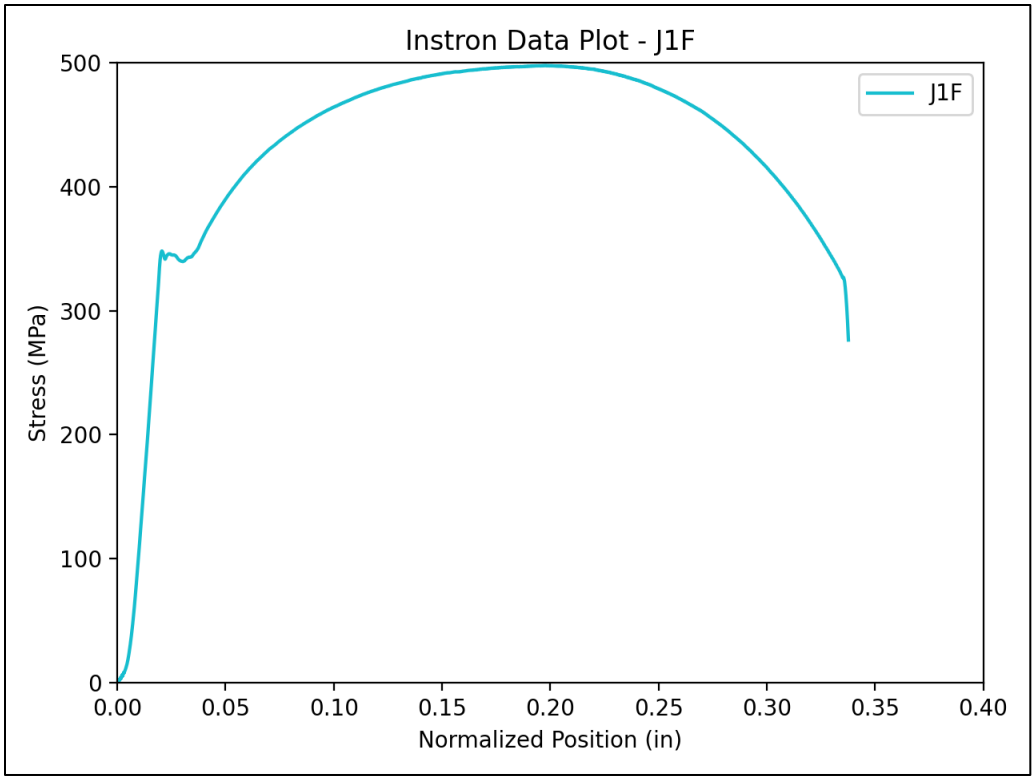
Instron Data Plot - J1F
J1F
Stress (MPa)
Normalized Position (in)
0
100
200
300
400
500
0.00
0.05
0.10
0.15
0.20
0.25
0.30
0.35
0.40

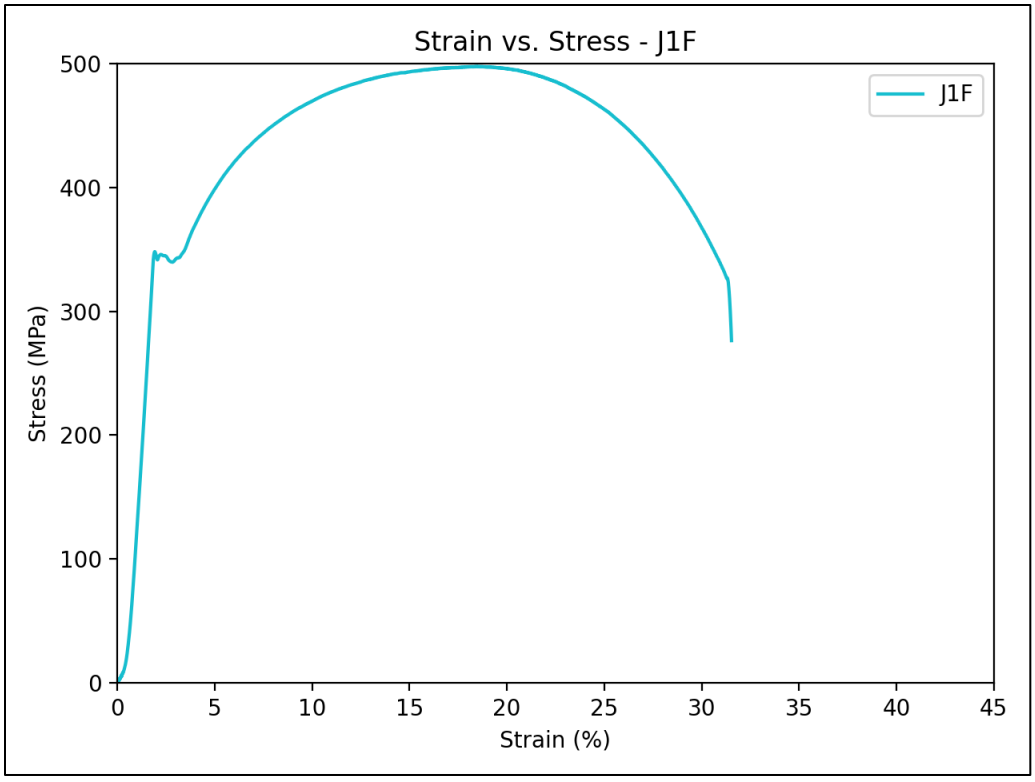
Strain vs. Stress - J1F
J1F
Stress (MPa)
Strain (%)
0
100
200
300
400
500
0
5
10
15
20
25
30
35
40
45

J1F

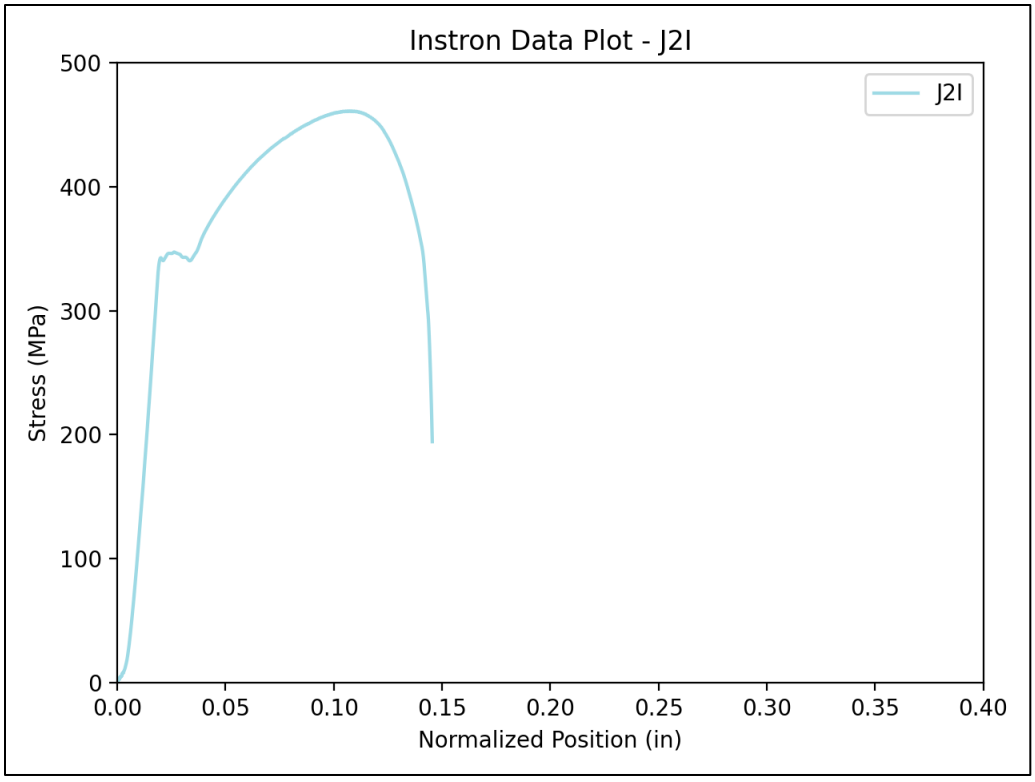
Instron Data Plot - J2I
J2I
Stress (MPa)
Normalized Position (in)
0
100
200
300
400
500
0.00
0.05
0.10
0.15
0.20
0.25
0.30
0.35
0.40

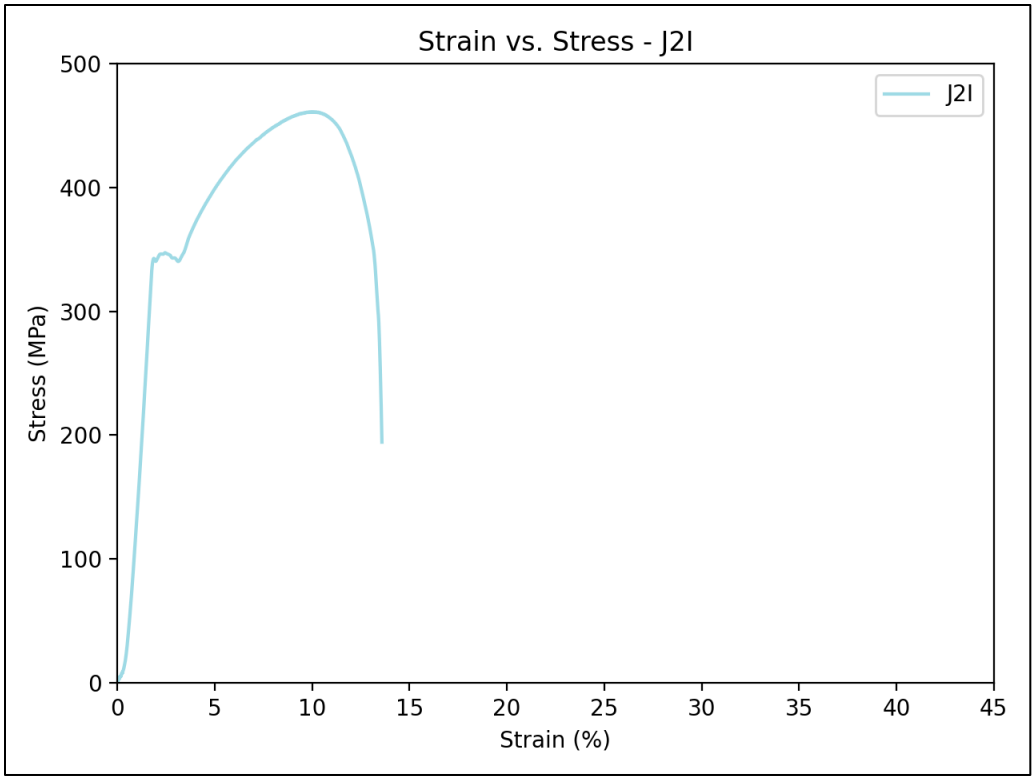
Strain vs. Stress - J2I
J2I
Stress (MPa)
Strain (%)
0
100
200
300
400
500
0
5
10
15
20
25
30
35
40
45

J2I

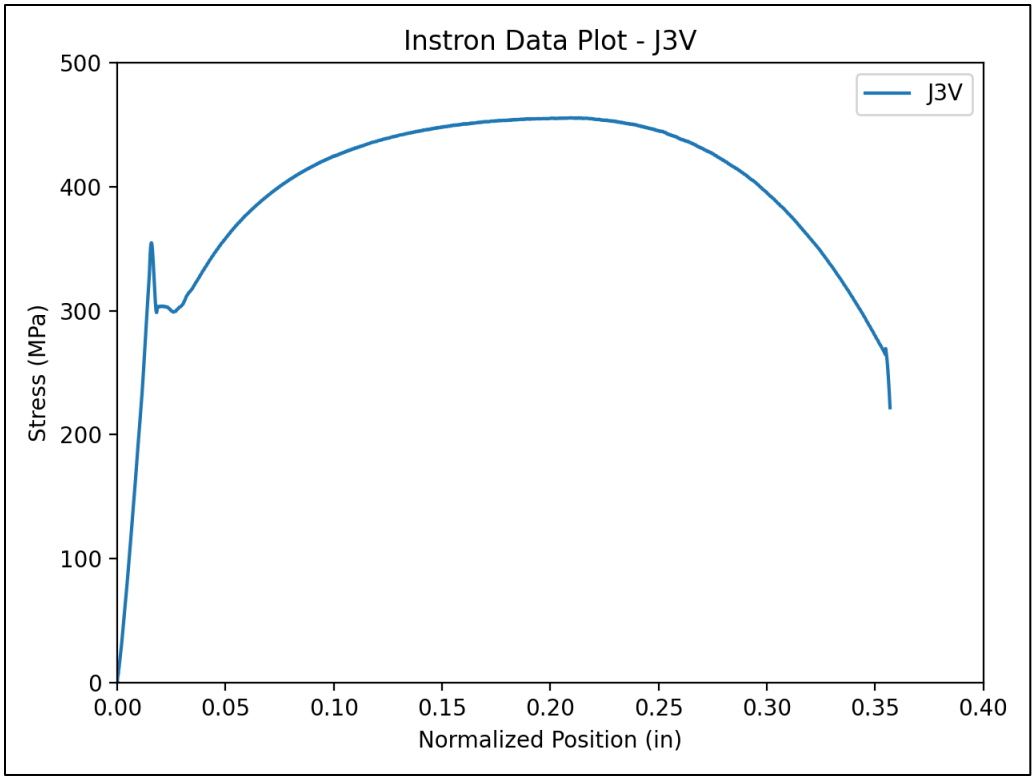
Instron Data Plot - J3V
J3V
Stress (MPa)
Normalized Position (in)
0
100
200
300
400
500
0.00
0.05
0.10
0.15
0.20
0.25
0.30
0.35
0.40

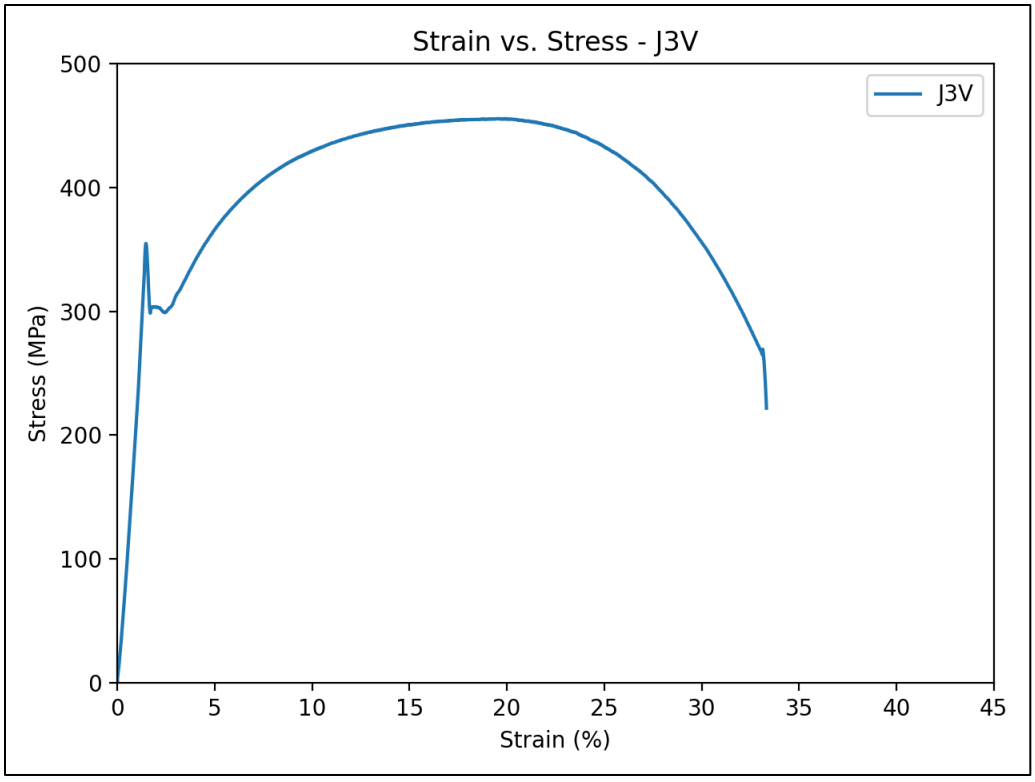
Strain vs. Stress - J3V
J3V
Stress (MPa)
Strain (%)
0
100
200
300
400
500
0
5
10
15
20
25
30
35
40
45

J3V

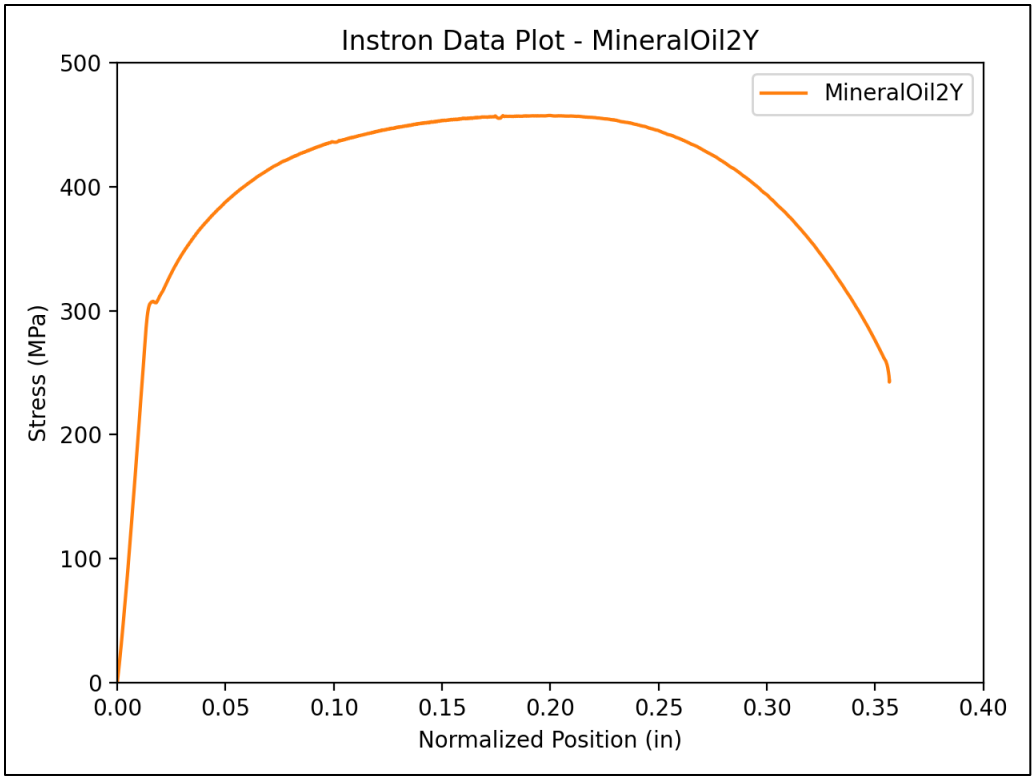

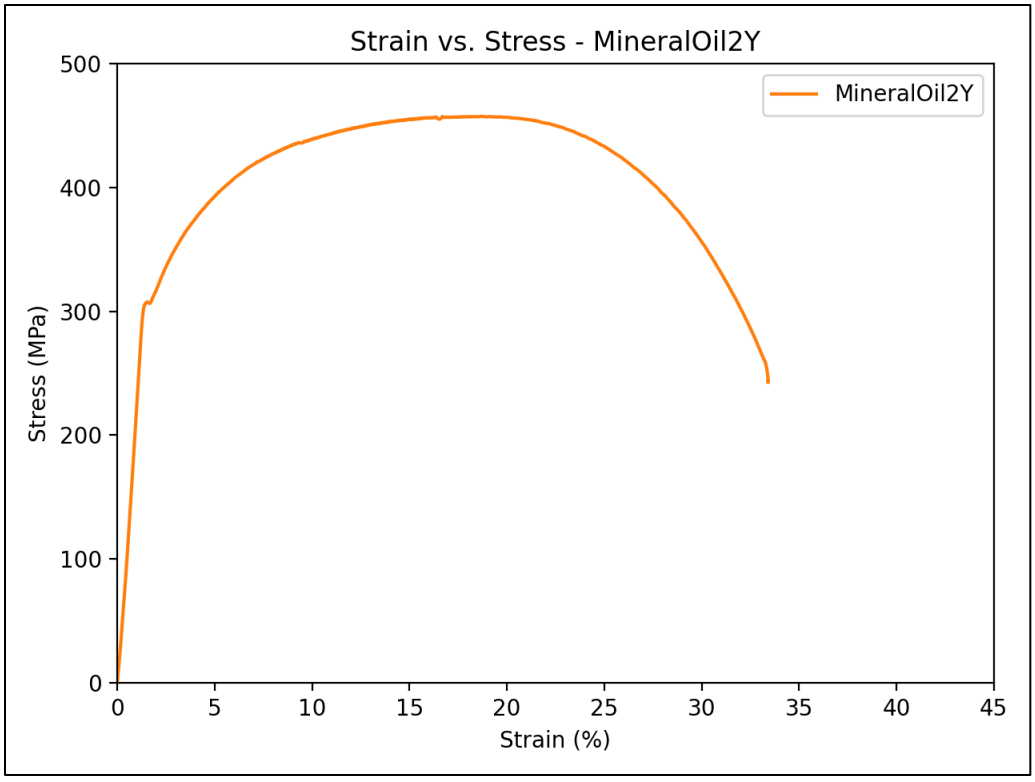

Mineral Oil Test 2

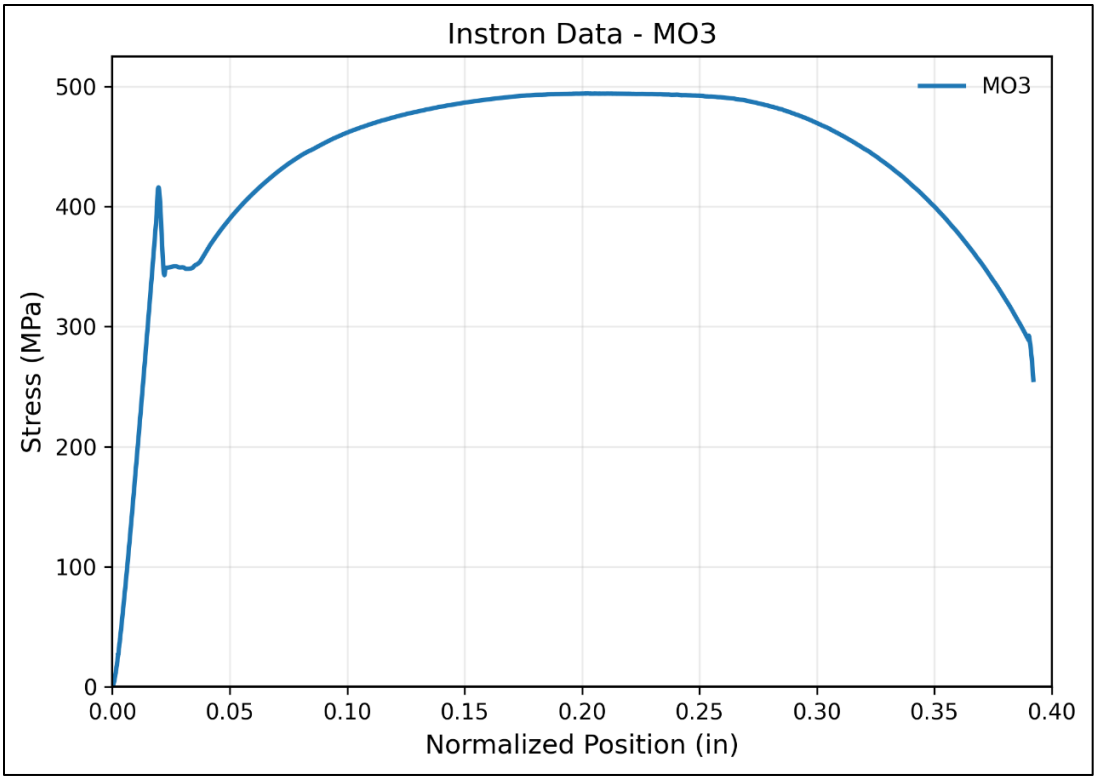

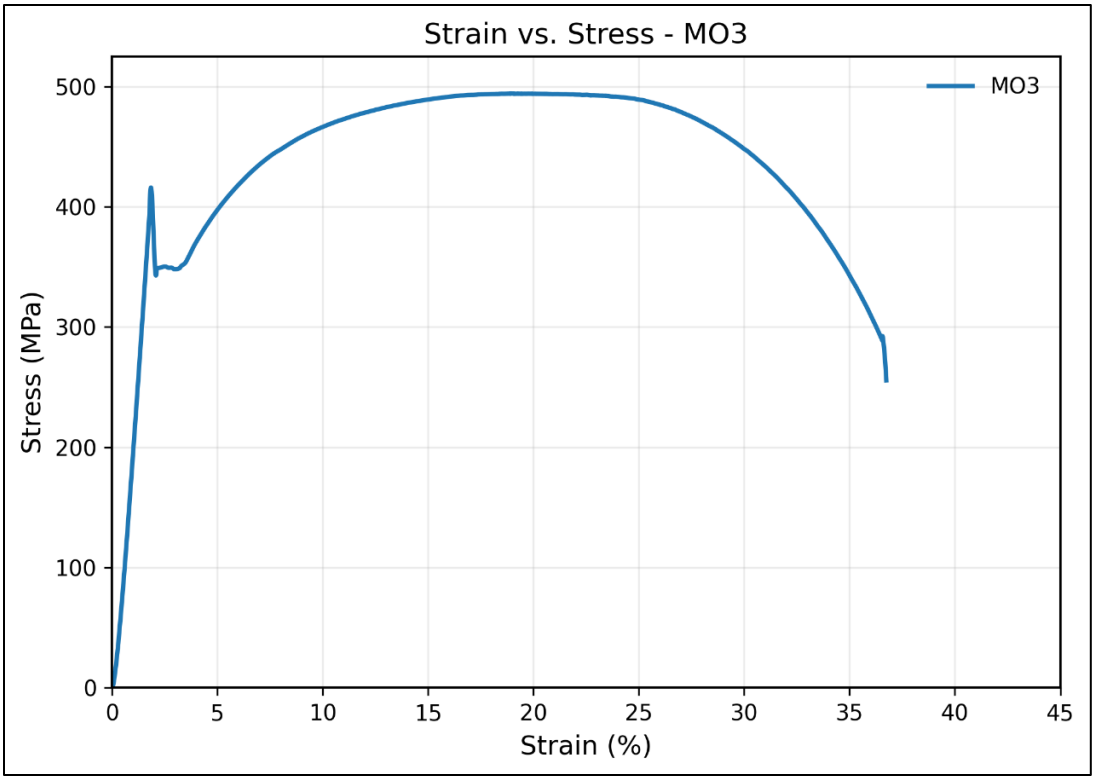

Mineral Oil Test 3

A.3 24 Hour Open Circuit Potential Measurement

This section shows the 24 hour OCP vs. time plots for each simulant. The reference electrode that was utilized was the Saturated Calomel Electrode (SCE).

Savitzky–Golay filter was used to smooth data by fitting a polynomial of a designated order, p, via least-squares fitting within a sliding window of length w. For each data point (x_i, y_i) the polynomial $P_{w,p}\ (x)$ is fitted to the window of data point in Equation 2.

$$\widehat{y_i} = P_{w,p}(x_i) \quad \textbf{2}$$

To select fitting parameters w and p for each dataset, a weighted objective function of residual variance, $R = \frac{MAD(y-\hat{y})}{MAD(y)}$, and proportion of variance explained, $V = \frac{MAD(y)-MAD(\hat{y})}{MAD(y)}$, where MAD is the median absolute deviation, and was minimized based on the weighting of, J in Equation 3.

$$J = R + \beta V \quad \textbf{3}$$

The value of β was set to 0.1 to provide adequate noise suppression without overly smoothing the data. By iterating over candidate values of p and w, a combination that minimizes J was selected. Samples A4Q and A5R below are shown as examples of the raw OCP data and the filtered plots using this process.

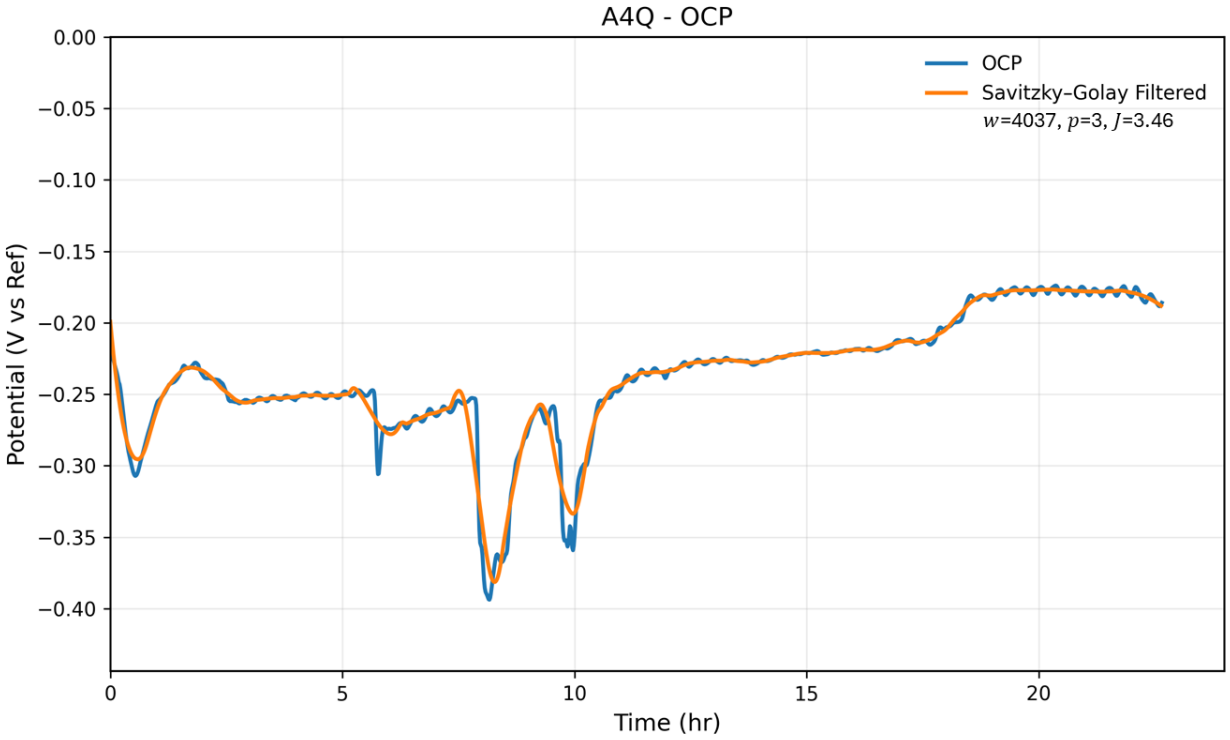

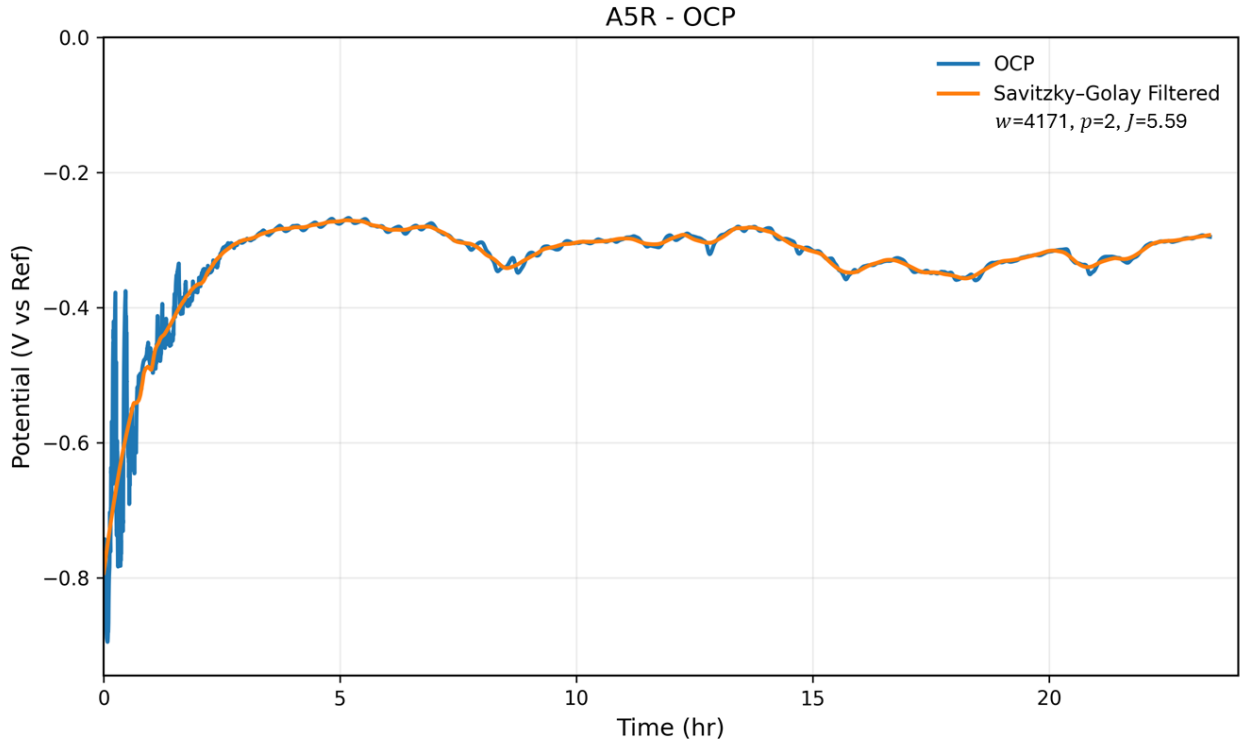
A5R - OCP
OCP
Savitzky–Golay Filtered
w=4171, p=2, J=5.59
Potential (V vs Ref)
Time (hr)
0.0
−0.2
−0.4
−0.6
−0.8
0
5
10
15
20

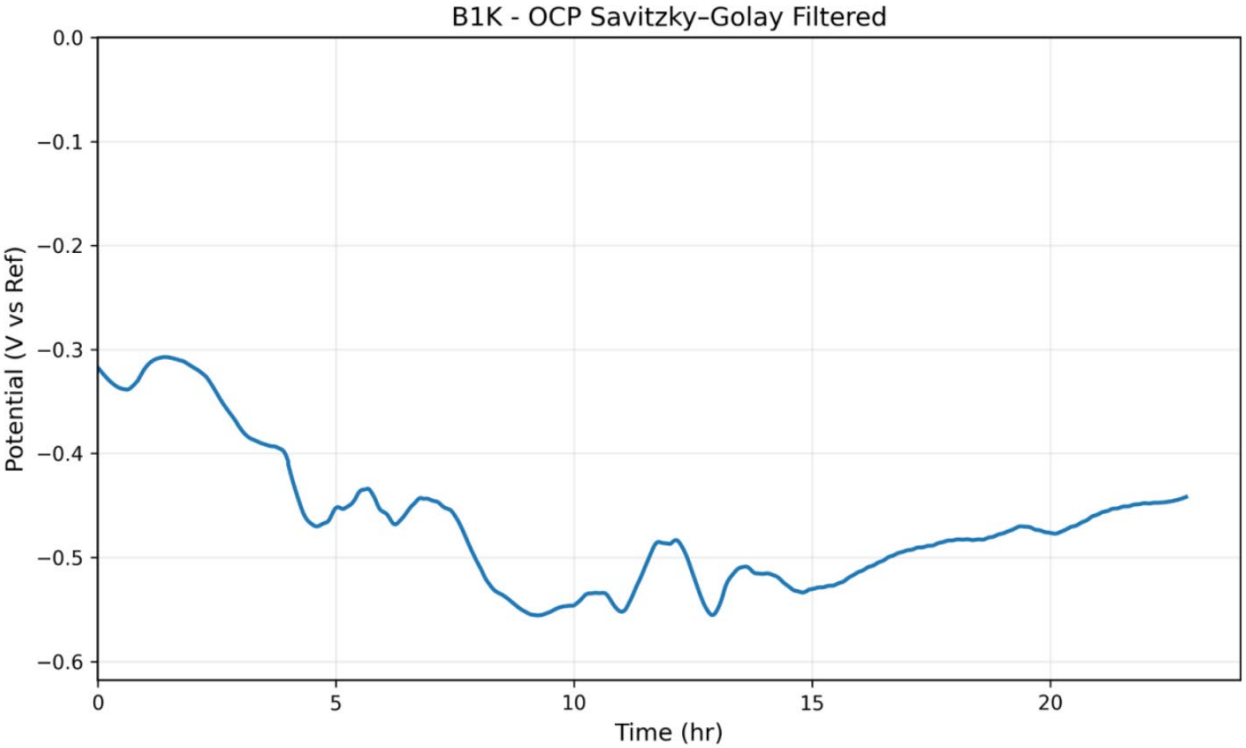
B1K - OCP Savitzky–Golay Filtered
Potential (V vs Ref)
Time (hr)
0.0
−0.1
−0.2
−0.3
−0.4
−0.5
−0.6
0
5
10
15
20

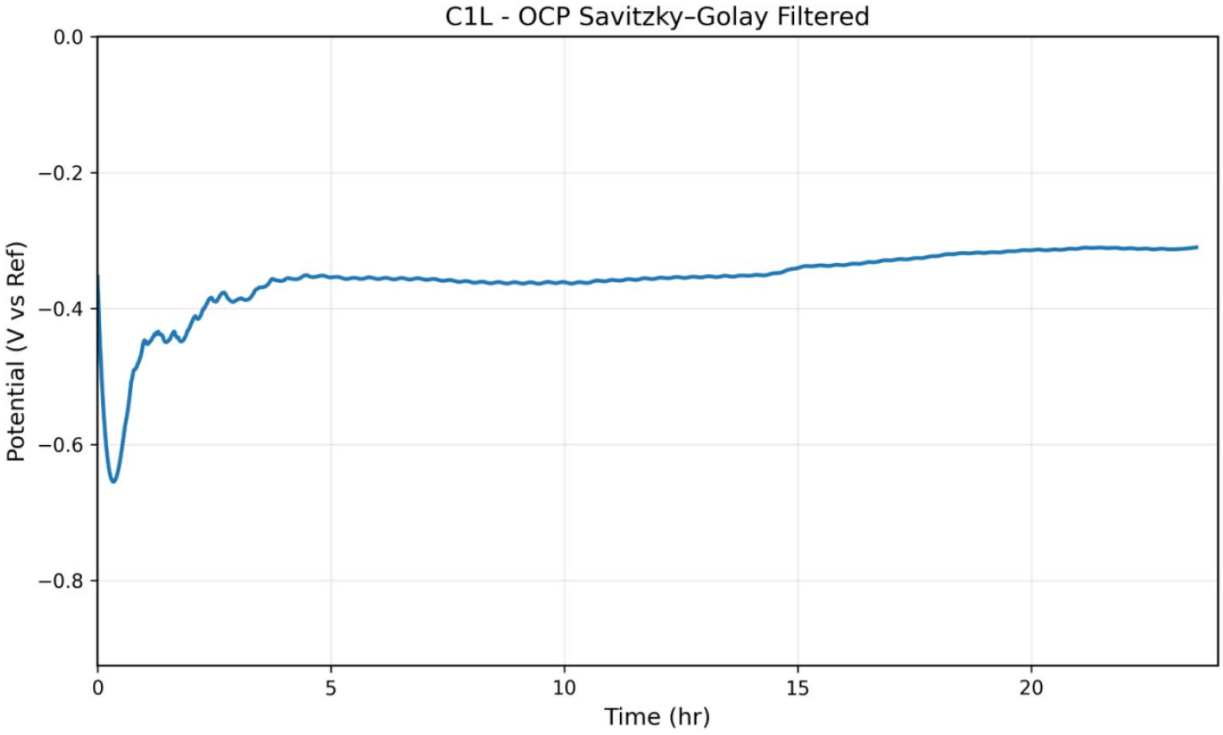
C1L - OCP Savitzky–Golay Filtered
Potential (V vs Ref)
0.0
−0.2
−0.4
−0.6
−0.8
0
5
10
15
20
Time (hr)

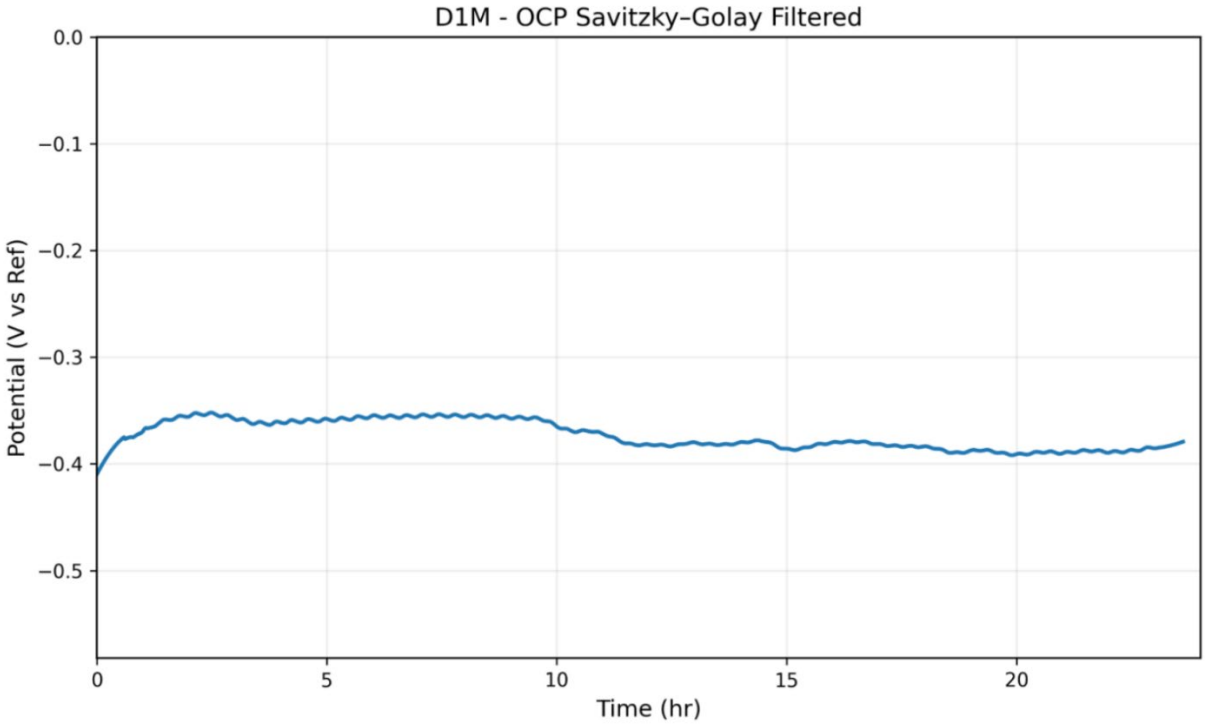
D1M - OCP Savitzky–Golay Filtered
Potential (V vs Ref)
0.0
−0.1
−0.2
−0.3
−0.4
−0.5
0
5
10
15
20
Time (hr)

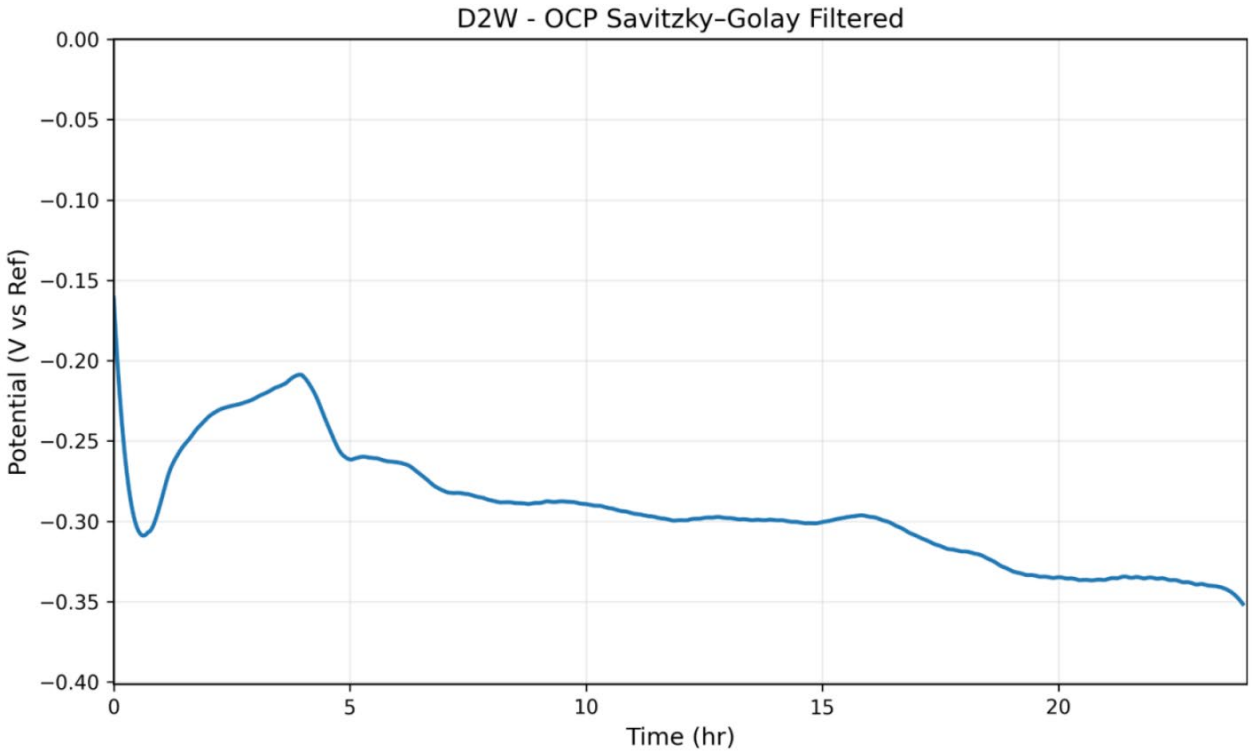
D2W - OCP Savitzky–Golay Filtered
Potential (V vs Ref)
0.00
−0.05
−0.10
−0.15
−0.20
−0.25
−0.30
−0.35
−0.40
0
5
10
15
20
Time (hr)

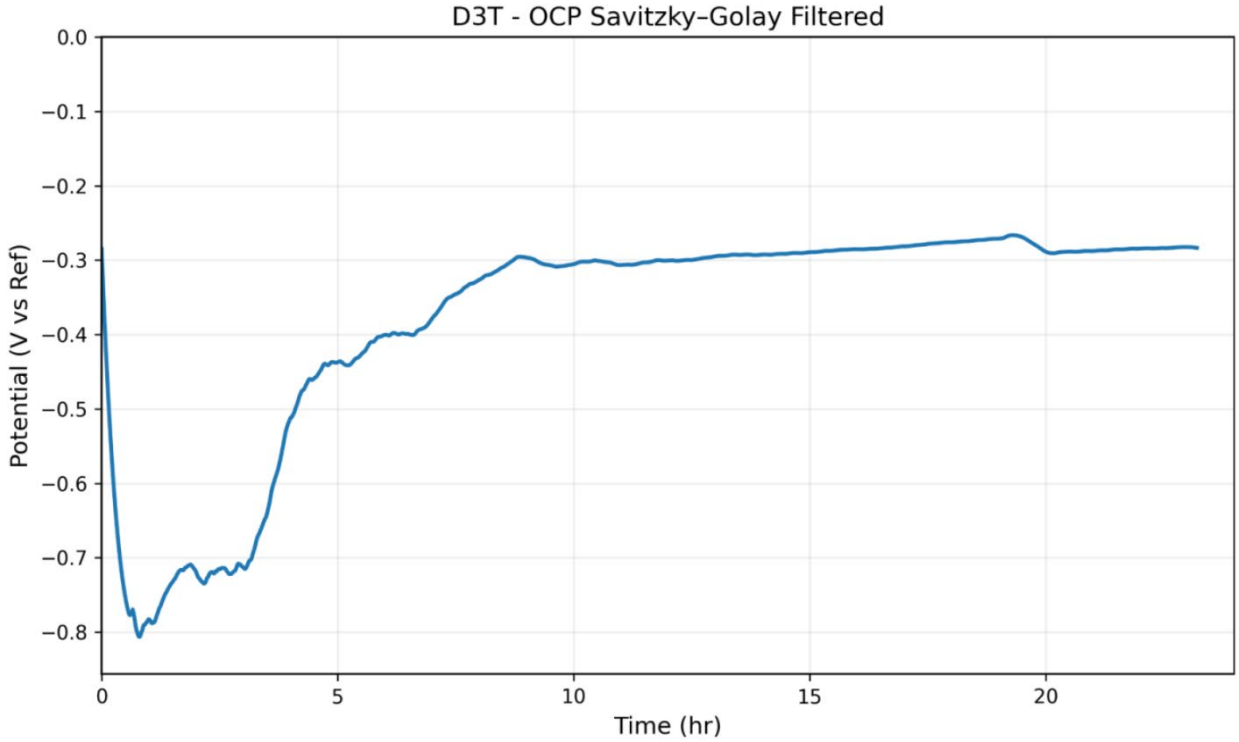
D3T - OCP Savitzky–Golay Filtered
Potential (V vs Ref)
0.0
−0.1
−0.2
−0.3
−0.4
−0.5
−0.6
−0.7
−0.8
0
5
10
15
20
Time (hr)

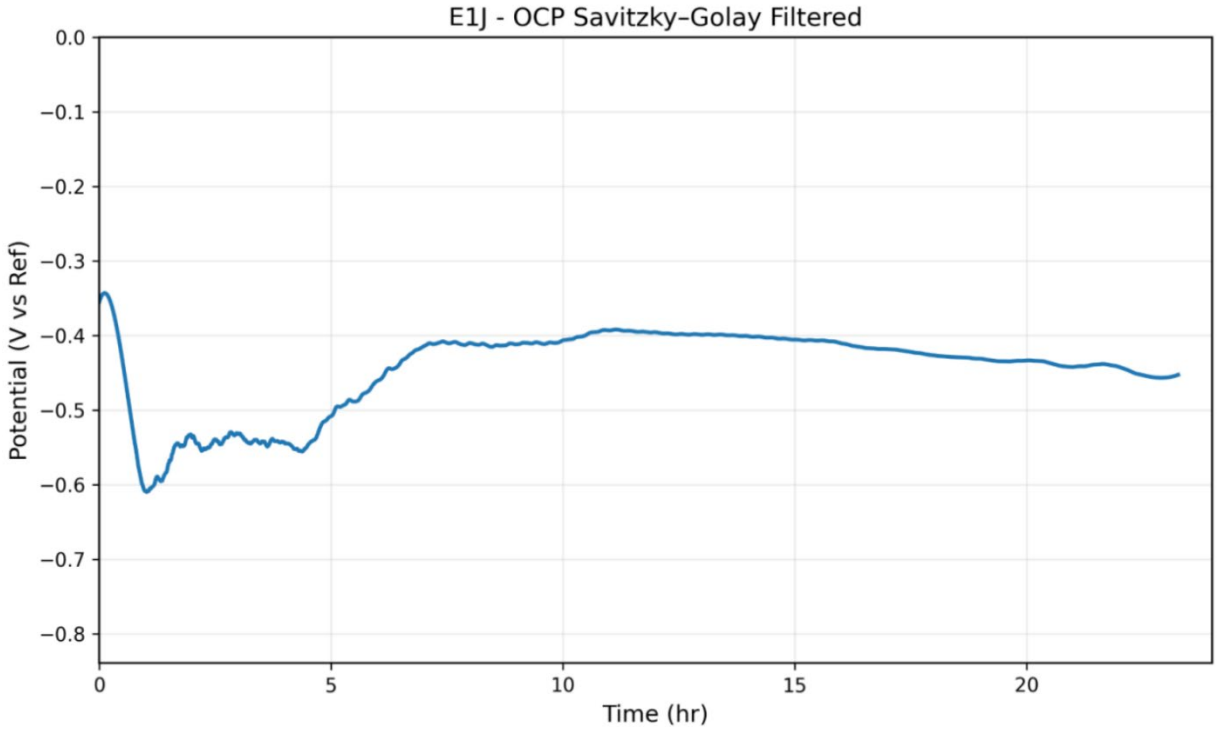
E1J - OCP Savitzky–Golay Filtered
Potential (V vs Ref)
0.0
−0.1
−0.2
−0.3
−0.4
−0.5
−0.6
−0.7
−0.8
0
5
10
15
20
Time (hr)

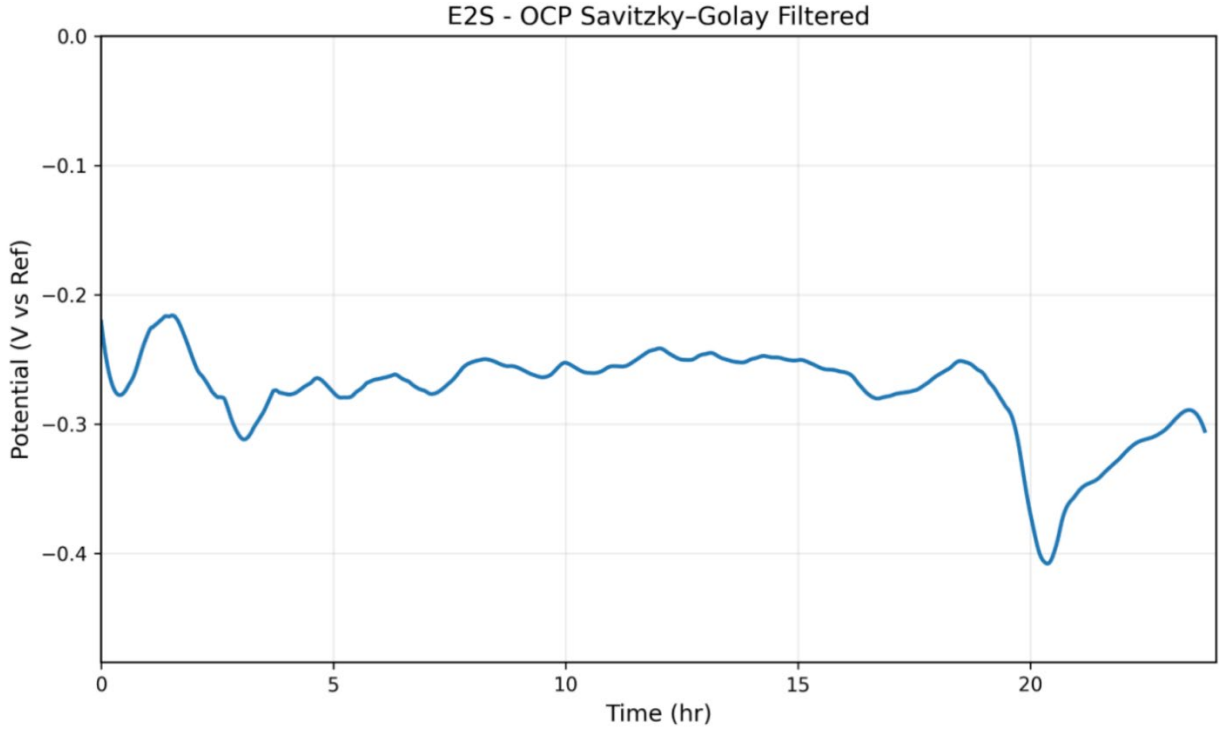
E2S - OCP Savitzky–Golay Filtered
Potential (V vs Ref)
0.0
−0.1
−0.2
−0.3
−0.4
0
5
10
15
20
Time (hr)

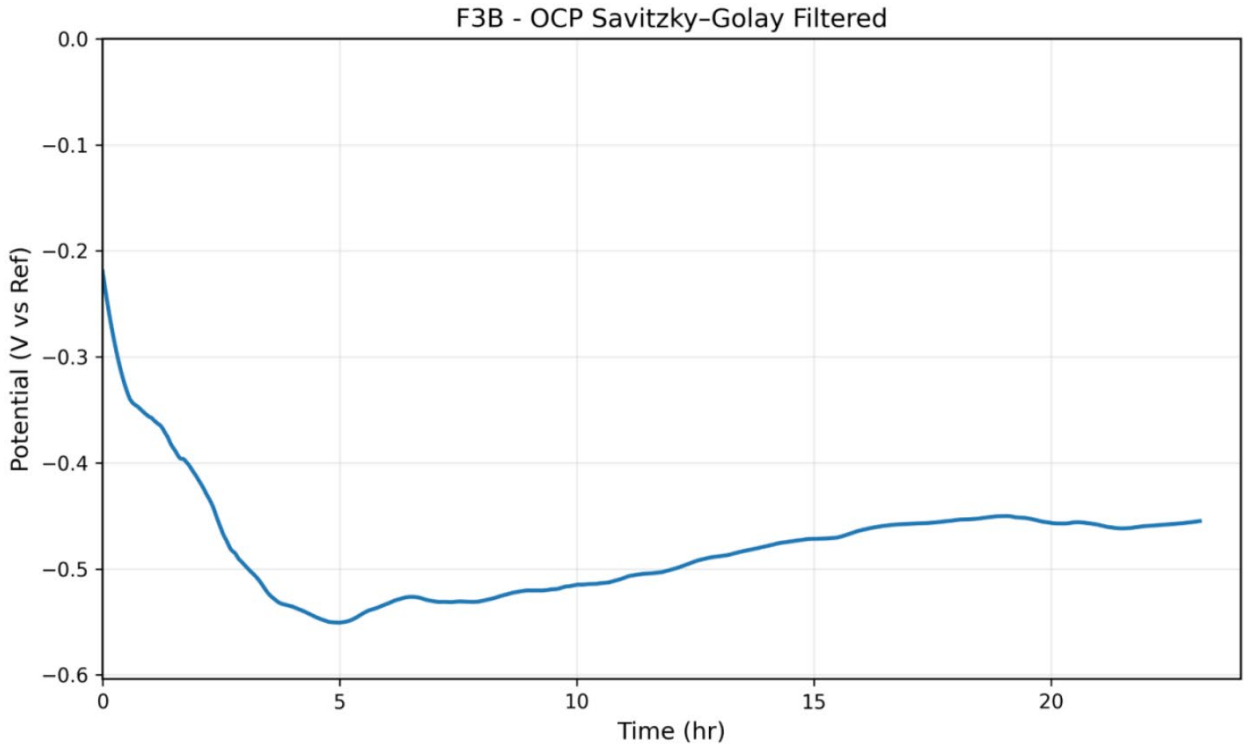
F3B - OCP Savitzky–Golay Filtered
Potential (V vs Ref)
Time (hr)
0.0
−0.1
−0.2
−0.3
−0.4
−0.5
−0.6
0
5
10
15
20

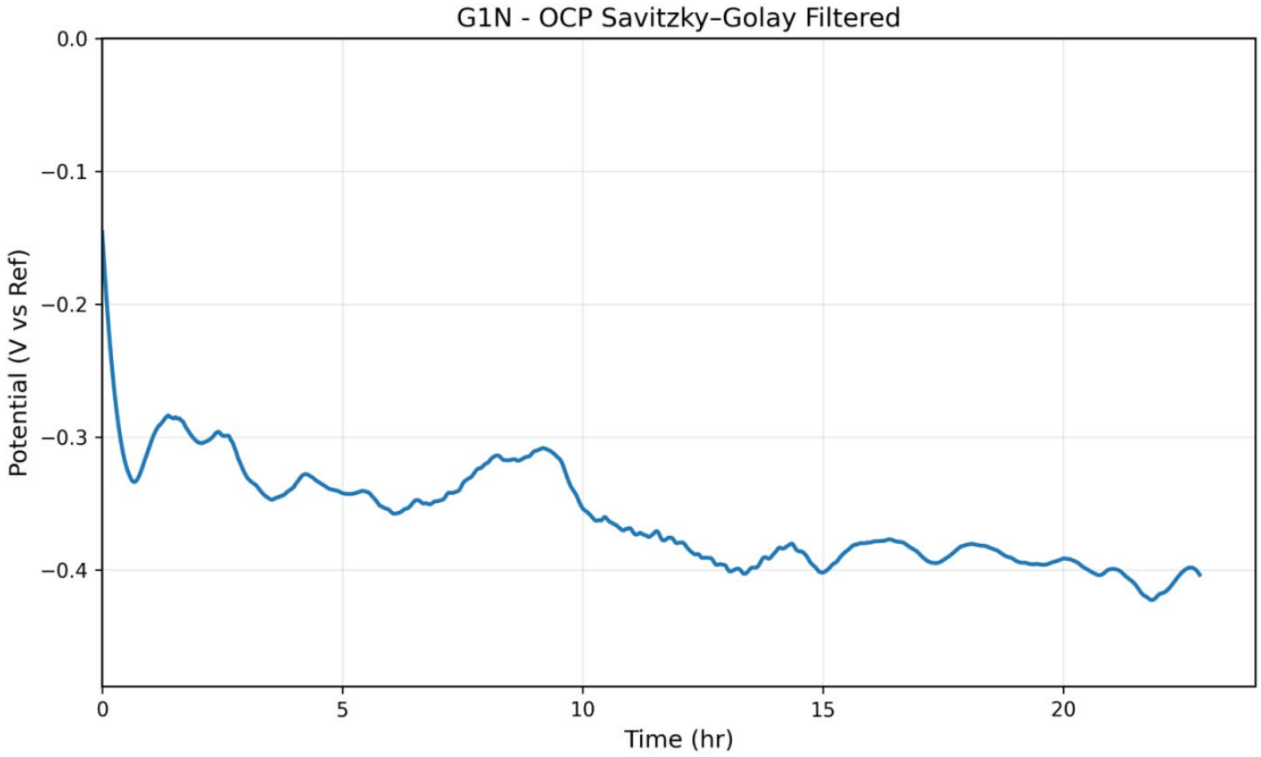
G1N - OCP Savitzky–Golay Filtered
Potential (V vs Ref)
Time (hr)
0.0
−0.1
−0.2
−0.3
−0.4
0
5
10
15
20

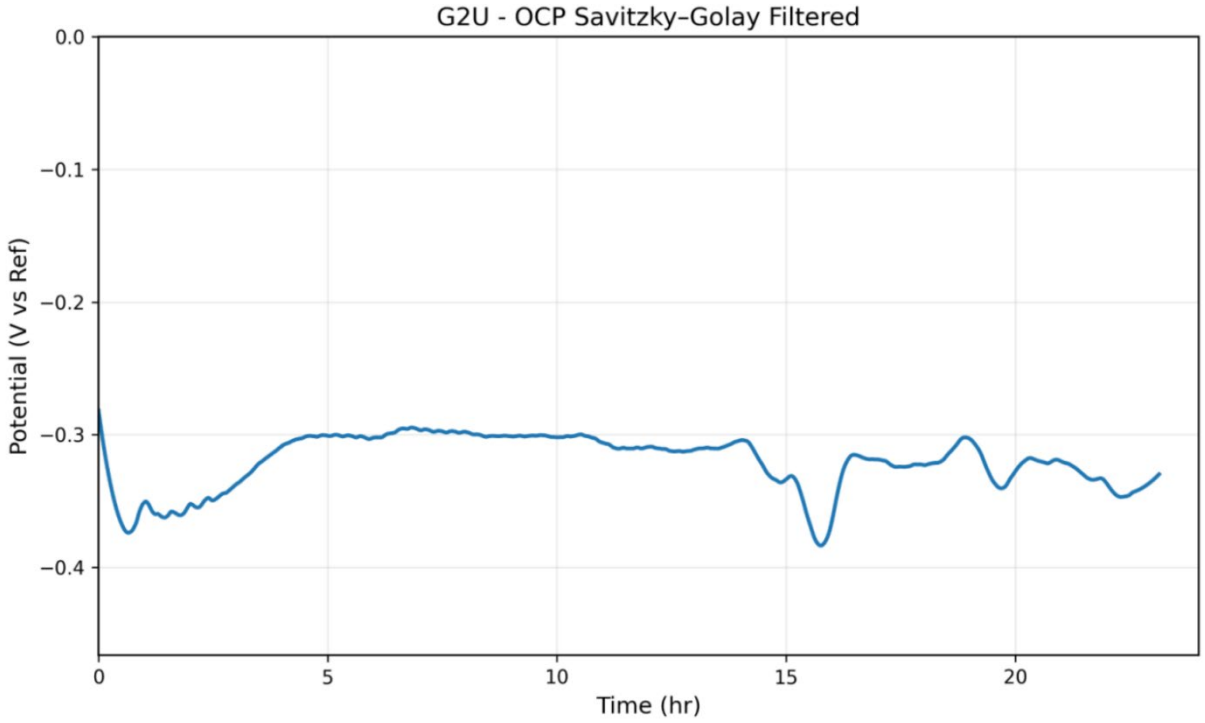
G2U - OCP Savitzky–Golay Filtered
Potential (V vs Ref)
0.0
−0.1
−0.2
−0.3
−0.4
0
5
10
15
20
Time (hr)

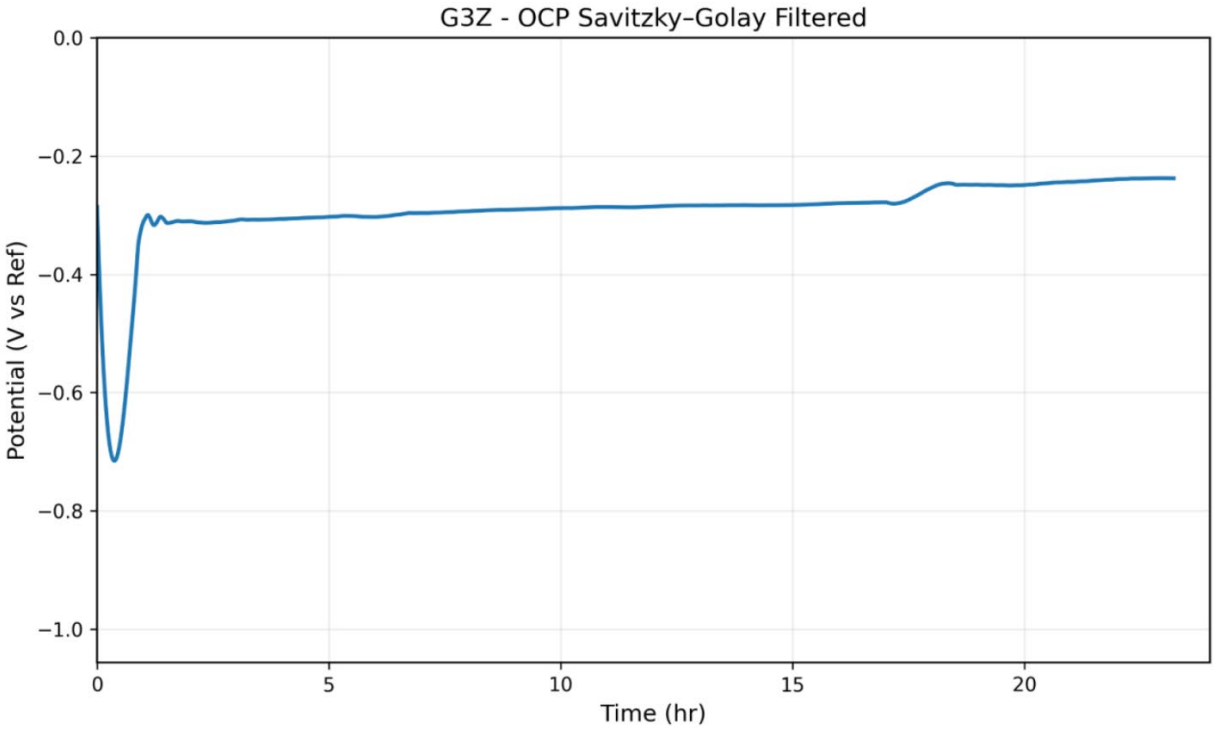
G3Z - OCP Savitzky–Golay Filtered
Potential (V vs Ref)
0.0
−0.2
−0.4
−0.6
−0.8
−1.0
0
5
10
15
20
Time (hr)

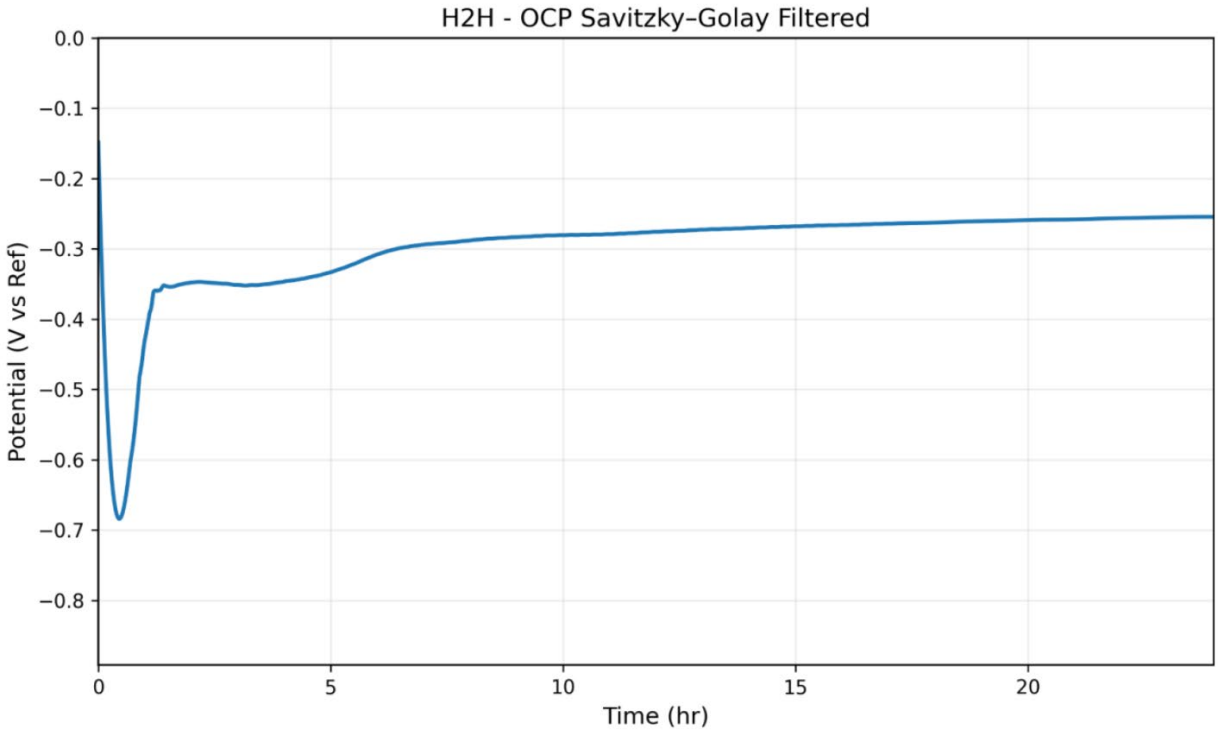
H2H - OCP Savitzky–Golay Filtered
Potential (V vs Ref)
0.0
−0.1
−0.2
−0.3
−0.4
−0.5
−0.6
−0.7
−0.8
0
5
10
15
20
Time (hr)

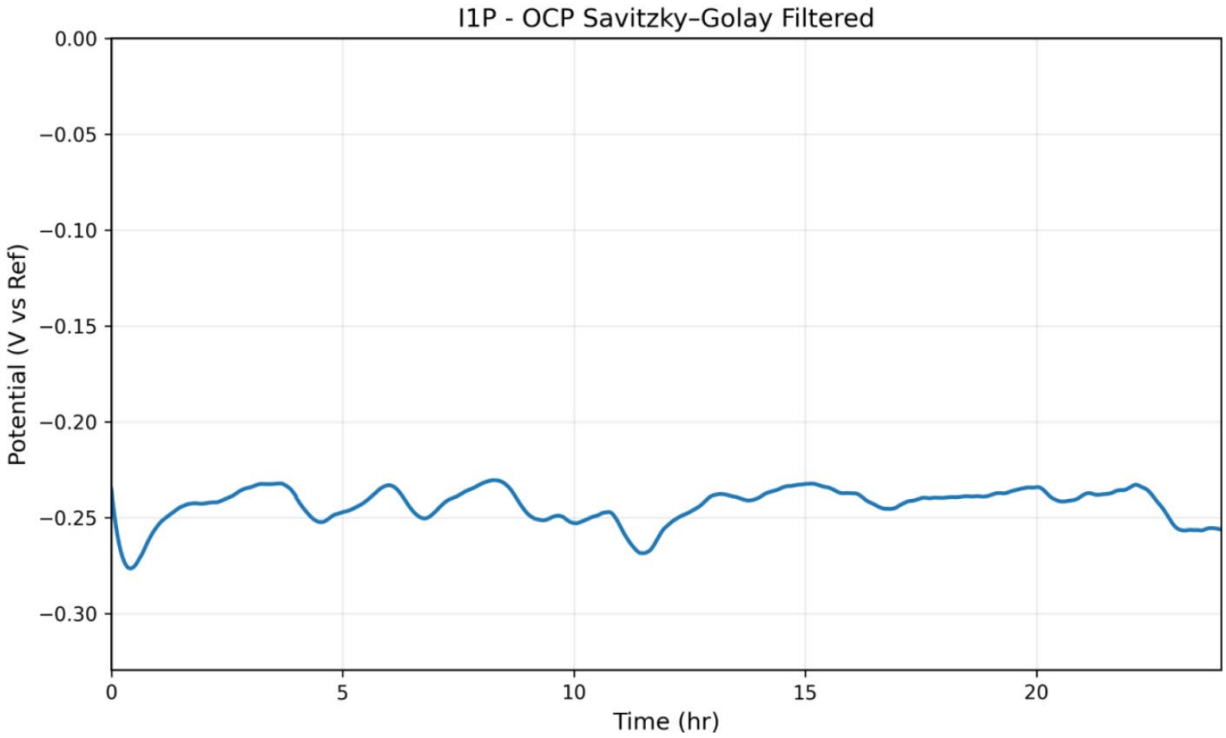
I1P - OCP Savitzky–Golay Filtered
Potential (V vs Ref)
0.00
−0.05
−0.10
−0.15
−0.20
−0.25
−0.30
0
5
10
15
20
Time (hr)

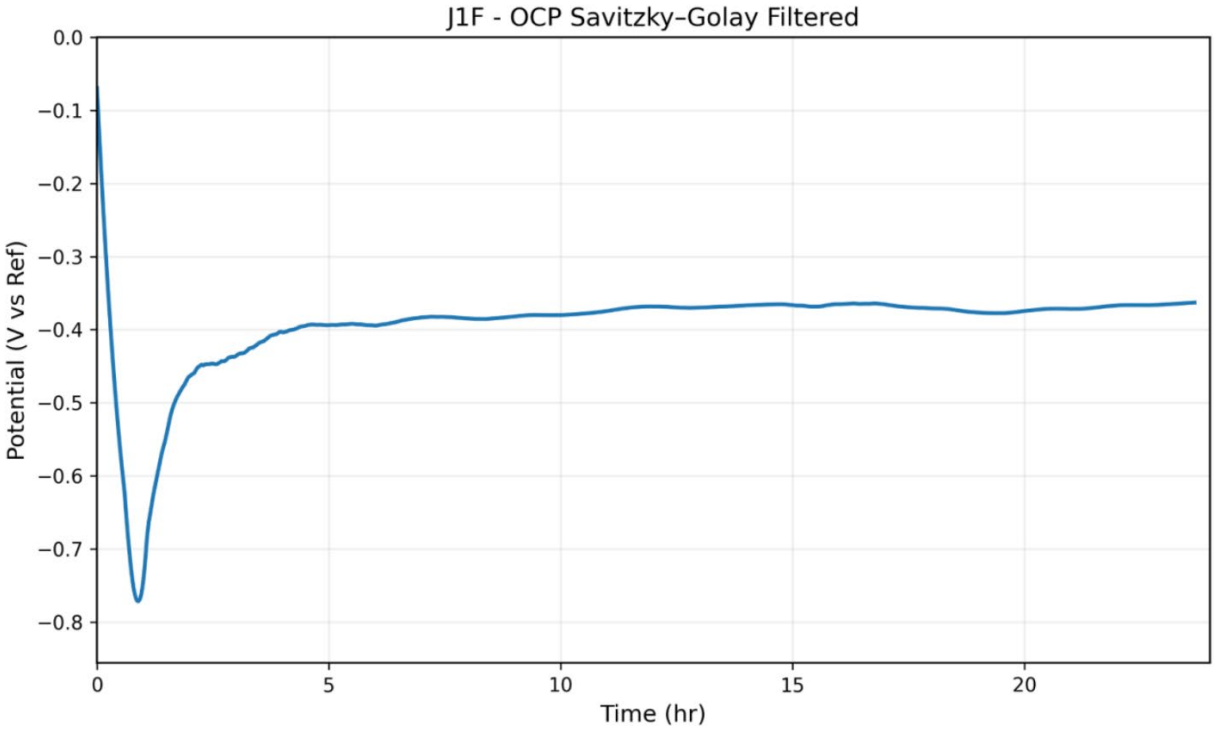
J1F - OCP Savitzky–Golay Filtered
Potential (V vs Ref)
0.0
−0.1
−0.2
−0.3
−0.4
−0.5
−0.6
−0.7
−0.8
0
5
10
15
20
Time (hr)

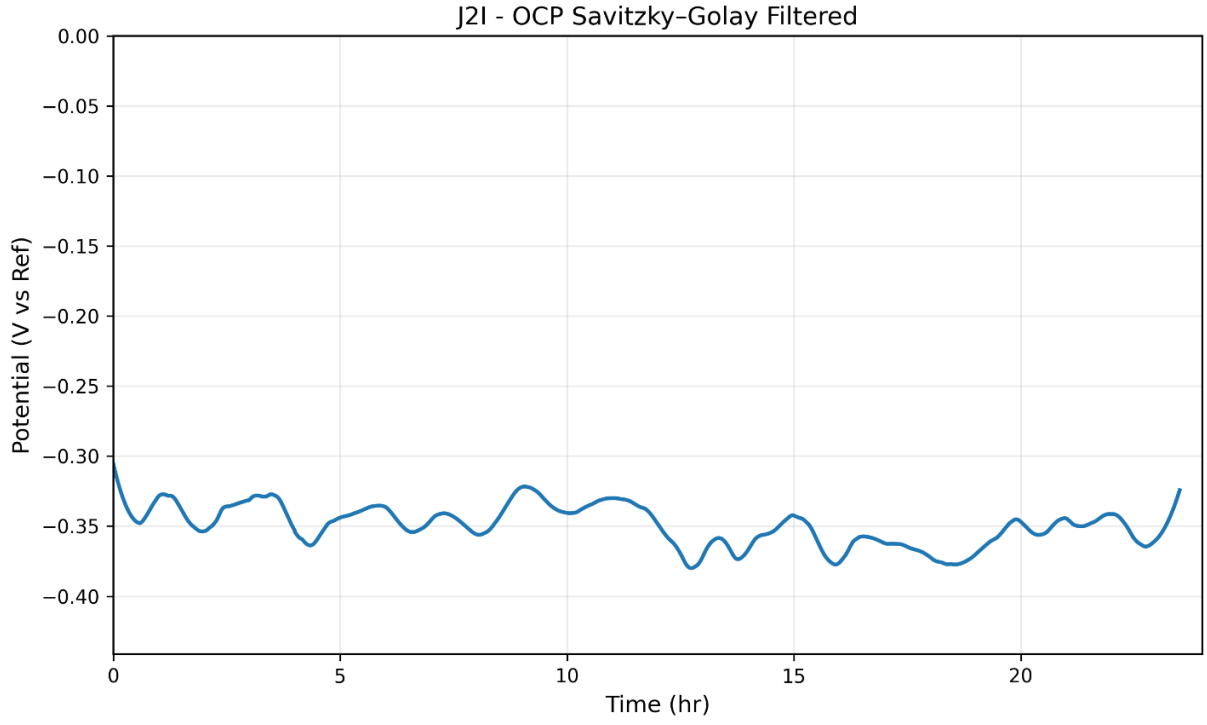
J2I - OCP Savitzky–Golay Filtered
Potential (V vs Ref)
0.00
−0.05
−0.10
−0.15
−0.20
−0.25
−0.30
−0.35
−0.40
0
5
10
15
20
Time (hr)

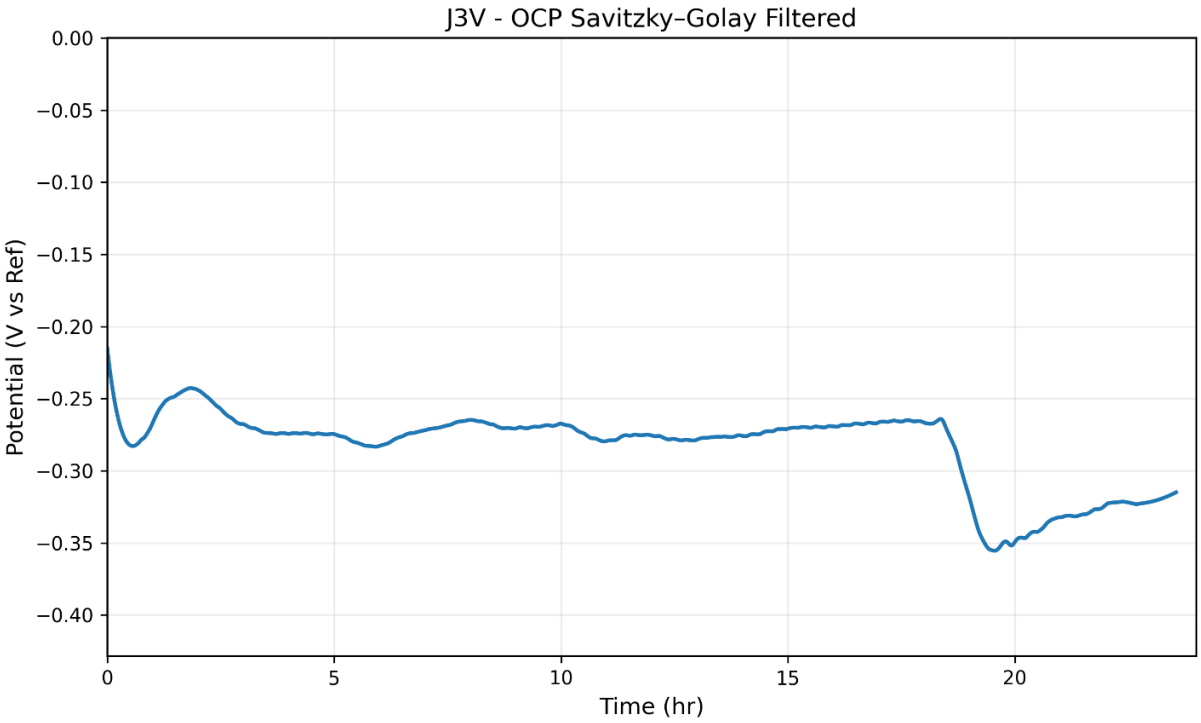
J3V - OCP Savitzky–Golay Filtered
Potential (V vs Ref)
0.00
−0.05
−0.10
−0.15
−0.20
−0.25
−0.30
−0.35
−0.40
0
5
10
15
20
Time (hr)